

THESIS FOR THE DEGREE OF DOCTOR OF PHILOSOPHY

Building Blocks for the Assembly of Nanostructures



CHALMERS
UNIVERSITY OF TECHNOLOGY

Tina Gschneidtner

Department of Chemistry and Chemical Engineering

CHALMERS UNIVERSITY OF TECHNOLOGY

Gothenburg, Sweden 2017

Building Blocks for the Assembly of Nanostructures
Tina Gschneidtner

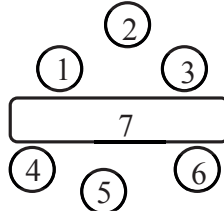
ISBN 978-91-7597-600-6
© Tina Gschneidtner, 2017.

Doktorsavhandlingar vid Chalmers tekniska högskola
Ny serie nr: 4281
ISSN 0346-718X

Department of Chemistry and Chemical Engineering
Chalmers University of Technology
SE-412 96 Göteborg
Sweden
Telephone + 46 (0)31-772 1000

Cover Illustration

1. TEM image of a Au 90 nm and Pd 25 nm nanoparticle
2. Schematic of the molecules we synthesized for metal surfaces
3. SEM image of lithographic Au discs and colloidal Pd 25 nm nanoparticles assembled on it
4. SEM image of heterodimer of Au 90 nm and Pd octahedron 130 nm. Inset shows the surface crystallographic facet (111)
5. UV/Vis spectra of several nanoparticles synthesized
6. Schematic of a molecule covering a lithographic Ag nanostructure



Printed by Chalmers Reproservice
Gothenburg, Sweden 2017

Building Blocks for the Assembly of Nanostructures

Tina Gschneidtner

Department of Chemistry and Chemical Engineering

Chalmers University of Technology

Gothenburg, Sweden

ABSTRACT

The natural world and many man made technologies are driven by self-assembly, involving the autonomous organization of individual components as a result of specific local interactions into functional structures. Self-assembly is a platform from which to construct materials with a high complexity, in high precision, with an inbuilt error-correction system due to its dynamic nature. For example, in nature this principle allows us to encode our genome by the controlled opening and closing two stands of DNA. In addition, linear protein chains fold into elaborate 3D structures for specific functions, cells assemble and divide for example into embryonic tissue and form the basis of reproduction. In fact, all these biological components have a high degree of organization owing to specific interactions at molecular level. The principle of self-assembly is also used in technology for example for drug delivery through liposomes made out of lipid bilayers to carry the drug through membranes to reach specific tissues. It is also the basis of many type of biosensors, such as glucose sensors used by diabetics to monitor their blood sugar level. But also future computer based technology may need ordered arrays of molecules, such as rotaxanes. Rotaxanes for example assemble and switch between two states, which is a promising step towards future molecular-based computers. Indeed, society is in a demand for more powerful computers and therefore its working components ideally need further miniaturization.

This thesis is focusing on different aspects of the self-assembly. The molecular level, the design of new molecules for the self-assembly on surfaces. We designed several molecules and dyes, such as terpyridines, rhodamines and photolabile molecules, which assemble on metal surfaces. Another aspect of this thesis is the testing and evaluating for possible application, such as in biosensing on surfaces with photolabile compounds. Furthermore, the complex strengths of osmium cations and terpyridin was determined using terpyridine molecules assembled on an AFM tip and on a metal surface. Moreover, a plasmon-exciton hybrid was observed by assembling rhodamine dyes on metal nanostructures. Spectral dips in the scattering spectrum appear due to strong coupling between the molecule and the metal. A third aspect of this work was the synthesis of nanoparticles and its assembly into discrete aggregates such as dimers using different approaches, such as molecular linkers or electrostatic interaction. Heterodimeric NPs were tested in hydrogen uptake experiments on individual particles.

Keywords: Self-Assembly, molecules, nanoparticles, sensing, plasmon

LIST OF PUBLICATIONS

This thesis is based on work reported in the following papers, referred to by Roman numerals in the text:

- I. Gschneidtner, T., Chen, S., Christensen, J. B., Käll, M., Moth-Poulsen, K. “**Toward Plasmonic Biosensors functionalized by a photo-induced surface reaction**”, *J. Phys. Chem. C.*, **2013**, 117, 14751-14758.
- II. Hao, X., Zhu, N., Gschneidtner, T. Jonsson, E., Zhang, J., Moth- Poulsen, K., Wang, H., Thygesen, K., Jacobsen, K., Ulstrup, J., Chi, Q., “**Direct measurement and modulation of single-molecule coordinative bonding forces in a transition metal complex**”, *Nature Communication*, **2013**, DOI: 10.1038/ncomms3121.
- III. Gschneidtner, T., Moth-Poulsen, K., “**A photolabile protection group strategy for terminal alkynes**”, *Tetrahedron Letters*, **2013**, 54, 5426-5429.
- IV. Gschneidtner, T., Diaz-Fernandez, Y., Syrenova, S., Westerlund, F., Langhammer, C., Moth-Poulsen, K. “**A versatile Self-Assembly Strategy for the Synthesis of Shape-Selected Colloidal Noble Metal Nanoparticle Heterodimers**”, *Langmuir*, **2014**, 30, 3041-3050.
- V. Gschneidtner, T., Diaz-Fernandez, Y., Wadell, C., Fornander, L., Lara-Avila, S., Langhammer, C., Westerlund, F., Moth-Poulsen, K., “**The Conquest of Middle-Earth: combining top-down and bottom-up nanofabrication for constructing nanoparticle based devices**”, *Nanoscale* **2014**, 6, 14605-14616 (cover).
- VI. Dewi, M., Gschneidtner, T., Elmas, S., Ranford, M., Mouth-Poulsen, K., Nann, T. “**Monofunctionalization and Dimerization of Nanoparticles Using Coordination Chemistry**”, *ACS Nano* **2015**, 9, 1434-1439.
- VII. Syrenova, S., Wadell, C. , Nugroho, F. A., Gschneidtner, T., Diaz-Fernandez, Y., Nalin, G., Świtlik, D., Westerlund, F., Antosiewicz, T. J., Zhdanov V. P., Moth-Poulsen, K., Langhammer, C. “**Hydride formation thermodynamics and hysteresis in individual Pd nanocrystals with different size and shape**” *Nature Materials*, **2015**, 14, 1236-1244.
- VIII. Zengin, G., Gschneidtner, T., Verre, R. Shao, L., Antosiewicz, T., Moth-Poulsen, K., Käll, M., Shegai, T. “**Evaluating Conditions for Strong Coupling between Nanoparticle Plasmons and Organic Dyes using Scattering and Absorption Spectroscopy**”, *J. Phys. Chem. C.*, **2016**, 120 (37), 20588-20596.

CONTRIBUTION REPORT

- I.** Main author, carried out the assembly of molecules on Au surfaces for all experiments. Sample preparation, data collection and evaluation of all QCM, FTIR, NMR and contact angle measurements. The plasmonic data collection was performed by Si Chen, and its evaluation was done in collaboration. Responsible for writing the manuscript.
- II.** Performed the synthesis and the characterization of the linker molecule. The AFM measurements were conducted by the group of Q. Chi. Responsible for writing the synthetic part of the paper and the proof reading.
- III.** Main author. Performed the design, the synthesis and the characterization of all compounds. Responsible for the stability study, the characterization of the photo-induced reaction, as well as the writing of the manuscript.
- IV.** Main author. Performed the synthesis of all nanoparticles, the assembly and the characterization with TEM and SEM together with Yuri Fernandez (no one was specialized in one area). The hydrogen uptake was measured by Svetlana Syrenova. Responsible for writing the manuscript except of the theoretical part.
- V.** Main author. Performed the surface functionalization with lipids, molecules and nanoparticles. Conducted the SEM and TEM images together with Yuri Fernandez (no one was specialized in one area). Proof reading. Design of the cover picture.
- VI.** Performed the synthesis of the molecules necessary to assemble the dimeric nanoparticles. The assembly was done by the group of T. Nann. Characterized some of the nanostructures via TEM and SEM. Part of the writing and proof reading.
- VII.** Performed the synthesis and characterization of the dimeric nanoparticles. The plasmonic evalution was done by C. Langhammers group. Part in writing and proof reading.
- VIII.** Performed the synthesis and characterization of the molecules necessary for the assembly on nanostructures. Spectral analysis was performed by Gülis Zengin. Proof reading.

LIST OF PUBLICATIONS NOT INCLUDED IN THIS THESIS

1. Gschneidtner, T., Fernandez, Y. A., Moth-Poulsen, K. "**Progress in Self-Assembled Single-Molecule Electronic Devices**" J. Mater. Chem. C, 2013, 1, 7127-7133. (cover)
2. Lehmuskerö A., Ogier, R., Gschneidtner, T., Johansson, P., Käll, M. "**Kilohertz spinning of submicron particles by absorption of light in aqueous medium**", Nano Letters, 2013, 13, 3129-3134.
3. Fernandez, Y., Sun, L., Gschneidtner, T., Kasper Moth-Poulsen "**Progress in synthesis of nanoparticle dimers by self-assembly**" APL Materials 2, 010702, 2014.
4. Sun, L., Diaz-Fernandes, Y., Gschneidtner, T., Westerlund, F., Lara-Avila, S., Moth-Poulsen, K., "**Single-molecule electronics: from chemical design to functional devices**", Chem. Soc. Rev., 2014, 43, 7378-7411.
5. **Handbook of Single Molecular Electronics**, Chapter in this book: Self-Assembly at Interfaces. Editor, Kasper Moth-Poulsen, Pan Stanford Publishing 2015
6. Ficker, M., Petersen, J.F., Gschneidtner, T., Rasmussen, A.-L., Purdy, T. N., Hansen, J. S., Hesselhøj Hansen, T., Husted, S., Moth-Poulsen, K., Olsson, E., Christensen, J. B. "**Being Two are Better than One — Catalytic Reductions with Dendrimer Encapsulated Copper- and Copper-Cobalt - Subnanoparticles**" Chem. Commun. 2015, 51, 9957-9960.
7. Bradley, S. Kroon, R.; Röding, M., Goreham, R. V., Gschneidtner, T., Moth-Poulsen, K., Schroeder, K., Andersson, M. and Nann, T. "**Heterogeneity in the fluorescence of graphene and graphene oxide quantum dots**" Microchimica Acta, 2017, 9, 673-683.
8. Eklöf, J., Lara-Avila, S., Gschneidtner, T., Nygaard, K., Moth-Poulsen, K., "**Controlling deposition of nanoparticles by tuning surface charge of SiO₂ by surface modification**" RSC Advances, 2016, 6, 104246-104253.

TABLE OF CONTENTS

| | |
|---|-----------|
| ABSTRACT | III |
| LIST OF PUBLICATIONS | V |
| LIST OF PUBLICATIONS NOT INCLUDED IN THIS THESIS | VII |
| TABLE OF CONTENTS | VIII |
| 1 Background | 1 |
| 1.1 Introduction | 1 |
| 1.2 Optical Properties of Metal Nanoparticles | 3 |
| 1.3 Synthetic Routes to Nanoparticles | 7 |
| 1.4 Self-Assembly | 13 |
| 1.4.1 Assembly of Discrete Dimeric Clusters | 16 |
| 1.4.2 Purification of Assembled Structures | 20 |
| 1.4.3 Assembly of Heterodimeric Structures | 21 |
| 1.5 Applications of nanostructured clusters | 23 |
| 1.6 Thesis Outline | 25 |
| 2 Design of Molecular Linker for Metal Nanostructures | 27 |
| 2.1 Molecular Linker | 27 |
| 2.1.1 Terpyridine Linker assembled on Surfaces to Measure the Strength of its Complexes with Heavy Metals (paper II) | 28 |
| 2.1.2 Rhodamine Linker Assembled on Gold Nanostructures to measure Strong Coupling (paper VIII) | 33 |
| 2.2 Photolabile Protection Groups | 40 |
| 2.2.1 Assembly of a Photolabil Nitroindoline on Gold Nanostructures as a LSPR based Biosensor (paper I) | 42 |
| 2.2.2 New Photolabile Protection Groups for Alkynes for self-assembly on plasmonic metal surfaces (paper III) | 46 |
| 3 Assembly of Colloidal Nanoparticles | 53 |
| 3.1.1 Terpyridine Linker to Assemble Dimeric Metal Nanoparticles (paper VI) | |
| 54 | |
| 3.1.2 Assembly of Dimers in Solution using Electrostatic Interactions and the Use of Heterodimers for Sensing Applications (paper IV and VII) | 58 |
| 3.1.3 Assembly of Nanostructures on Surfaces (paper V) | 65 |
| 4 Concluding Remarks and Outlook | 71 |
| REFERENCES | 73 |
| ACKNOWLEDGEMENTS | 83 |

Background

1.1 Introduction

Controlled self-assembly of nanoparticles to afford dimeric nanoparticle (NP) structures is an interesting challenge for many research areas, such as bio-medical science, physics and chemistry. Fundamental questions in material science and nanotechnology have the potential to be answered with nanoparticle dimers, such as the possible miniaturization of electronic and medical devices.^{1,2}

The current computer technology uses lithography for the production of silicon-based chips. This method is called “top-down” approach, in which devices are manufactured by removing material from larger entities. But to build more powerful and faster computer, these approach need to achieve the size of a few atoms, which is not possible with current top down technology yet.^{3,4} Current research on nanodevices focuses therefore on e.g. improving semiconductor based devices with the help of self-assembly of molecules and nanoparticles, via a method called “bottom-up” approach, see **Figure 1**.^{5,6}

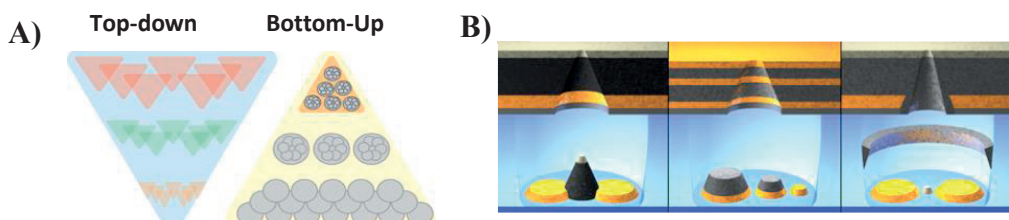


Figure 1: A) Schematic of the bottom-up vs top-down methodology to construct nanostructures; B) Example of constructing nanostructures by advanced hole-colloidal lithography. (©from reference⁹ 2014 ACS Publications)

A first step towards molecular computing is the development of new structures such as molecules with two stable states to be switched to, in order to form the binary 1 or 0 for memory devices. Examples are here Stoddards switches, the rotaxanes.⁶ Their performance, durability is still not comparable with current technology as used in computers, neither to nano machines in nature.⁷ Nature shows how to form structures in nanometer size, such as biological machines, e.g. the motor proteins myosin, which

is involved in muscle contractions and other motions in muscle tissue, or our DNA. But also the assembly of nanoparticles or even dimeric nanoparticles, as shown by Thomas Bjørnholm et al.⁸ can be used to form for e.g. nanoelectrodes.

Dimeric metal structures produced *via* top-down methods, are produced in a variety of different ways, for example by hole-mask colloidal lithography (see **Figure 1B**),^{9–11} by electron beam (EBL) or focused ion beam (FIB).¹² Common for all of these and other top-down techniques is the manipulation of larger structures to create nanostructures. Nanostructures prepared in this way can be positioned on top of each other or next to each other, but there are limiting factors including the fact that these nanostructures are in the size of several atoms, they are mostly not single crystalline and therefore special surface facets, which may exhibit specific catalytic efficiencies, cannot often be investigated by structures made in a top-down method.

Colloidal nanoparticles composed of different materials with a multitude of sizes and morphologies, displaying different facets, have previously been described in the literature. These include examples of palladium (Pd) NPs possessing different morphologies,¹³ gold (Au) nanorods in different aspect ratios,¹⁴ Au stars,¹⁵ iron oxides (Fe_xO_y),¹⁶ titania nanocrystals (TiO_2),¹⁷ Au shapes as cubes and octahedral¹⁸ and silver (Ag) triangles.¹⁹ Many others have also been well-studied and described.^{20–22} A key ambition of nanoscience is therefore to control the synthesis of nanoscaled materials using efficient and elegant bottom-up approaches, while aiming for a high yield production in order to implement it in practical applications. By controlling the surface properties of nanoparticles the assembly of nanostructures to, e.g., dimers on surfaces or in solution can give rise to new materials, new devices, and new catalysts.^{23–29}

Arising from this, the following scientific questions are discussed in my thesis: how can self-assembly of these well studied nanostructures be controlled to create new or better properties? Can we combine top-down and bottom up approaches to assemble nanostructures for devices? How can new functions of nanoparticle assemblies be achieved and analyzed?

In the following I am going to present some general information about metal nanoparticles, in particular their optical properties, which makes them especially interesting for nanocluster assemblies. This will include a historical overview, as well as a comprehensive overview on what has been done to assemble nanoparticle dimers and why this is such an emerging field of interest. **Chapters 2 and 3** describe the work done to address the scientific questions discussed above by working on different building blocks, important for the self-assembly, such as the synthesis of **molecular linkers**, **nanoparticles** and their **assembly** in solution and on the surface. The center of interest of **Chapter 2** lays on the development of special molecular linkers for metal

surfaces and its applications such as biosensors or to study strong coupling effects. These molecular linkers can be further used for the assembly of nanoparticle dimers as e.g. described in **Chapter 3.1**. **Chapter 3** focuses on the assembly of dimeric nanostructures using synthetic molecular linkers, as well as electrostatic interaction between nanoparticles. Furthermore, the controlled assembly of nanoparticles on surfaces is discussed.

1.2 Optical Properties of Metal Nanoparticles

Scientist have been fascinated by metal nanoparticles for over more than a century. As early as the 19th century, the optical properties of colloidal noble metal nanoparticles (NPs) were studied by Michael Faraday.³⁰ It was indeed due to their optical properties, that metal nanoparticles such as gold (Au) and silver (Ag) were utilized much earlier. Many famous church windows built during the middle ages, such as the Rayonnant rose³¹ window from Notre-Dame de Paris shown in **Figure 2**, were vividly colored by metal nanoparticles. These particles were used because they keep their color without fading over time.

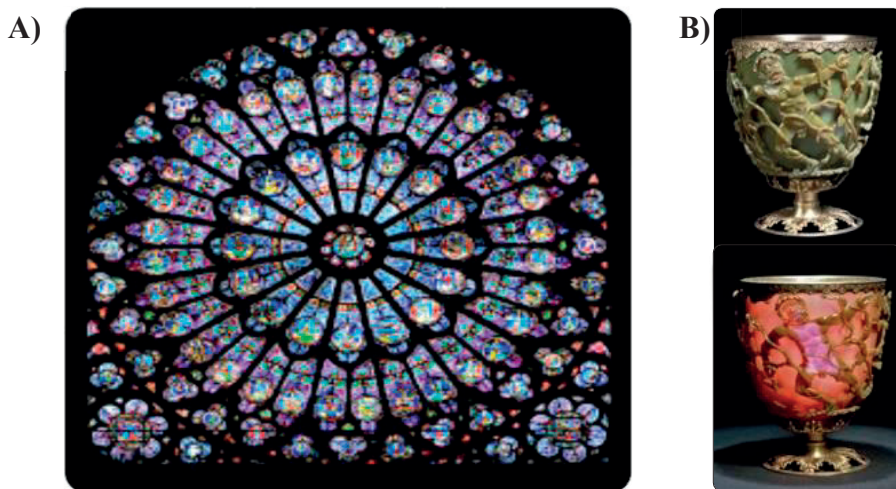


Figure 2: A) Rayonnant rose window from Notre-Dame de Paris. The photo is reproduced from a web page.³¹ B) Lycurgus Cup in the British Museum. The photos are reproduced from the web page of the British Museum.³² ©Trustees of the British Museum.

Another example in history is the Roman glass cage cup made in the 4th century, the Lycurgus Cup,³² also colored by nanoparticles. The cup changes its color whether it's illuminated from inside (red) or from the outside (green, **Figure 2**). The green or red color can be explained due to scattering and absorbing of either red light (green cup) or respectively green light due to the nanoparticles dispersed throughout the glass.

Metal NPs show well understood phenomena like intense light scattering and strong absorption, which can be used in many applications.^{33–35} NPs appear in a certain color due to the absorption and/or scattering of light. Small Au NP spheres, for example, are reddish, because the blue and green light is absorbed (350-550 nm) but the red light is transmitted, see **Figure 3A**. For larger NPs the scattering of light is more dominant and, the observer therefore sees the light scattered from the nanoparticles.

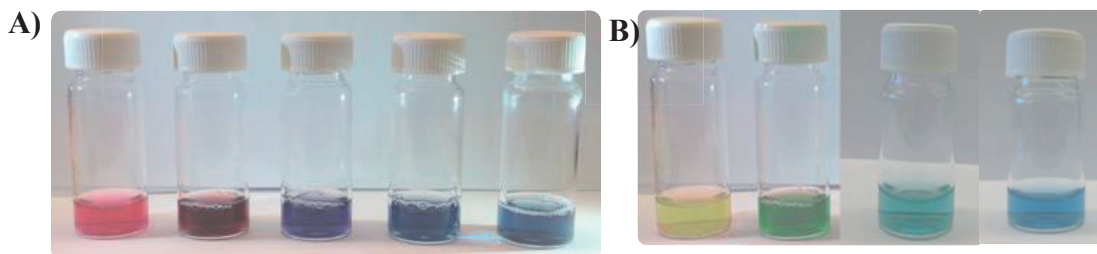


Figure 3: NPs synthesized in our lab: A) Au NPs of different size and different shape; B) Ag NPs of different size and different shape.

There is a relationship between the size and absorption in the UV/Vis. If the size of metal NPs are smaller or comparable with the wavelength of the incident light the conduction electrons in the metal can be excited to resonant collective oscillation, which is called localized surface plasmon resonance (LSPR). The electrons are displaced with respect to the ionic core of the metal, see **Figure 4A**. The electron cloud will want to return to its ion lattice due to Coulomb attraction, which causes a harmonic oscillation. At this resonance the electric field of the plasmonic NPs results in an enhanced absorption and scattering, which can be measured by the UV-Vis absorption spectrum of the NP solution, see **Figure 4B**.

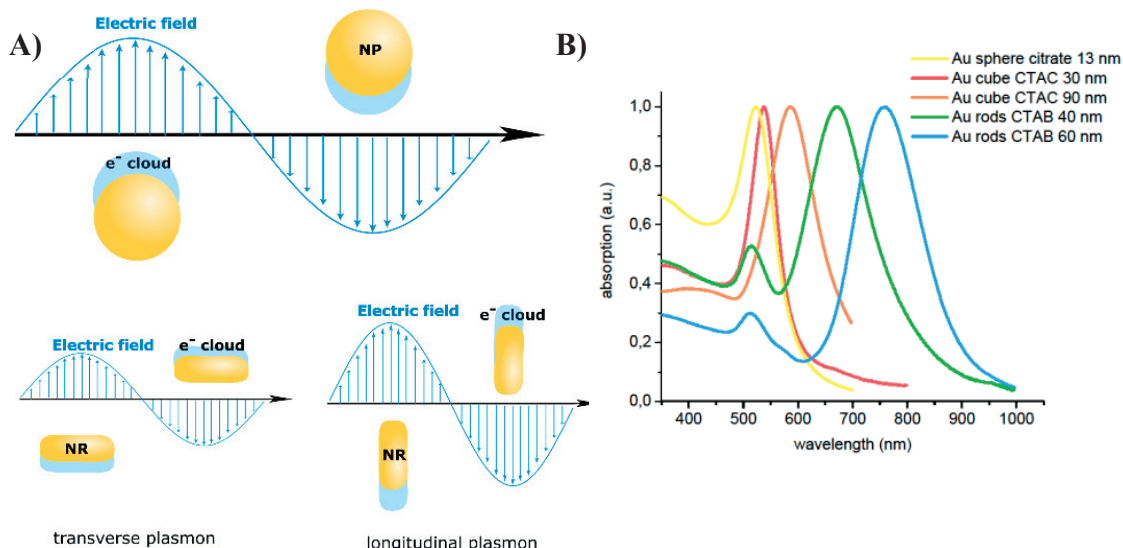


Figure 4: A) Light of the right wavelength excites the conducting electrons to a collective oscillation in metal NPs. Schematic visualizes the oscillation of the electron cloud (LSPR) of NPs and NRs. B) Absorption spectra of different Au based nanostructures, spheres, cubes, rods of different size, synthesized in our lab.

The oscillation, due to the Coulombic attraction, which pulls the electrons back to its positively charged lattice, is not only influenced by the size, shape, composition, permittivity of the NP, but also by the local dielectric environment.³⁶ The resulting LSPR peak can therefore be in the UV-Vis³⁷ or the near- IR region³⁸ of the electromagnetic spectrum. As depicted in **Figure 4B**, larger nanoparticles absorb at a longer wavelength than small nanoparticles and depending on the shape some special features can be seen. The rods for example possess two intense surface plasmon resonance peaks, originated from the long (longitudinal) axis and the short/transverse axis (see **Figure 4B**/ blue and green traces). Furthermore, the aspect ratio of the rod determines the position of the LSPR as well. Anisotropic nanoparticles show therefore characteristic features in their absorption behavior.

Due to this charge separation at the surface, a strongly enhanced electric field around the NP is generated. The electron oscillation (LSPR) can also be distributed over several NPs through interparticle coupling of plasmonic modes, called a collective plasmonic oscillation, which is strongly dependent on the distance between the NPs, the surrounding media and the type of metal.³⁹⁻⁴¹ NPs positioned close to each other such as in dimers demonstrate a spectral shift. In this near-field interaction, a coupled plasmonic mode, influences the electric field around the nanostructure assembly. As a result of this, the gap between assembled nanoparticles has a highly enhanced electric field, shown in **Figure 5**. Dielectric objects can be strongly affected by the localized electromagnetic field. One can envision many interesting applications, such as photo-chemistry of molecules,⁴² thermal processes assisted by plasmons,⁴³ nanoantenna behavior,⁴⁴ field enhanced spectroscopy^{45,46} including SERS (surface-enhanced Raman scattering) and many more.

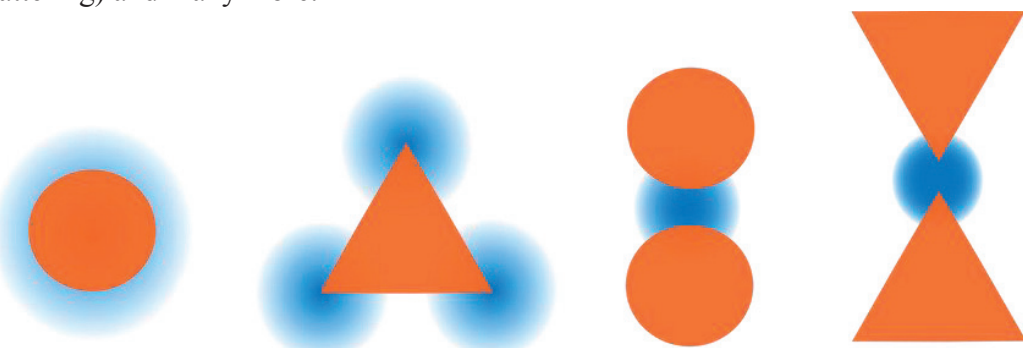


Figure 5: Schematic of the enhanced electric field close to the surface of plasmonic nanostructures. Sharp corners and gaps between particles show a very strong local enhancement of the electric field, called hot spot.

Spectroscopic techniques such as cathodeluminescence (electronic)⁴⁷ or dark-field spectroscopy (optical)⁴⁸ can map the plasmon resonance and visualize the enhanced fields around the particles or in the gaps. The gaps are called, “hot spots” because of this enhanced field.

Due to the special optical properties and the chemical inertness of noble metal NPs, a wide range of applications for plasmonic NPs ranging from photodynamic therapy, drug delivery, LSPR supported biosensing^{49,50} or single molecular electronics^{51–53} opens up.

Also non optically active NPs themselves could play important roles in many research fields, as catalysts (Pd, Pt...),^{54 55} as a tool to monitor labelled cells in real time by magnetic resonance tomography (MRT) (Fe_3O_4)⁵⁶ or for monitoring the storage of hydrogen in hydrogen driven cars with metal hydrides.

The assembly of discrete clusters such as dimeric structures of nanoparticles as well as metal and non-metal nanoparticles is a very interesting topic. **Chapter 1.4** highlights possible applications of discrete nanoparticle clusters, thus motivating our research efforts in this field. In order to give a better perspective into the assembly of nanoparticles, the following chapter presents synthetic methodologies into the formation of particles and how they are stabilized in solution.

1.3 Synthetic Routes to Nanoparticles

During the last decade the synthesis of various metal NPs with different shapes, sizes and compositions has been developed and improved. Spheres, stars, cubes, rods and many others can be synthesized according to known procedures.

Due to the large surface to volume ratio of NPs, resulting in a high surface energy, NPs tend to aggregate resulting in sintering if not properly stabilized. The stabilization ideally should occur during the synthesis and the growth process in order to avoid aggregation. In this way a narrow size distribution of NPs can be achieved simultaneously. Typical ways of stabilization are maintained through steric or electrostatic interactions, as depicted in **Figure 6**.

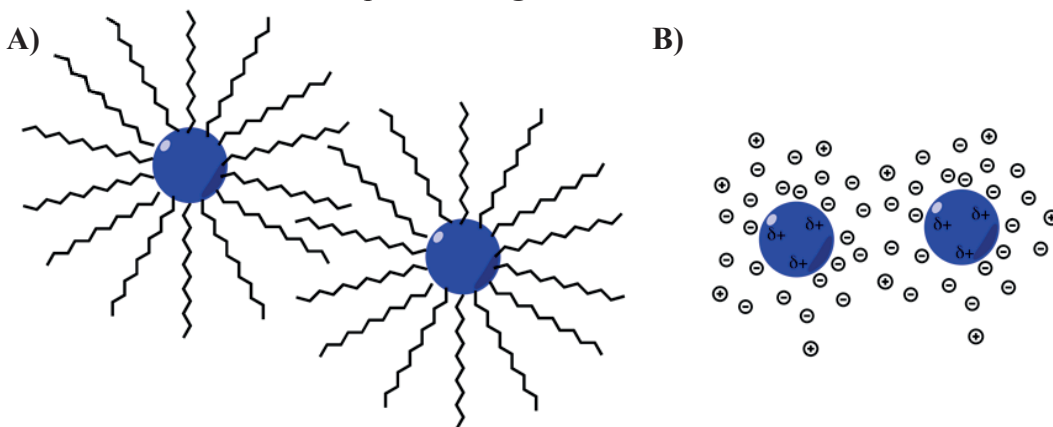


Figure 6: Schematic of colloidal NPs stabilized by A) steric and B) electrostatic interaction.

Steric stabilization, see **Figure 6A**, can be achieved by employing polymers, surfactants or long alkanes preventing the particles from sintering. A common way is using molecules with specific anchoring groups to the corresponding metal. Every metal and metal oxide has a certain affinity for anchoring groups, for example Au binds almost covalently (40-50 kcal/mol) to thiols, and even stronger binding occurs with di- or trithiols.⁵⁷ Ligands anchored with functionalities such as phosphanes, nitriles, carboxylic acids and many more are known to be very stable as well, though the Au-anchor bond for these functional group is not as strong as that found for the Au-S and most likely not covalent in nature. The binding affinity of the ligand to the metal nanoparticle decreases following the HSAB principle of Pearson from S > P > N > O. In this principle most metals are soft acids and form therefore covalent bonds with soft base ligands such as thiols. Silver (Ag), palladium (Pd), platinum (Pt), copper (Cu), zinc (Zn) show a similar behavior. Metal oxides like titanium dioxide (TiO_2), iron oxides (Fe_xO_y), or oxidized silicon (SiO_2) however are better stabilized by non-covalent bonding anchors with oxygen groups like carboxylic acids, phosphoric acids, or alkoxides. They can, however also be stabilized by very stable covalent bonds, such as in the case with silicon dioxide stabilized *via* silanes such as alkyltrichlorosilanes.⁵⁷

Electrostatic stabilization, see **Figure 6B**, can be achieved by Coulomb repulsion between two neighboring particles charged by adsorbed ions and their counter ions which form an electrical double layer around the particle. Many metal NPs are typically stabilized by adsorbed citrate anions, but also other donor molecules such as phosphines or amines can be used. The double layer depends on temperature and the ionic strength. It has been assumed that the adsorbed citrate anions on the metal surface show no interacting with each other, but only electrostatically stabilize the metal NP solution. However, Shumaker-Parry et al.⁵⁸ confirmed in recent studies that the citrate anion adsorbs by the central carboxylate group and further interacts with the adjacent citrate anions on the surface, forming a 1-D citrate chain. The citrate anions in the chain interact through Van-der-Waals interaction between CH₂ moieties but also with dangling citrate molecules through hydrogen bonds between the terminal carboxylic acid groups.

Most synthetic procedures of Au NPs are based on the same principle, the reduction of a metal salt *via* a reducing agent in the presence of a stabilizing ligand in aqueous or organic solvent. The particle size and shape depend strongly on the choice of the ligand, the solvent, the reaction temperature and reaction time, as well as the stoichiometry of metal, ligand and solvent and pH.⁵⁹ A famous procedure from 1994 is the Brust-Schiffrin method, used to synthesize small monodisperse Au NPs in organic solvent.⁶⁰ In this, Faraday inspired method, an aqueous solution of gold salt is reduced with sodium borohydride (NaBH₄) in a two-phase system. The gold salt needs to be transferred to the organic phase using a phase transfer agent like tetraoctyl ammonium bromide (as a counter ion pair) and is reduced and stabilized in the organic phase *via* alkanethiols as ligands.⁶¹ The procedure can also be performed in methanol as a monophasic reaction mixture, and NPs in the size range of 1.5-5 nm can be produced. Interestingly, the average size can be tuned by changing the ratio between Au and ligand.⁶² This method was varied and improved in many ways. One example is by Stucky *et al.*,⁶³ who describe the synthesis of “real” monodisperse NPs by using a weaker reducing agent. Exchanging the reducing agent sodium borohydride with borane complexes reduces the rate of the reduction of Au³⁺ to Au⁰, resulting in a better growth control.

Another notable method to produce water soluble Au NPs from as early as 1951 is the synthetic procedure by Turkevich *et al.*^{64,65} and has been the subject for further improvements by Frens *et al.*^{66,67} Tetrachloroauric acid (HAuCl₄) is heated with trisodium citrate to reduce but also stabilize the particles. By differing the citrate/Au ratio the size can be tailored.

Silver NPs can be synthesized in similar fashion to the Brust and Turkevich method, with the precursors silver nitrate or silver acetate and the stabilizers citrate, oleylamine or dodecanethiol.⁶⁸⁻⁷⁰

These methods show, that stronger reducing agents such as sodium borohydride tend to give smaller NPs compared to the use of weaker reducing agents such as citrate.

The mechanism during the formation of nanoparticles is still under discussion, but two different growth mechanisms have been proposed: growth via diffusion and growth via coalescence, see **Figure 7**. SAXS (small angle X-ray scattering) analysis show that borohydride⁷¹ initiates a rapid and complete conversion of Au^{3+} into atomic Au^0 and forms gold nuclei, the particle grows *via* coalescence of nuclei into bigger particles. Citrate as a reducing agent shows a fast initial formation of small nuclei as well, they coalesce into bigger particles, followed by growth by diffusion, which is a slow step due to an ongoing reduction of Au precursor. Finally, Au^{3+} is all reduced and a rapidly growing step finalizes the Au NPs. They grow slowly while the reduction to Au^0 is still ongoing, see **Figure 7B**.⁷²

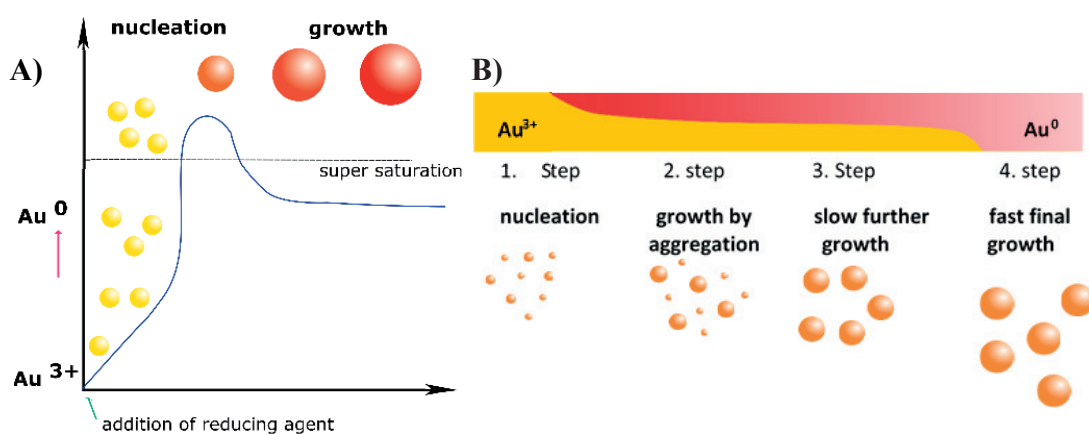


Figure 7: A) Schematic of the nucleation and growth of Au NPs by reducing Au^{3+} to atomic Au^0 with NaBH_4 . Small particles nucleate and after reaching a certain concentration of Au^0 , they start to grow via coalescence. B) Schematic of the growth of Au NPs by using citrate as a reducing agent. The particles grow while still more Au^{3+} is reduced. Two different growth modes are seen here, step 2: growth via coalescence, step 3 and 4 growth via diffusion.

In summary, Au NPs grow in the presence of a strong reducing agent *via* coalescence, **Figure 7A**. Alternatively, Au NP growth while using a weaker reducing agent arises from coalescence/aggregation first (**Figure 7B** steps 1-3) but later by diffusion (**Figure 7B** step 4).⁷³

In addition to sodium citrate and borohydride many other reducing agents such as potassium tartrate can be used to produce nanoparticles. Furthermore, organic solvents such as DMF can reduce Ag^+ / Au^{3+} to Ag^0/Au^0 thus forming NPs, however this approach usually requires higher reaction temperatures.⁷⁴⁻⁷⁶

The synthetic routes described so far lead to “monodisperse” spherical NPs. Other shaped particles can be formed, by using for example surfactants such as ammonium salts. Around 2000, the first wet chemical method by seeded growth synthesis by Jana,

Murphy, El-Sayed, and others was developed to produce Au nanorods.^{77,78} In order to get shaped NPs such as stars, rods, cubes, octahedral and many more, most synthetic procedures are now using surfactant molecules. These form micellar structures through self-assembly, when they are dissolved in water above their critical micelle concentration (cmc).⁷⁹ Furthermore, small organic molecules or counter ions such as iodide or bromide adsorb selectively on special planes of the growing particle and direct the synthesis of the noble metal NP; they induce symmetry breaking steps.⁸⁰ The size and the shape is controlled by the nucleation growth kinetics and also by the type of formed micelles, *e.g.* rodlike micelle templates result in high-quality anisotropic nanorods.⁸¹

In order to synthesize shaped NPs in CTAB (cetyltrimethyl ammonium bromide) for example, often a seed-mediated growth in aqueous solution is used. The seeds can be small citrate seeds, as synthesized by Turkevich *et al.*⁶⁵ or small CTAB covered NPs.⁸² Typically, the seeds are added to the growth solution containing additional Au salt and a weak reducing agent such as ascorbic acid, plus some extra agents (ions or small molecules) to direct the growth. Ascorbic acid as a reducing agent is widely used, since it is too weak to reduce freely dissolved gold salts from Au^{3+} to Au^0 , and hence no new nuclei can be formed.

CTAB is the most widely used stabilizing and form-giving surfactant in recent years. CTAB builds very dense double layers and is therefore a suitable stabilizing agent for metal nanoparticles. It forms 6 nm spherical micelles in a >1 mM solution, cylindrical micelles at > 20 mM solution or elongated rodlike micelles by using organic solubilizers.^{81,83} Nanorods, for example are favored when one is reaching the second cmc at very high CTAB concentrations and CTAB can therefore act as a soft template for the formation of Au nanorods.⁸⁴ Furthermore, temperature influences micelle assembly, since micelle formation and shape is temperature sensitive as well.

Many proposed growth mechanisms of shaped particles, *e.g.* rods, suggest a preferential interaction of the surfactant with specific crystallographic facets, *e.g.* along the side of the rod. This allows growth of the particle in the micelle at the ends of the rods and less on its sides.⁸⁵ Furthermore, it is suggested that the counter ion bromide (Br^-) has a strong influence on the shape of the NP as well. One theory about the growth mechanism for Au nanorods suggests, that CTAB adsorbs to the side of the rod on its [100] and [110] facet *via* chemisorbed bromide counterions, so the growth is promoted at the ends.⁸⁵ Another interpretation by Liz-Marzán *et al.* describes the AuCl_4^- ion displacing Br^- ions on the growing particle surface, followed by the binding of CTA^+ ions, which then form the micelle. AuCl_4^- ions are then reduced to AuCl_2^- at the micelle surface, meaning that the micelle determines the growth at different rod facets.⁸⁶

To form an even more densely packed CTAB double layer, silver nitrate (AgNO_3) is often added to the reaction to reduce the repulsion between adjacent ammonium head groups of CTAB, see **Figure 8**.⁸⁰ However, it might also be that the deposition of AgBr (Br^- originated from CTAB) on specific facets of the rods directs the growth, due to a more rapid incorporation of gold on less hindered facets.⁸⁵ Another theory suggests, that a silver monolayer protects the [110] facets.⁸⁷

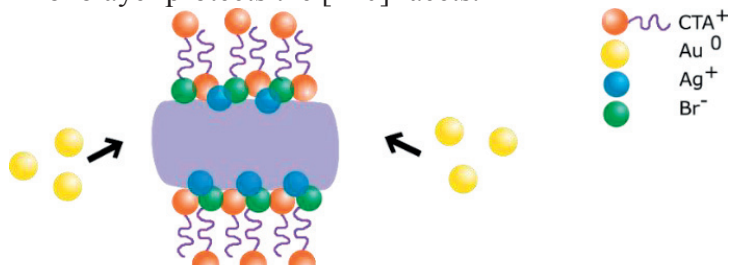


Figure 8: CTAB double layer stabilizing growing Au nanorod. Synthesis in the presence of AgBr .

In conclusion, it seems that additives can have an impact on the bilayer formation and their influence is promoting or inhibiting the adsorption and growth along specific facets and therefore in specific dimensions, even though rods were traditionally produced without additives. Vaia *et al.*⁸⁸ followed each growth step and even goes as far as to rationalize the formation of different type of rods, such as with a dumbbell profile, flattened end facets or octagonal prismatic structures.⁸⁰

Other nanoparticles with interesting shapes derived from different metals have been prepared in a similar manner. For instance, palladium NPs can be synthesized by reducing a palladium salt (PdCl_2 which forms H_2PdCl_4 by adding HCl to the salt to solubilize the insoluble PdCl_2) with ascorbic acid in the presence of CTAB at elevated temperature.⁸⁹ These small cubic seeds can be grown by seed-mediated growth in CTAB, H_2PdCl_4 and different amounts of potassium iodide (KI) with different temperatures to bigger cubes, truncated cubes, octahedral crystals, rhombic dodecahedrals and others possessing a variety of palladium facets.¹³

Besides the prominent stabilizing ligand CTAB being used to form shaped NPs, other stabilizers such as PVP (poly(vinylpyrrolidone)) are also often used. PVP can itself act as a reducing agent and at the same time regulate the size of the synthesized particles, as a stabilizing agent.⁷⁴ For example, Ag rods from its precursor silver nitrate (AgNO_3) can be synthesized in PVP.⁹⁰ It is thought that the lone-pair electrons on the oxygen of enol form of PVP oxidize Au^{3+} to Au^0 atoms in water by forming an Au-O-C bond in a polymer-metal coordination complex. Furthermore, high temperature reactions with DMF as a reducing agent can form shaped nanoparticles at high temperatures as well.^{74-76,91}

Figure 9 shows a few examples of shaped nanoparticles synthesized during my PhD.

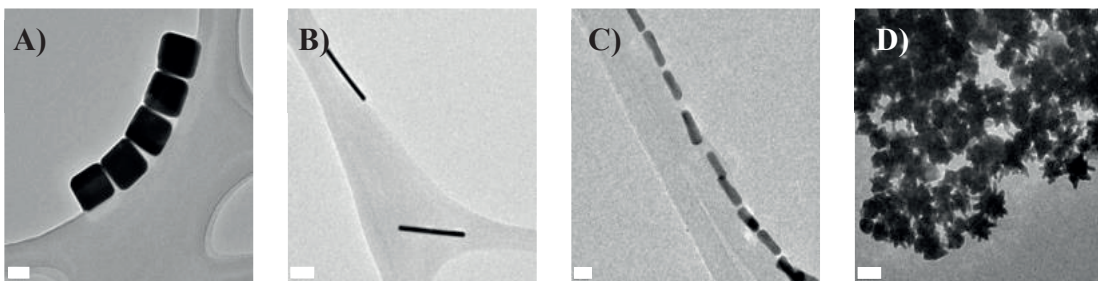


Figure 9: Synthesized shaped Au NPs stabilized with CTAB/C,¹⁸ A) Au cubes in CTAC; B) high aspect ratio Au rods in CTAB,²⁰⁶ C) low aspect ratio Au rods in CTAB;⁹⁹ D) Au stars surfactant free²⁰⁷ (synthesized according to known procedures). Scale bars from A) to D) are 50 nm, 100 nm, 20 nm and 50 nm.

As described above, most NPs are synthesized with a stabilizing ligand. These, often chemisorbed, ligands on nanoparticle surfaces can be exchanged by others with either stronger surface interactions or a competitive ligand present in higher concentrations in the surrounding medium.⁹² Even the strongly covalently bound thiol ligands on Au surfaces are labile and thus capable of undergoing exchange, shown by Rotello *et al.* in 2000.⁹³ This makes it possible to functionalize NPs with other molecules of interest, be it to obtain greater solubility or introduce additional function. The most facile being the exchange of NPs stabilized by citrate, since citrate is a relatively weak stabilizer due to its low affinity for the Au surface and can be exchanged with e.g. thiols, which bind much more strongly to Au.^{94,95} Conversely, it is difficult to effect exchange of thiols. Yet monovalent ligands are still dynamic and exchangeable by exposing the NPs to competing ligands in higher concentrations or by introducing stronger ligands such as multivalent thiols.⁹⁶ For a long time CTAB was considered a very difficult stabilizer to exchange, since it forms a stable bilayer around its particles due to Van-der-Waals interactions between the long alkane chains. Destabilization of the bilayer can occur when subjecting these nanoparticles to different solvents such as acetonitrile,⁹⁷ or isopropanol or reducing the CTAB concentration drastically, however, most CTAB covered nanostructures can be further functionalized in different ways.⁹⁸ CTAB stabilized NPs are toxic to biological cells and denature proteins, therefore development of methods in post functionalization is of great interest for biological applications.^{99–101}

More elaborate tailor made ligands to connect particles with each other or surfaces are subject to our research interest. **Chapter 1.4** will feature examples what has been done historically in the assembly of nanoparticles into discrete clusters using ligands, electrostatic interactions or surfaces to achieve this goal.

1.4 Self-Assembly

Self-Assembly describes the ability to form organized structures out of disordered systems without external guidance.¹⁰² Indeed, many processes in biology rely on molecular self-assembly, *via* Van-der Waals interactions, hydrophobic interactions and hydrogen bonding. Peptides, proteins and nucleic acids fold *via* self-assembly, membranes are formed by the assembly of lipid bilayers, nanoscale motions like those found in myosine are made possible due to the self-assembly of small complexes. Nature gave us these tools which are capable of assembling and disassembling when required without human intervention. Chemists try to mimic this behavior by synthesizing molecules, which reversibly bind their counterpart in a specific way, and this field in chemistry has been called supramolecular chemistry. Here, relatively weak non-covalent interactions such as metal coordination, Van-der-Waals forces, π - π -interactions, hydrogen bonding or electrostatic interactions are used to assemble molecules to form vesicles, liquid crystals, Langmuir films and many more organized macrostructures. Very notable examples of supramolecular chemistry include the so-called catenanes and rotaxanes which were pioneered by Stoddart *et al.*^{6,103} These are macrocyclic rings looped around linear or other macrocyclic structures, see **Figure 10A+B**. Other examples include the formation of grids by Jean Marie Lehn *et al.*,¹⁰⁴ in which metal-ligand interactions are used to form grid like structures, (**Figure 10C**). Sir J. Fraser Stoddart even won the Nobel Prize in chemistry together with Jean-Pierre Sauvage and Bernard L. Feringa for the design and synthesis of molecular machines in 2016, as well as Jean-Marie Lehn together with Donald J. Cram and Charles J. Pederson in 1987 for their development and use of molecules with structure-specific interaction of high selectivity.

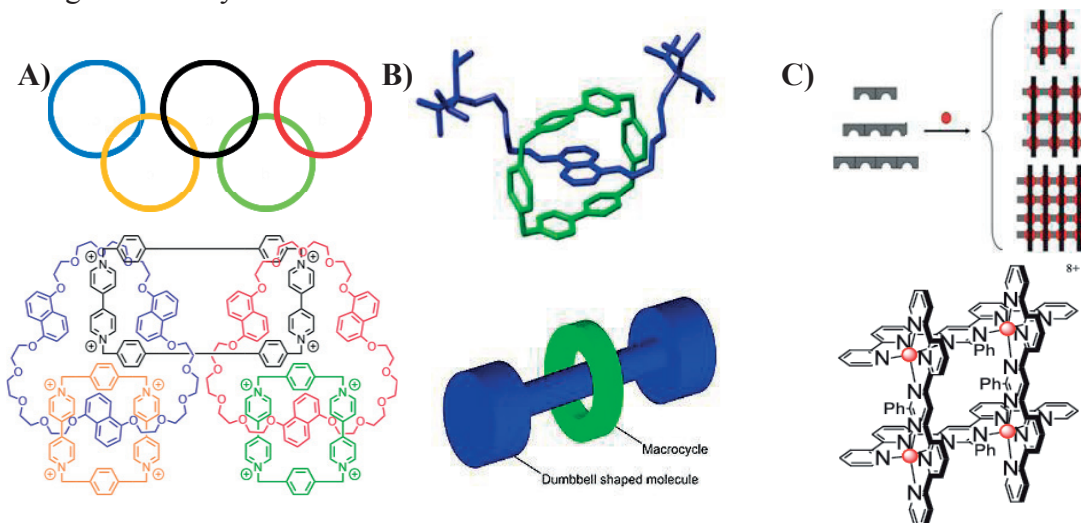


Figure 10: Supramolecular Chemistry, A) Stoddards Olympiad, B) Dumbbell-shaped rotaxanes, (These photo are reproduced from a web page, reprinted with permission from reference⁶ 1998 John Wiley & Sons;) C) metallo grids from planar polytopic organic ligands coordinating metals. (Reprinted with permission from reference¹⁰⁴ ©2011 NZIC)

In the field of single molecule electronics, the self-assembly of organic molecules onto metal surfaces is a main process to connect molecules of interest with, for example electrodes for the purpose of investigating conductivity through organic bridging units. In a famous example by Weiss *et al.*¹⁰⁵ in 1996, a tunneling current though a π -conjugated single conducting molecule was measured using an STM tip. The molecule protrudes from a self-assembled monolayer (SAM) consisting of an ensemble of non-conductive molecules, see **Figure 11**.

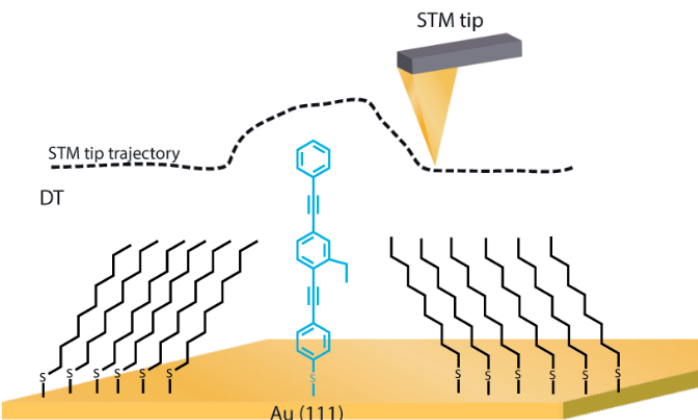


Figure 11: STM measures the tunneling current of a single conducting molecule in a mixed SAM layer on Au.

As nanoscale building blocks, nanoparticles are particularly interesting candidates for self-assembly, especially due to their interesting catalytic and electronic properties. The combination of nanoparticles of the same type (chemical composition, size, and shape) but also of different types pose interesting scenarios for this research field. The following paragraph will describe the assembly of nanoparticles to form bigger constructs, which can be used for example for plasmonic sensing, or to form a protein transistor. Examples such as these motivate our research interest in nanoparticle assembly.

We are particularly interested in the assembly of NPs into discrete well defined units. It is envisaged that this can be reached *via* different approaches such as electrostatic interactions or with molecular linkers, (**Figure 12**).

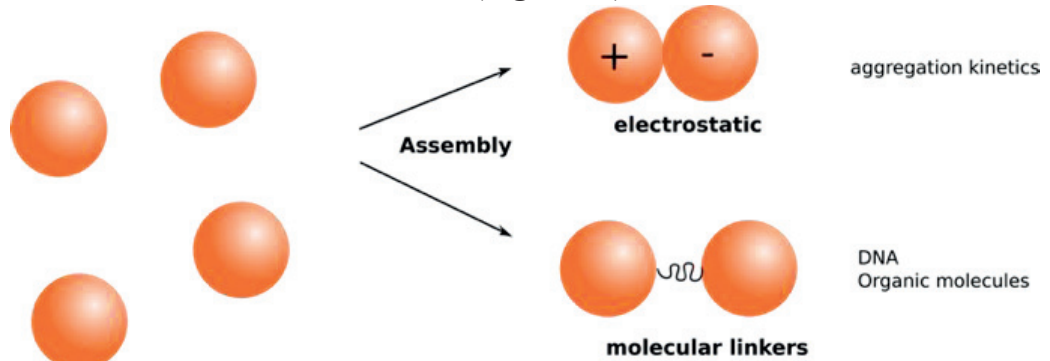


Figure 12: Schematic of the assembly of NPs via electrostatic interactions or with molecular linker molecules.

The assembly of Au NPs to discrete clusters by controlling the kinetics of aggregation caused by electrostatic interaction has already described by Turkevich *et al.*⁶⁵ in 1963. They studied the assembly of 20 nm citrate covered Au NPs by varying the salt concentration in solution, which allows the negatively charged particles to get closer to each other, or by changing the ratio between positively and negatively charged particles and/or playing with the coagulation times, they managed to control the assembly to aggregated NPs. They were able to achieve linear aggregates (see **Figure 13A**), when the repulsion of the negatively charged NPs was reduced in low ionic strength by partly neutralizing the surface charge. This early example of fine-tuning the balance between Van-der-Waals interactions of the particles and their electrostatic interaction through the charged ligand can be improved using more specific interactions, as shown in nature, using DNA and its complementary recognition features. Some pioneering work was demonstrated by Alivisatos *et al.*¹⁰⁶ and also by Mirkin *et al.*¹⁰⁷ around 1995, see **Figure 13B**, where complementary DNA strands are used to form NP assemblies. Furthermore, synthetic polymers can be used, as for example Rotello *et al.*¹⁰⁸ describes in 2000. Nanoparticles shrouded in non-polar alkane thiols have been subjected to place exchange with small amounts of thiols bearing functional units capable of forming strong hydrogen bonds with partnering thiolated nanoparticles bearing small amounts of reciprocated hydrogen bonding units (diaminotriazine-thymine).

Larger nanoconstructs were made in 2009 by the Alivisatos¹⁰⁹ group such as pyramids using DNA as a specific template to arrange NPs, see **Figure 13C**.

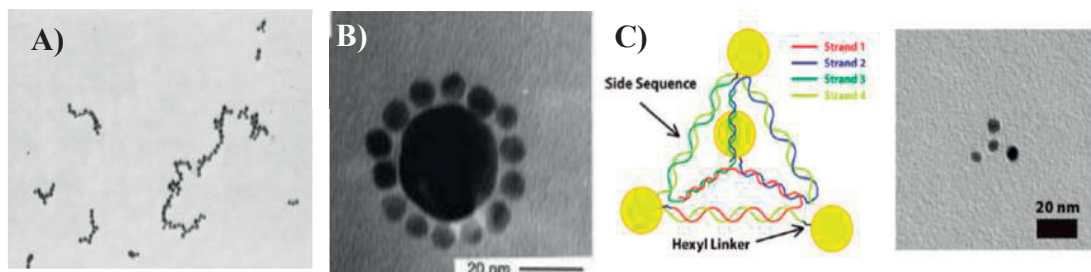


Figure 13: A) Linear aggregates of Au NPs via electrostatic and van-der Waals interactions (Reprinted with permission from reference⁶⁵ © 1963 American Chemical Society) B) specific interactions using DNA to assemble NPs(Reprinted with permission from reference¹⁰⁷ ©1998 American Chemical Society); C) Discrete pyramids of DNA assembling Au NPs (Reprinted with permission from reference¹⁰⁹ © 2008 American Chemical Society).

Our group is interested in the assembly of smaller structures, especially dimeric clusters, therefore in the following the focus will be more on what has been done to produce dimers.

1.4.1 Assembly of Discrete NP dimers

Au dimers were assembled by using DNA as a molecular linker as early as 1999 by Alivisatos and Schultz *et al.*¹¹⁰, see **Figure 14**. These structures are very interesting in terms of plasmonic applications, since they should have the so called hot-spot between the NPs and can be used for all types of plasmonic applications. Complementary sequences of single strand DNA (ssDNA) on each particle were used to selectively find each other. By modifying the length of the ssDNA the spacing between the NPs can be varied. DNA is flexible and can bend, which makes it difficult to assemble reproducibly dimers with the same fixed distance between the NPs.¹¹⁰ A few years later, in 2002, the same group could reach dimeric NPs with 80% yield by purifying the crude product with electrophoresis, but it was important here to have mono-functionalized NPs (only one DNA strand per NP) to obtain dimers with this approach.¹¹¹

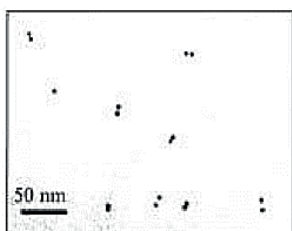


Figure 14: Dimeric Au NP assembly via DNA. (Reprinted with permission from reference¹¹⁰ ©1999 John Wiley and Sons)

Besides DNA, rigid organic molecules can be utilized to assemble NP dimers and these can overcome the issue of the varied spacing between the NPs. Highly π -conjugated phenyl-acetylenes could be used as bridging units, see **Figure 15**, leading to a yield of 30% of dimeric structures.¹¹²

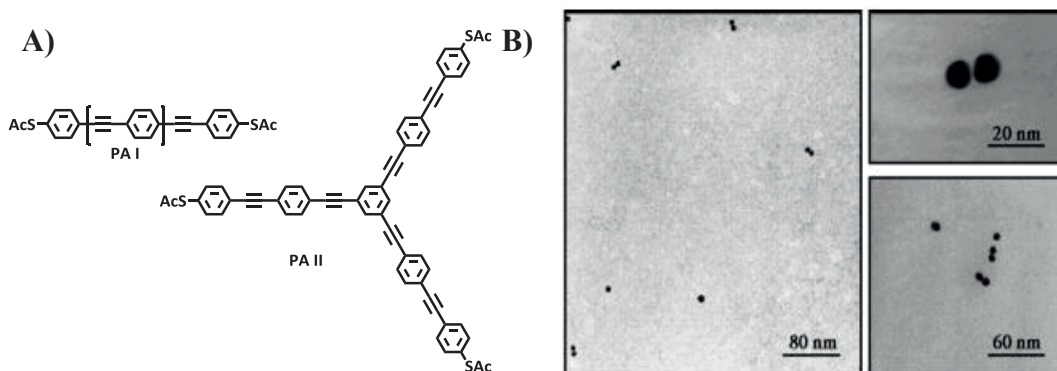


Figure 15:A) Rigid phenyl-acetylenes to build dimers (PA I) and trimers (PA II); B) TEM images of PA I bridges Au dimers. (Reprinted with permission from reference¹¹⁰ ©1999 John Wiley and Sons)

Another noteworthy example from Bar-Joseph *et al.*⁵¹ in 2005, is the use of thiolated conjugated organic molecules such as 4,4'-biphenyldithiol (BPD, fully conjugated), bis-(4-mercaptophenyl)-ether (BPE, conjugation broken in the center by the oxygen of the ether) and 1,4-benzenedimethanethiol (BDMT, broken conjugation near the contact

to the electrode) to measure differences in conductivity of a single molecule through an Au dimer, see **Figure 16A**. The dimers were obtained in a 50% yield, by using a large excess of Au NPs relative to the linker molecule.

A wide range of bifunctional molecules such as dithiols have been used to obtain NP dimers. Bjørnholm *et al.*¹¹³ used polyethylene glycol dithiol to combine Au seeds, which grow as dimers to linked Au nanorods. This appears to be an interesting way of integrating single-molecule linked nanoclusters in electronic devices. Another method is to mix two ligands, such as 4,4'-biphenyldithiol and ω -mercapto-alkanoic acid, to obtain dimers. The second linker, ω -mercapto-alkanoic acid, helped reducing the repulsion between two negatively charged citrate Au NPs.¹¹⁴

Mayor *et al.*^{115,116} were able to obtain “real” monofunctionalized Au dimers, by using a dendrimer, which wrap around one single Au NP, and bearing only one linker moiety. The linker is an acetylene, which undergoes dimerization *via* a copper catalyzed homocoupling and forms in this way the molecular bridge, see **Figure 16B**.

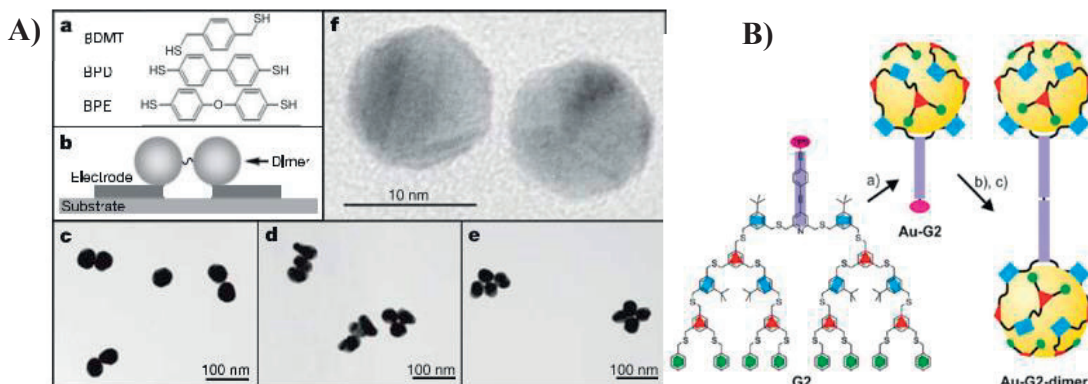


Figure 16: A) a)Structure of the molecules BDMT, BPD, BPE ; b) schematic of Dimer on electrode, b-f) TEM images of the dimers consisting of 50 nm Au; (Reprinted with permission from reference⁵¹ © 2005 Nature Publishing Group) B) Schematic on forming monofunctionalized Au dimers by encapsulating them with a dendrimer. (Reprinted with permission from reference¹¹⁶ ©2012 American Chemical Society)

The use of DNA as a molecular linkers is still prominent, as in the group of Bidault who uses it to study the optical properties of dimers, its application in SERS, or to learn about the distance dependency of dimeric structures and many more.¹¹⁷⁻¹¹⁹ Also Kuang *et al.*¹²⁰ presented a mercury (II) sensor using SERS from DNA conjugated nanostars. Another approach to form dimers is to asymmetrically functionalize NPs by immobilizing one part of the NP on a surface and functionalizing the other half. Sardar *et al.*¹²¹ reported the formation of dimers, due to immobilizing Au NPs on amine functionalized glass surfaces. The immobilized Au particles could be further functionalized with active linker molecules on the Au surface opposite of the glass and finally removed by sonication while a passivating thiol ligand (*e.g.* a thiol alkanol) is present to cover the newly generated naked NP side, see **Figure 17**. This so called Janus

NP can then react in solution with a second NP, prepared in the same manner but with a complementary functionality on the other Janus NP capable for instance of hydrogen bonding, *e.g.* carboxylic acid and amine, and form dimers see **Figure 17**.

A very similar study was published in 2011, which focused on the use of multivalent ligands. As mentioned earlier, especially monovalent thiol linkers are dynamic and therefore the asymmetric structure generated on the NP (Janus particle) might not be that stable. The authors mention that multivalent ligands are less dynamic and can keep

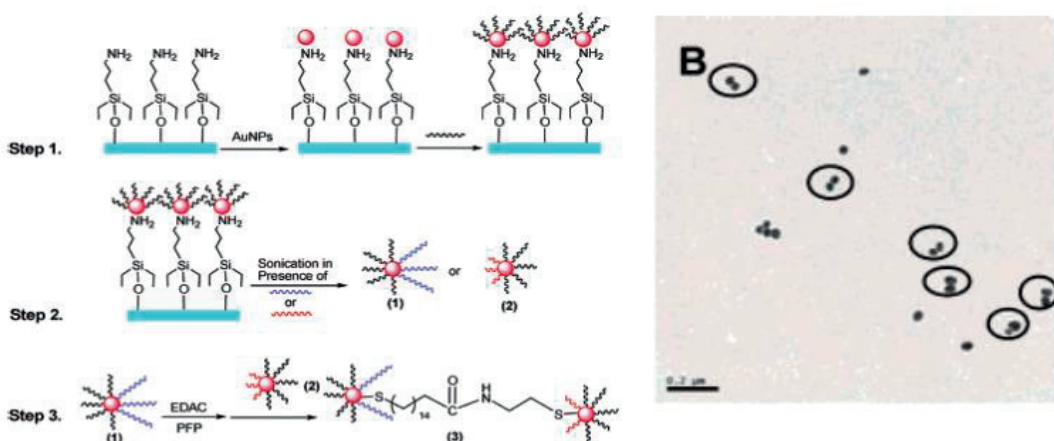


Figure 17: Au NP dimers due to asymmetric functionalization of the NPs on the surface. (Reprinted with permission from reference¹²¹ © 2007 American Chemical Society)

the locally confine functionalization better. Monovalent thiols might get exchanged or move on the surface and the regioselective functionalization might be lost. Here NP dimers were formed by a complementary regioselective functionalization with N-hydroxysuccinimide esters and amino functionalities, see **Figure 18**.¹²²

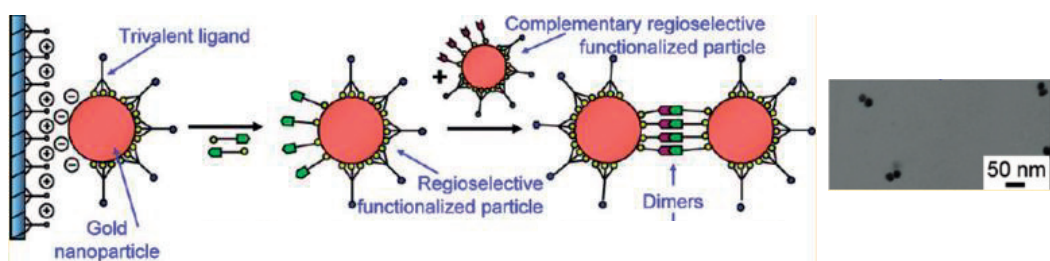


Figure 18: Formation of Au NP dimers via the binding of citrate Au NPs on amino silanized glass, the functionalization of the NPs with trivalent thiol ligands on the opposite site of the glass, isolating the NP off the glass with a specific functionalized linker and combine it in solution with a complementary regioselective functionalized particle to form dimers. (Reprinted with permission from reference¹²² © 2011 American Chemical Society)

By using bigger NPs (<50 nm), the risk of generating larger clusters of NPs than dimers increases, due to a higher degree of functionalization of ligands with linking units and therefore binding area, as shown by Yoon *et al.*¹²³, see **Figure 19C**. They prepare dimers with a 90% yield, by forming them directly on the surface by using a similar way as described before (see **Figure 19A**). Amino silane functionalized glass captures Au citrate NPs, the glass is desilanized to prevent the binding of a second citrate Au NP on the surface. The first NP is functionalized with a dithiol based molecular linker to bind specifically on top of it with a second NP, see **Figure 19A-C**.

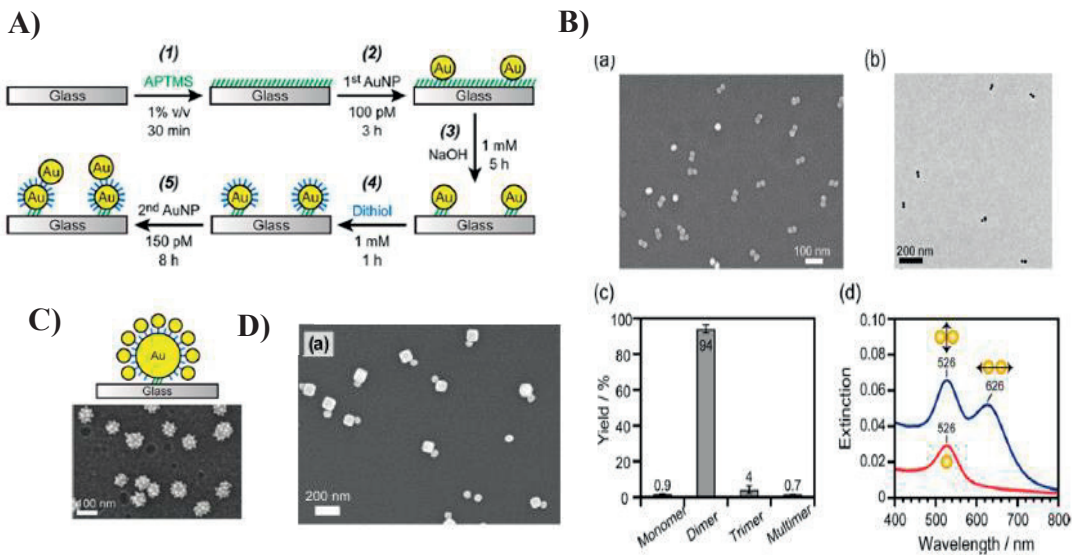


Figure 19: A) Schematic of the assembly: A amine functionalized glass surface captures Au NPs, the glass is desilanized, the Au NP functionalized with a dithiol which binds a second NP; B)a) SEM, b)TEM, c) yields, d) scattering spectra of Au (25 nm each) dimers linked by 1,8-octanedithiol; C) SEM of a Au (50 nm)- Au (12 nm) core-satellite assembly; (Reprinted with permission from reference¹²³ © 2014 American Chemical Society) D) SEM of a Au cube-Au sphere (Reprinted with permission from reference⁹⁷ © 2015 American Chemical Society).

In a follow up paper,⁹⁷ they follow step 1 and 2 as depicted above, immobilizing citrate Au NPs, but bind CTAB covered (positively charged) cubic particles as the second particle on the surface, see **Figure 19D**, heterodimers of cubes and spheres. The desilanization step (step 3, NaOH) is skipped, to keep the positive charge of the amine group on the surface, so that the positively charged CTAB particles are repelled and bind just specifically via the molecular linker on the first NP to the particle. The solvent acetonitrile can be used in the assembly to disintegrate the CTAB bilayer regioselectively on the vertices and edges, which results in binding of the molecular linker at the edges and connects them to the spheres on the glass surface.⁹⁷

1.4.2 Purification of Assembled Structures

As described above, dimers can be assembled in numerous ways, either electrostatically or with molecular linkers, symmetrically in solution or asymmetrically on surfaces. If not produced on a surface, a purification method is usually required, to obtain a quality sample of dimers.

Electrostatics is used to assemble NPs seen in a report of Chen *et al.*¹²⁴ They fine-tune the electrostatic interaction by inducing aggregation upon the addition of HCl. In order to purify the assemblies, they need to be stabilized by isolating them in a diblock copolymer (polystyrene₁₅₄-block- poly(acrylic acid)₆₀)(PSPAA) in DMF/H₂O. Prior to the encapsulation a thiol-ended hydrophobic ligand is used to bind on the citrate Au NPs to allow the particles to connect with the diblock copolymer. By using a CsCl solution gradient to microcentrifuge the assembly, a high purity of discrete nanoaggregates (95%) can be separated in well resolved bands containing single particles, dimers or trimers, see **Figure 20**. This method of purification is called differential centrifugation and used in different forms by other groups as well.

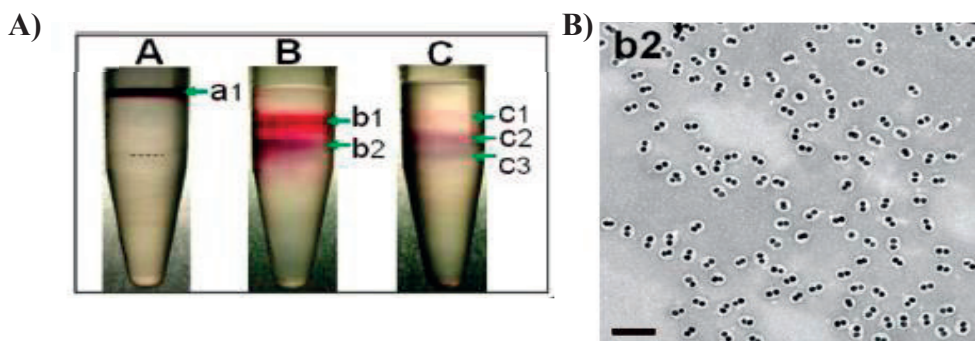


Figure 20: A) Differential centrifugation in 62% and 11% CsCl and encapsulated Au-NPs in PSPAA, B) TEM image of the fraction b2 resulting in dimers (Reprinted with permission from reference¹²⁴ © American Chemical Society).

A similar method was described by Whitesides *et al.*¹²⁵ in 2012, which is based on a density gradient centrifugation. They demonstrate the separation of nanoparticles of different shapes and sizes without applying high ionic strength unlike the method by Chen *et al.*¹²⁴ with CsCl and therefore the need to encapsulate them, stabilize them within a polymer dispersion is omitted. Here, a three phase system consisting of molecules and polymers (such as sucrose, Ficoll, Brij) with different densities, can separate rods from nanospheres and larger particles, which are products from a Au nanorod synthesis. This zonal centrifugation uses the differences in hydrodynamic behavior to separate the different particles. Three different zones with three different viscosities in the same medium are layered on top of each other, to collect NP in narrow regions according to their hydrodynamic behavior.

Another successful purification method, which has been widely used, since the first dimers were reported, is gel electrophoresis. Here, charged NPs migrate in a gel under

the influence of an electric field. Depending on the size and the charge of the NPs the migration behavior differs and can therefore be separated. By using ssDNA to assemble nanoparticle dimers, Alivisatos *et al.*¹¹¹ managed to separate dimers with electrophoresis, already in 2002. The group of Bidault also extensively employs electrophoresis to separate assembled dimers from other aggregates. In 2012 they presented a 90% yield in DNA assembled dimers, which can reversibly switch the interparticle distance. They do so by using a DNA template with a loop, which folds by itself forming a small gap between the dimeric particles, or the DNA loop hybridizes with additional DNA strands in the surrounding to achieve a big gap in between the NPs¹¹⁸

1.4.3 Assembly of Heterodimeric Structures

Most of the aforementioned instances, are concerned with the assembly of homodimers, more specifically of Au NPs due to their inertness, optical properties and the wide range of possible applications. Nevertheless, Ag NPs have also been used to form dimers, despite greater oxidative sensitivity. They show a very similar surface chemistry to Au and can be treated in much the same way. Therefore, Au-Ag or Ag-Ag dimers are often produced in the same manner as described above.

The assembly of heterodimers between metal and metal oxides have not been extensively studied, since their surface chemistry is very different and other methods must be used to assemble them, as opposed to the described “simple” electrostatic approach or using molecules such as dithiols as linkers. Despite these challenges, some examples have been reported.

Crut *et al.*⁴⁰ reported the assembly of hybrid nanoclusters between Au NPs and core shell Ag@SiO₂ NPs, see **Figure 21D**. The Ag@SiO₂ NPs were positively charged through polyelectrolytes and interact electrostatically with the negatively charged Au NPs. Au-TiO₂ NPs were assembled by Chen *et al.*¹²⁶ by transforming hexanethiolated Au NPs in toluene into Janus particles using a water surface with hydrophilic ligands on a Langmuir-Blodgett trough. The hydroxyl functional groups of the NPs were used as anchoring groups to grow TiO₂ NPs in a sol-gel process. Chen *et al.*¹²⁷ used nanoscopic phase separation of different metals to form dimers, see **Figure 21A**. Pietryga *et al.*¹²⁸ showed a general way to assemble quantum dot-dielectric-metal hybrids. A silicon shell on top of the metal structure is used to attract the quantum dots, see **Figure 21B**. Zhang *et al.*¹²⁹ present the synthesis of Au nanorods on AgCdSe seeds, see **Figure 21C**.

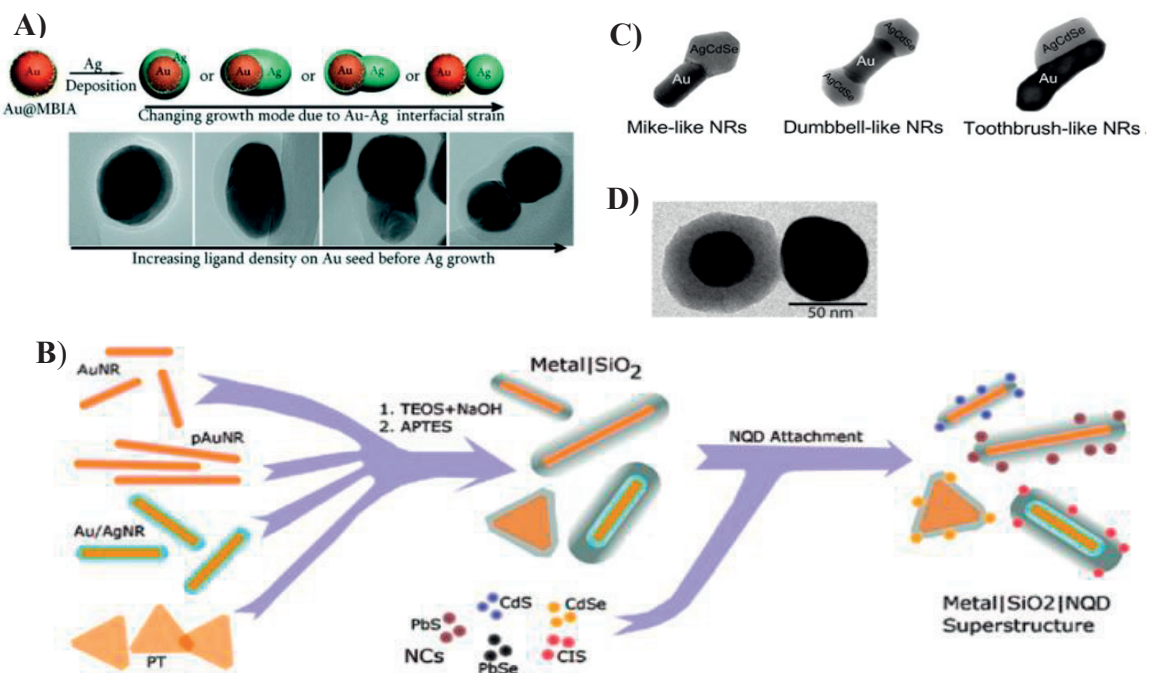


Figure 21: A) Nanoscopic phase separation to form Au-Ag hybrid nanoclusters (Reprinted with permission from reference¹²⁷ © 2012 American Chemical Society); B) Quantum dots on Au structures via a silicon shell (Reprinted with permission from reference¹²⁸ © 2012 American Chemical Society); C) AgCdSe –Au hybrids (Reprinted with permission from reference¹²⁹ © 2012 American Chemical Society); D) Au-Ag@SiO₂ hybrid materials (Reprinted with permission from reference⁴⁰ © 2013 American Chemical Society).

This quick overview demonstrates, that there exist examples of heterodimer assemblies, however these have not been studied to the same extent as the homodimers and are not as straight forward to achieve and/or applicable to a broad spectrum of particles.

The assembly of homo- and heterodimers is still a growing field, with room for improvement. Further homo-and heterodimers have many possible applications, as described in **Chapter 1.5**, making these topics relevant for us to work on as well.

1.5 Applications of nanostructured clusters

The special optical properties of metal NPs, on the account of their very specific localized surface plasmon resonance (LSPR), introduced in **Chapter 1.2**, give rise to a wide range of applications, such as imaging and detection in the fields of biology and medicine,^{130,131} or even catalysis.¹³² To quickly reiterate, the LSPR depends on the dielectric property of the surrounding of the NPs as well as their composition, size and shape. Furthermore, by combining two NPs a red shift of the LSPR is expected as well as a change in the peak appearance. The electrical field in the gap, hot spot, is expected to be enhanced. These specific features of the LSPR allow us the use of plasmonic NPs for many applications. By varying the composition, the size, the shape of the NPs and/or by putting e.g. molecules in the hot spot between two NPs, the LSPR changes or gives an amplifying effect in for example the Raman signal of molecules, the absorption, the catalysis of reactions and many more.

A change in the surrounding medium can be detected by the plasmonic particle, or better by its LSPR. This property can be used for indirect nanoplasmonic sensing, which is schematically shown in **Figure 22**. Some metal NPs such as Pd don't have a strong LSPR signal and a reaction on their surface, for instance hydride formation (PdH), coming about from hydrogen absorption onto Pd NP, expands the lattice of the palladium and changes its volume, can barely be seen in the scattering spectra, **Figure 22A**. By placing another metal with a strong LSPR signal in the close proximity of the Pd NP, such as Au, which is sensitive to its surroundings, allows the hydride formation on a Pd NP to be probed by examining the LSPR shift ($\Delta\lambda$) of the plasmonic NP, see **Figure 22B**.^{27,41,133,134}

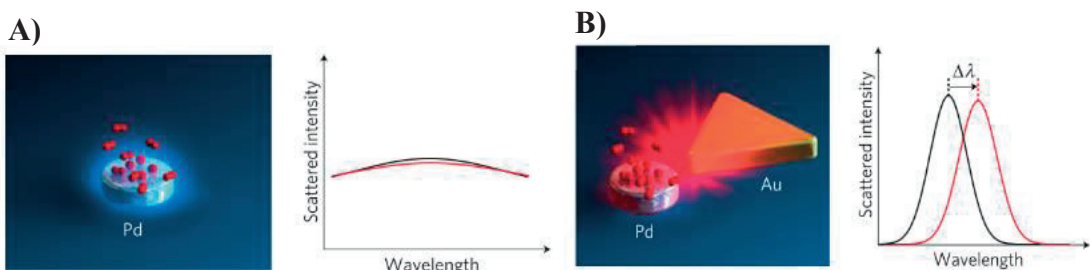


Figure 22: Schematic of indirect sensing of hydrogen by a Au nanostructures, A) Hydrogen molecules and hydrogen atoms (red) absorb on palladium, which induces a little shift in the scattering spectrum; B) Hydrogen sensing by a resonant antenna-enhanced scheme. Pd NP placed at the nanofocus of a gold antenna; scattering spectra shows strong resonance shift ($\Delta\lambda$) a lot, due to the change in the dielectric function (Reprinted with permission from reference¹³³ © 2011 Nature Publishing Group).

These nanostructures can be on top or side-by-side and manufactured in different ways such as double electron-beam lithography in a combination with a double lift-off procedure,¹³³ or by hole-mask colloidal lithography,¹³⁴ see **Figure 23**. Our work (paper **VII**) describes a new approach to achieve this indirect sensing of hydrogen absorbed

onto Pd NPs with dimers assembled in solution on a single particle level, see details in **Chapter 3.1.2**.

Plasmonic shifts of dimeric structures depend strongly on the distance between the particles, which allows the use of dimers as plasmonic rulers. This principle makes it possible to measure biomolecular distances,^{135,136} or to detect molecules, for example, molecular linkers between dimers, which can change conformation on the account of binding.¹³⁷

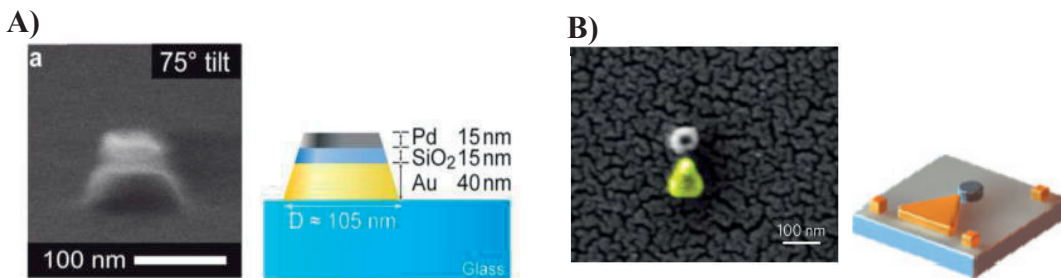


Figure 23: A) ESEM image and schematic depiction of an approx. 40 nm high truncated Au nanocone with a nominal base diameter of 105 nm, covered by a 15 nm SiO₂ spacer layer and a Pd particle with the dimensions of 75 nm x 15 nm on the tip (Reprinted with permission from reference¹³⁴ © 2011 John Wiley and Sons); B) SEM image schematic of a single palladium- Au antenna (Reprinted with permission from reference¹³³ © 2011 Nature Publishing Group).

The enhanced field in a gap makes NP dimers suitable as optical antennas, for coupling light to molecules. This can enhance the Raman signal from adsorbed molecules, which allows even single-molecule sensitivity.^{138,139} The fluorescence,¹⁴⁰ absorption,¹⁴¹ light-harvesting properties in dye-sensitized solar cells,¹⁴² and other properties can also be enhanced due to the strong electromagnetic field.

By combining two or more materials, the selectivity as well as the activity of a catalyst can be increased compared to the pure catalytic compound.^{143–146} The assembly of heterodimeric structures is undoubtedly a growing field.

Finally, I want to mention the assembly of proto-devices with single molecules based on colloidal nanoparticles, which is a big topic in single molecular electronics. Some examples were already mentioned earlier, such as Bar-Joseph *et al.*⁵¹, which is one of the first examples in this field at all, in which they studied differences in conductivity of molecules between a dimer; or an example from Bjørnholm *et al.*¹¹³, in which assembled nanorod dimers were placed between electrodes. In addition, more advanced structures based on antibodies can be used to connect to gold nanoparticles and form a “protein transistor”, see **Figure 24**.¹⁴⁷

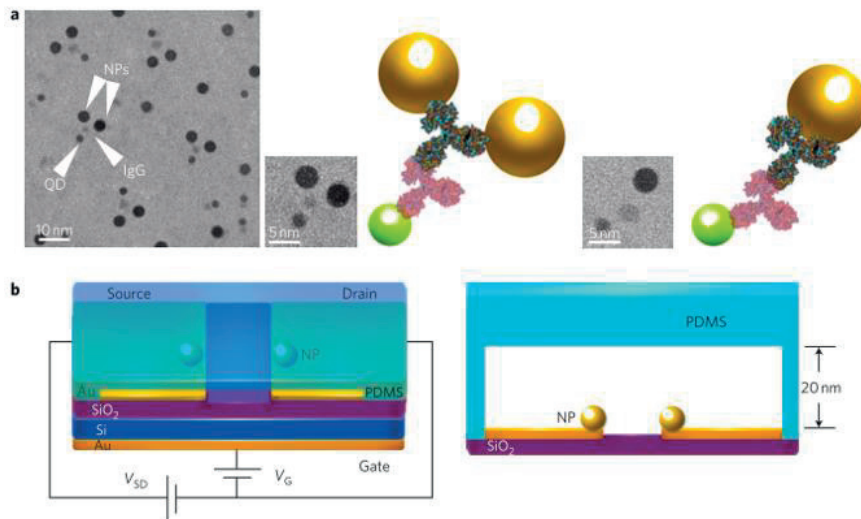


Figure 24: a) Au dimers are connected by a IgG antibody, which also binds a quantum dot (left) or Au monomer binds the antibody and its conjugated quantum dot (right), b) schematic of the protein transistor (Reprinted with permission from reference¹⁴⁷ © 2012 Nature Publishing Group).

Single molecular electronics is a growing field and requires exactly the discussed dimeric structures, and there is a need for improvement in terms of yields, reproducibility and, monodispersity of the particles, and a universal accessibility.

1.6 Thesis Outline

The background chapter visualizes the complexity of the assembly of nanoparticles, either in solution or on surfaces. Many building blocks are involved here, such as the synthesis of the nanoparticles and its stability, the formation of dimeric structures and its purification in order to achieve high purity samples. Additionally, the synthesis of the molecules binding to different type of materials for the assembly of discrete clusters as well as allowing such particles to assemble on surfaces are a key focal point of this thesis. Furthermore, the functionality of the assembled structures needs to be proven to enable the system to be used for certain purposes.

Many of the discussed issues are kept in mind in our research questions: how can self-assembly of these well studied nanostructures be controlled to create new or better properties? Can we combine top-down and bottom up approaches to assemble nanostructures for devices? How can new functions of nanoparticle assemblies be achieved and analyzed?

The following **Chapter 2** and **3** describe the synthesis of linker molecules, nanoparticles, the assembly of dimeric nanostructure clusters as well as its usage for biosensing, as well as a hydrogen sensor.

2

Design of Molecular Linker for Metal Nanostructures

From Synthesis to Application

2.1 Molecular Linker

Molecular linkers are an important tool for the self-assembly of NPs on metal surfaces or for the assembly of discrete NP clusters. As described in **Chapter 1**, each type of metal surface shows a different affinity for specific anchoring groups, e.g. Au forms strong covalent bonds with thiol anchors. Both, functional gold surfaces and Au NPs hold interest in many applications, such as electronics or the field of plasmonics, and in these instances mostly thiol based anchor groups are used. Self-assembled monolayers (SAMs) are widely used in for example STM measurements (see **Figure 11**) to measure *e.g.* the conductance of a single molecule. Conductivity has been measured on single molecules in SAMs and for that matter also in break junction but placing between the NPs may allow for the possibility of arranging these units in an ordered ensemble for a device by for example the aid of lithography. The ability of these molecular linkers to assemble on surface but also connect NPs to it or connect NPs with each other, makes them an import tool for our work.

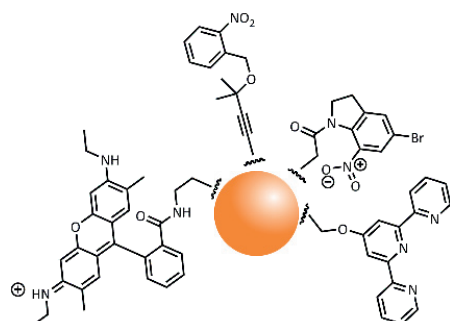


Figure 25: Schematic summary of this Chapter, visualizing the use of different molecular linker molecules for metal surfaces and nanoparticles.

In this chapter I am going to introduce some interesting linker molecules that we synthesized in order to answer several unanswered questions in the field of coordination chemistry (**Chapter 2.1.1.**) and the strong coupling between NP plasmons and organic dyes (**Chapter 2.1.2.**) giving rise to changes in the optical properties. Furthermore, we

demonstrate the application of a photo-labile molecular linker for biosensing (**Chapter 2.2.1.**), as well as the development of new, very specific molecular linkers for photo induced reactions (**Chapter 2.2.2.**), see **Figure 25**.

2.1.1 Terpyridine Linker assembled on Surfaces to Measure the Strength of its Complexes with Heavy Metals (paper II)

The nature of metal-ligand interactions is a fundamental aspect of coordination chemistry, which became a rapidly growing field around 1890.^{148,149} Interestingly, transition metal complexes play a big role in chemistry, biochemistry, protein science and catalysis.¹⁴⁹ The character of a bond between a transition metals and neutral ligands is a so called coordinative bond, which is mostly a dipolar, covalent bond or a dative covalent bond. The full understanding of electronic interactions between ligand and metal is complex and still is the subject of many investigations. Therefore in fact, the study of ligand substitution reactions is an important aspect of transition metal complexes and especially pertinent to the field of catalysis. This is notable in palladium catalyzed C-C bond forming reactions such as Sonogashira, Suzuki, Stille, Heck and in the case of nickel, Kumada reaction, just to mention a few examples. Most experimental work about the kinetics of the association/dissociation of metal complexes as well as their energies and enthalpies are done by ensemble measurements of a host of molecules. This work was therefore instead focused on determining the strength of a metal-ligand complex coordination by measuring a single metal-ligand interaction.

For this interdisciplinary study, the design of a molecular linker, which has a greater metal linker interaction than the coordinative bonding force of a transition metal complex, was required. This would allow to study the strength of the coordinative bond. The design of the molecular linker also needs to be equipped with functionality to bind to a gold surface, by *e.g.* a thiol group, which has a bonding force to Au of around 2 nN, and furthermore coordinate a metal ion of interest.^{150,151}

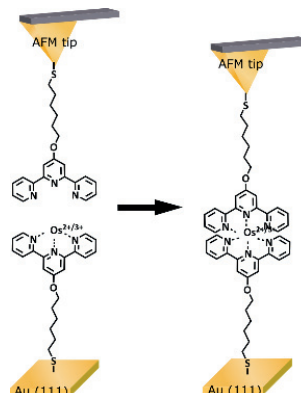
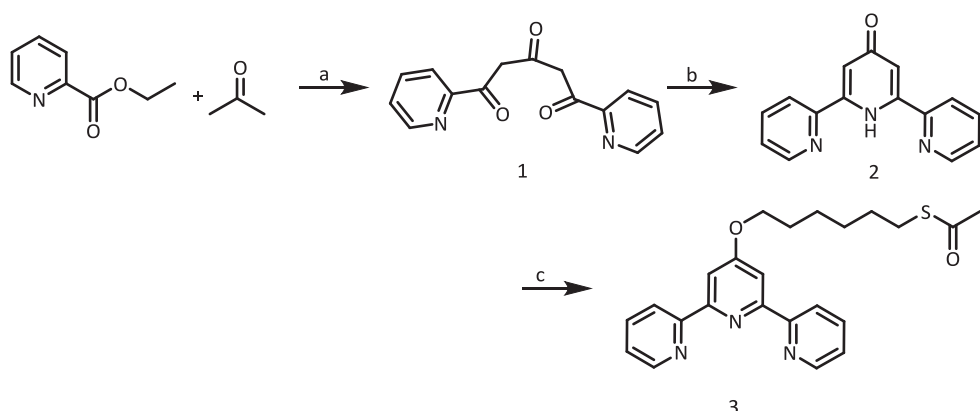


Figure 26: Schematic of the study of the coordinative bonding force of a transition metal complex; molecular linker binding on Au surface or on a gold tip.

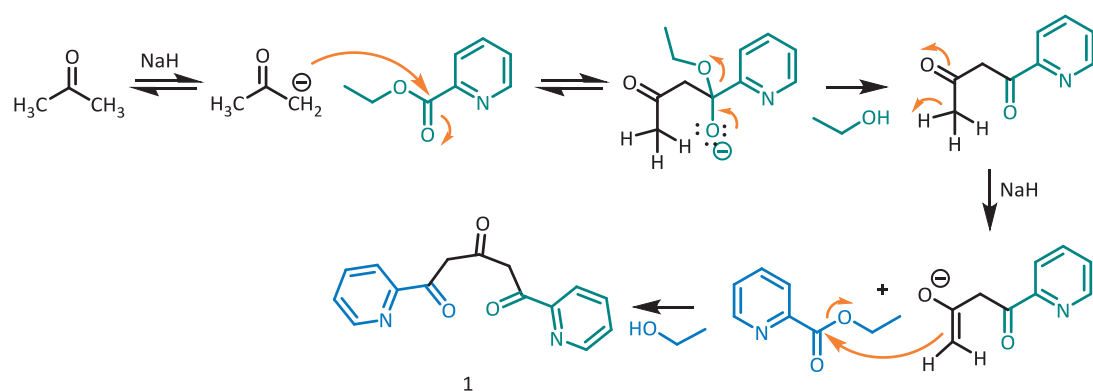
The idea was to use an electrochemically controlled atomic force microscope (EC AFM) to analyze the single molecule force, see **Figure 26**.

A *N*-heterocycle, 2,2':6'2''terpyridine, seemed to be a great candidate here. Terpyridine shows a high affinity towards transition metal ions. Therefore, a terpyridine with a thiol anchor moiety (compound 3) was synthesized, by the following procedure:



Scheme 1: Synthesis of the terpyridine thiol anchor. A) NaH, DME, reflux, 6 h; b) EtOH, NH₄Ac, reflux, 1 h; c) S-(6-bromohexyl)ethanethioate, K₂CO₃, DMF, 70°C, 12 h.²⁰⁸

Firstly, acetone reacts in a two-fold Claisen condensation reaction with ethyl picolinate. The Claisen reaction results in the formation of a new carbon-carbon bond by reacting two esters or as here an ester and another carbonyl compound, such as a keton. After the deprotonation of the acetone in the presence of a strong base, sodium hydride (NaH), the carbanion (keto-enol tautomer) can react with the electrophilic ester of ethyl picolinate, firstly giving a tetrahedral intermediate followed by the expulsion of ethoxide leaving group. Ethoxide acts as to deprotonate this intermediate and facilitate the attack on a second ethyl picolinate, see **Scheme 2**, to form a dipicryl triketone, compound 1.

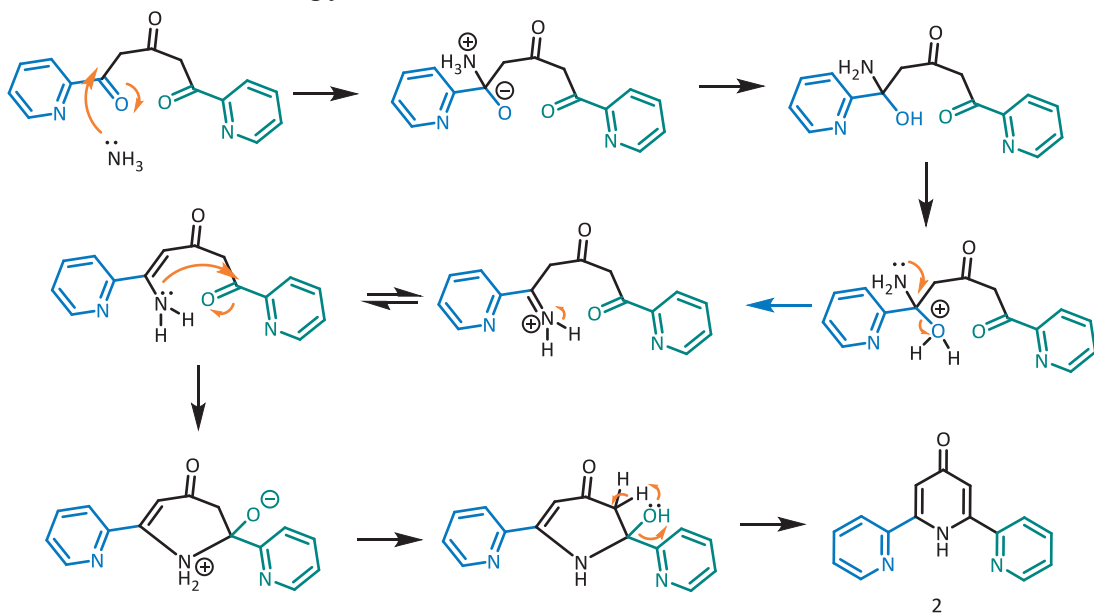


Scheme 2: Reaction mechanism for the formation of terpyridine, part A. Claisen reaction between ethyl picolinate and acetone.

Compound 1 can react two times with ammonium acetate (from the equilibrium between ammonium acetate and ammonia and acetic acid) *via* a nucleophilic attack of

the ammonia to a terpyridine unit, compound 2, see **Scheme 3**, similar to the Hantzsch pyridine synthesis.¹⁵² Firstly, ammonia can condense with the ketone and the acetic acid assist with the proton transfer giving an imine/iminium which can tautomerize to give the enamine. The driving force is the formation of an extended π conjugated system in the enamine form. The lone pair nitrogen can facilitate an intramolecular condensation resulting in the formation of the heterocycle, pyridinone, compound 3.

During the first nucleophilic attack one carbonyl is transformed into an imine, which is in an equilibrium with its enamine (imine-enamine tautomer), and the carbonyl is eliminated by condensation. This ester enamine reacts intramolecularly with the other ketone and forms the terpyridine under condensation.



Scheme 3: Reaction mechanism for the formation of terpyridine, part B. According to Hantzsch pyridine synthesis, formation of a pyridine out of a diketone.

The final step, shown in **Scheme 1**, involves the attachment of the anchoring group through the oxygen atom to the terpyridine. This can be made possible by subjecting the pyridinone with base, deprotonating the amine. The negative charge is delocalized sharing the charge with the oxygen atom, which is then capable of behaving as a nucleophile with S-(6-bromohexyl) ethanethioate in an $\text{S}_{\text{N}}2$ reaction. Furnishing the desired terpyridine, compound 3.

Terpyridine can form transition metal complexes with many transition metal cations, including ruthenium(II), zinc(II), manganese, iron(II) and copper(II).¹⁵³ In these instances, two terpyridine units are capable of coordinating to a cation, which possesses an octahedral geometry. In order to investigate the strength of the bis terpy metal complexes, AFM was employed as the tool to gauge this. Organic linker containing one terpy unit was attached to a gold surface, likewise the same molecule was attached to the gold tip of the AFM. If one ion, in this case osmium, was introduced to either the

tip or the flat surface (II and III in **Figure 27A**) and the tip is brought close to the surface gave the bis terpy complex, a coordinative bond force between the osmium and two terpyridine is measured as a force peak feature of 100 pN (see **Figure 27B**). The AFM measurements were performed by Qijin Chi's group at DTU Denmark.

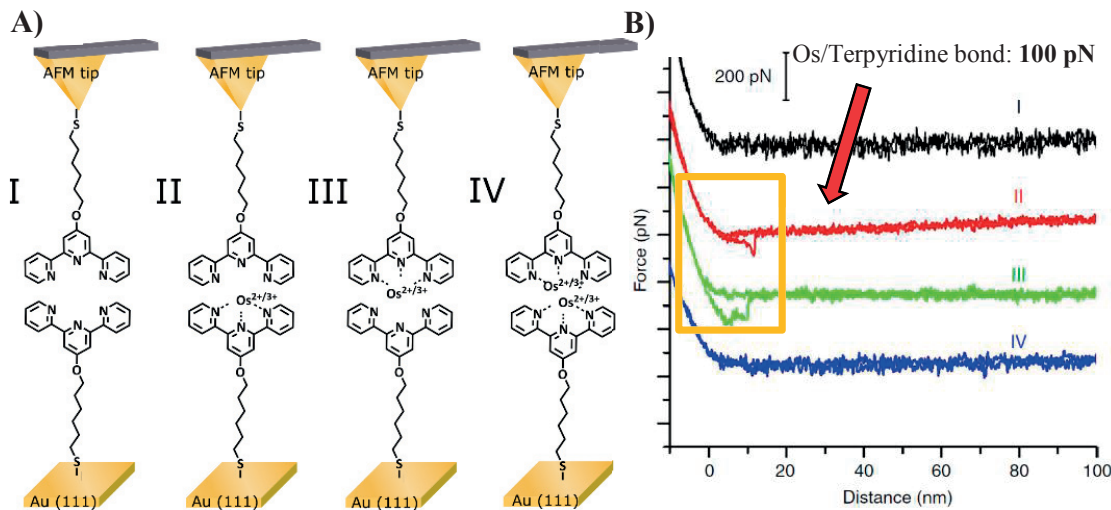


Figure 27: A) Schematic of the four experimental set ups: I: no Os on Au surface, II: Os pre-bound on Au surface, III: Os pre-loaded on AFM tip, IV: Os pre-loaded on tip and surface; B) Force-extension curves for the four set ups. B is reprinted with permission from reference²⁰⁹ (paper II) © 2013 Nature Publishing Group.

By coordinating the ion on both sides, no coordination bond can be measured, since all binding sites are already saturated, **Figure 27A, IV**.

Several hundreds to thousands force-distance curves for the four different experiments, shown in **Figure 27A**, were measured to obtain a statistical analysis for the determination of the bonding strength. Single force peaks as shown in **Figure 27B** suggest that the coordination comes from a single bis terpy osmium complex in the junction. Around 5-8% of the experiments showed multiple peaks due to multiple terpyridine molecules interacting with the surface.

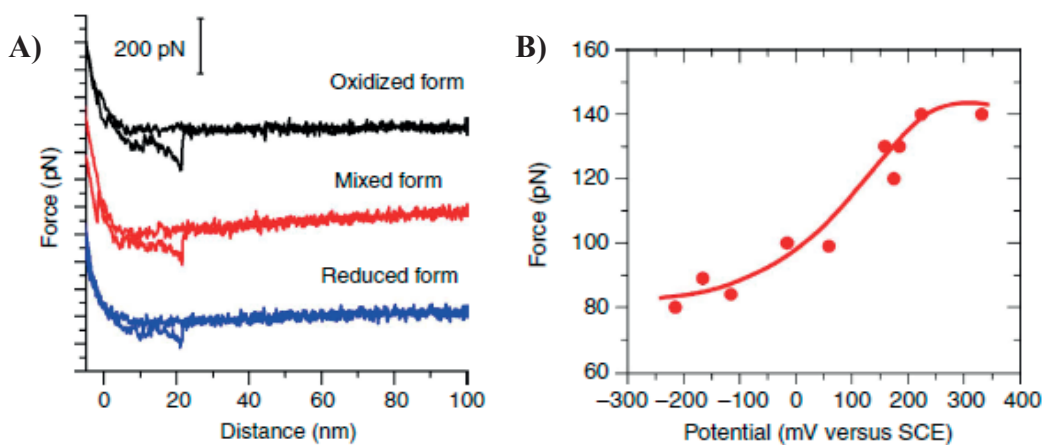


Figure 28: A) Force-extension curves at different potentials from fully oxidized to partially reduced and fully reduced osmium ion; B) The average unbinding force depending on the redox states controlled by the electrochemical potential. Reprinted with permission from reference²⁰⁹ (paper II) © 2013 Nature Publishing Group.

Furthermore, the redox state of the central metal atom has an impact on the metal-ligand interaction, which can be controlled by using an (electrochemical controlled) EC AFM. The coordination force can be measured while controlling the oxidation state of the metal, by applying different electrochemical potentials. Upon full oxidation of osmium, an average force of 130 pN can be measured. 100 pN is measured when the Os ion component was partially reduced ($\text{Os}^{2+/\text{3}^+}$) and the force was further lowered to 80 pN by fully reducing it, see **Figure 28**. The force to break the Au-S bond is with around 2 nN, higher than the measured bonds.

This technique makes it possible to look not only at other metal cations such as zinc, manganese, iron, which can have different redox states, but this can also be used to examine the relative strengths of metals with differences in binding sites (single to multiple binding). Furthermore, external factors influencing the binding force can be studied.

2.1.2 Rhodamine Linker Assembled on Gold Nanostructures to measure Strong Coupling (paper VIII)

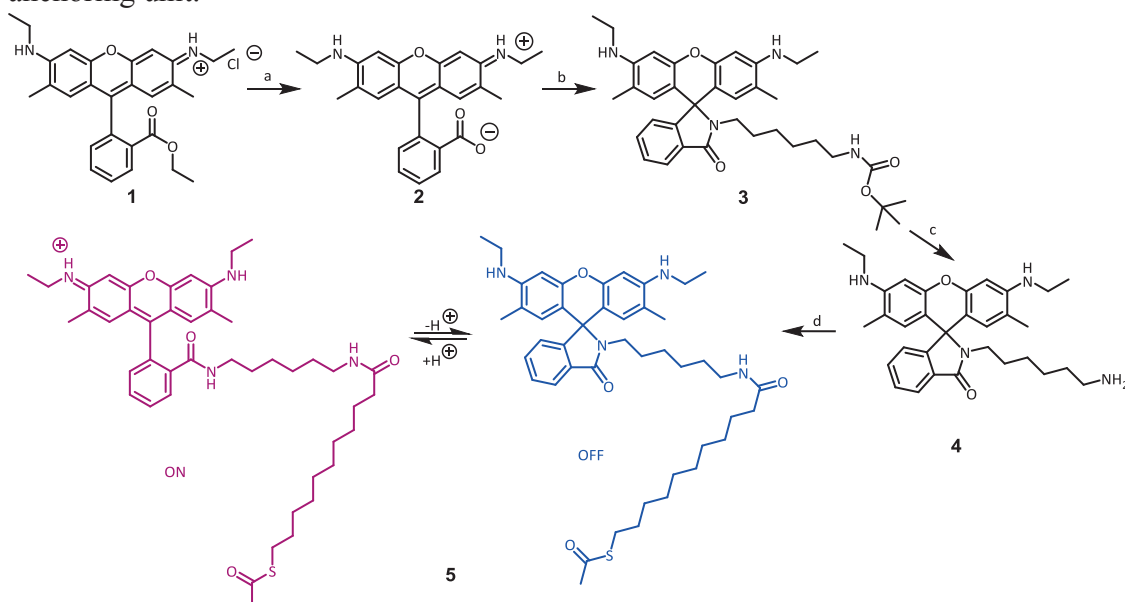
Due to the special optical properties of noble metal nanostructures, produced via top-down or colloidal NPs *via* bottom-up, as introduced in **Chapter 1**, many possible applications can be envisaged. One field is the interaction of metal nanostructures with dye molecules. Indeed, the LSPR of a metal nanostructures can in fact couple with the resonance of a molecule resulting in properties suitable for many applications, such as enhanced fluorescence, absorption, enhanced light-harvesting, SERS, just to mention a few. Another example of exploiting the coupling of LSPR of metal nanostructures and molecules is strong coupling, which is the coupling of a plasmon of the nanostructure with an exciton of an excited dye. This field is a more fundamental research field, but also interesting in terms of quantum optical applications. To achieve a strong coupling regime, the nanostructure and the dye must be adjusted in many parameters such as spectral overlap,¹⁵⁴ mode volume,^{155,156} the oscillator strength,^{157–159} number of molecules attached to the nanostructure,¹⁶⁰ and the positioning and orientation of the attached molecule.¹⁶¹ Strong coupling of a unified plasmon and molecule forming a hybrid, a coupled plasmon-exciton, means that molecules could influence the NPs plasmon or *vice versa*. This phenomenon can be seen as spectral “dips” in absorption or scattering spectra. We show here that very high concentrations of the molecular linker attached to plasmonic structures results in strong coupling, however lower surface loading show small scattering dips which are due to a surface enhanced absorption and not due to strong coupling.

To best study the plasmon-exciton interaction, required a dye with the following properties: photostability, good solubility, high fluorescence quantum yield and an absorption band overlapping with an available laser wavelength. As the dye was to be attached to NP, functionalization with a strongly binding anchoring group was also necessary to ensure a high loading on the nanostructure.

A commonly used dye is rhodamine 6G (R6G), which fulfills all these requirements, even though it has a relatively weak transition dipole moment of $\mu_{R6G} = 1.74$ Debye. It was of interest to see what concentrations were necessary to achieve a strong coupling. Molecules with strong transition dipole moments can easier reach a strong coupling regime, such as certain J-aggregates of different dyes.¹⁶² Furthermore the absorption of R6G overlaps well with the Ar⁺ line (514.5 nm) and the Nd:YAG (2nd harmonic 532 nm) laser. To allow it to self-assemble on nanostructures, we modified the dye and synthesized a derivative with a thioacetate group, which was capable of anchoring strongly to gold *in situ*.

All prior published work in this field used unspecific adsorbed ordinary rhodamine 6G (R6G) molecules, a novelty is therefore to use the derivatised R6G capable of self-assembling on noble metal based nanostructures, which in turn enabled observation of strong coupling.

Starting from the commercially available R6G (**Scheme 4**, compound 1), the ester functionality was hydrolysed under strongly basic conditions to the free carboxylic acid ((**Scheme 4**, compound 2) and then coupled using HBTU (2-(1H-benzotriazol-1-yl)-N,N,N',N'-tetramethylaminium hexafluorophosphate) and base DIPEA (diisopropylethylamine), with tert-butyl (6-aminohexyl)carbamate (**Scheme 4**, compound 3). These are typical peptide coupling conditions, which can be performed at room temperature and this reaction went in almost quantitative conversion. The BOC (tert-butyloxycarbonyl) protecting group was conveniently removed under acidic conditions (TFA (trifluoroacetic acid) (**Scheme 4**, compound 4)) and the liberated amine further coupled under peptide coupling conditions (DMAP (4-(N,N-Dimethylaminopyridine)) and EDC (1-Ethyl-3-(3-dimethylaminopropyl)carbodiimide)) with 11-(acetylthio)undecanoic acid, **Scheme 4** step c and d compound 5. In this way we synthesized a R6G, both with a long alkyl chain bridging between the dye and the anchoring unit.



Scheme 4: Synthesis of the R6G thiolated molecular linker. a) NaOH , EtOH , 95°C , 7 h; b) HBTU, DIPEA, RT, 1.5 h; tert-butyl (6-aminohexyl)carbamate, RT, 12 h; c) TFA, DCM, RT, 12 h; d) 11-(acetylthio)undecanoic acid, DMAP, EDC, DCM, RT, 4 h; rhodamine, RT, 16 h.

As can be seen in **Scheme 4**, protonation or deprotonation of the rhodamine core results in a fluorescence (purple in scheme) and non-fluorescence (blue in scheme) rhodamine dye, which can be switched back and forward. This opening and closing to a spirolactam form of the rhodamine dye can be observed in UV/Vis as well as fluorescence of the two forms, as depicted in **Figure 29**.

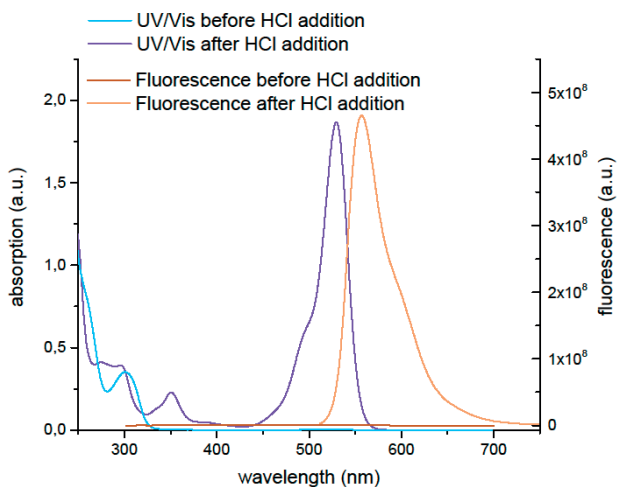
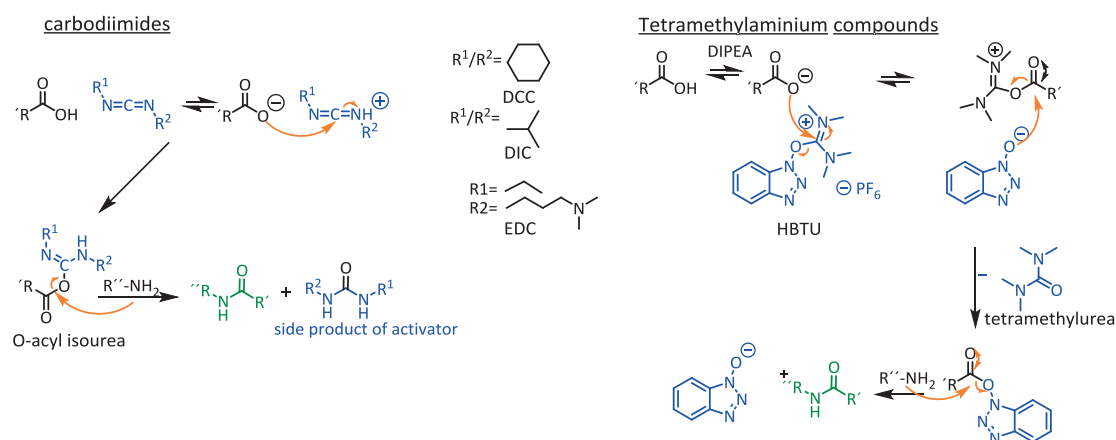


Figure 29: UV/Vis and fluorescence spectra of the fluorescent and non-fluorescent R6G. Upon the addition of HCl the spirolactam ring opens and R6G becomes fluorescent.

The main reaction steps to the thiolated R6G (compound 5) are peptide coupling reactions, in which amide bonds between amines and carboxylic acids are formed, in a condensation reaction. In peptide synthesis mild conditions and high yields are crucial, therefore activation of the carboxylic moiety is achieved firstly by reacting it with an activating reagent to form a reactive intermediate, usually an activated ester, here in **Scheme 4** and o-acyl iso-urea. During the second step, an acylation of the amino group, the intermediate is attacked by the amine, as a nucleophile.

We used two different activators, the more traditional, water soluble EDC, which is one of the more widely used carbodiimides (EDC, DCC, DIC and others), and a coupling agent from the family of the tetramethylaminium compounds, HBTU hexafluorophosphate salt. Others could be TBTU the analog tetrafluoroborate, or HATU and TATU, the azobenzo derivatives, in which a base has to be present. The coupling mechanisms for both reagents can be described as depicted in **Scheme 5**.



Scheme 5: Mechanism of the condensation reaction between carboxy acids and amines activated by carbodiimides (left) and tetramethylaminium compounds (right).

The thiolated R6G as well as the ordinary unmodified R6G were adsorbed onto 80 nm Ag structures in pure methanol as well as in methanol: water mixtures as depicted in **Figure 30**. The SEM images of the Ag nanodiscs, as well as photographs and dark-field images of all the samples are shown in **Figure 30**. The Ag nanostructures were chosen to match the spectral properties of the dye.

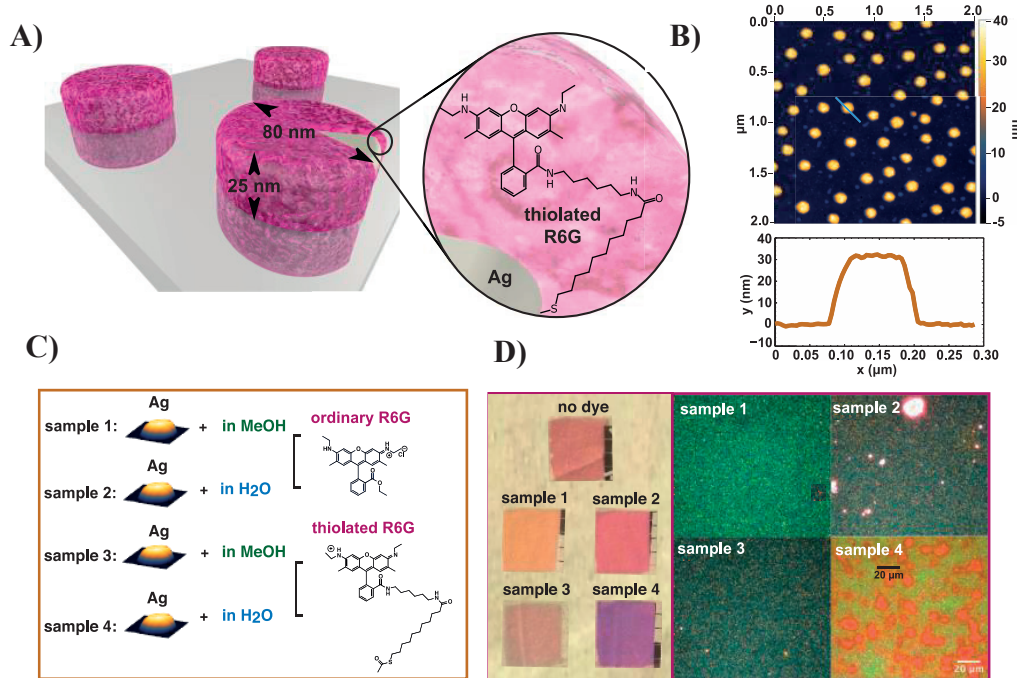


Figure 30: A) Illustration of the covalent attachment of R6G on Ag nanodisks; B) SEM of the Ag disks, made by colloidal lithography on a glass substrate, C) the four sample preparations in which the commercially available as well as the newly synthesized R6G is assembled on the disc; D) photographs and dark-field images of all samples. Reprinted with permission from reference²¹⁰ (paper VIII) © 2016 American Chemical Society.

Figure 31 demonstrates representative scattering spectra of the Ag nanoparticles covered with ordinary (1 and 2) and thiolated (3 and 4) R6G, measured by Gülis Zengin in the group of Timur Shegai at Applied Physics at Chalmers. The green dashed traces in the spectra for the solutions of nanodisks represent pure Ag disks, the magenta colored traces the hybrids (coupled dye-Ag NP) and the blue ones the photobleached spectra. In the photobleached spectra, no features of the molecular absorption are observed, it only shows the recovery of the plasmon resonance of the Ag nanodisks, which proves that the spectral dips were an optical response of the nanoparticle caused by R6G.

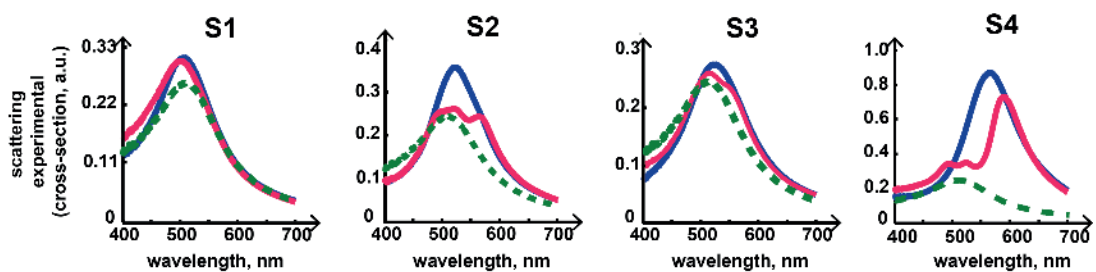


Figure 31: Scattering spectra of the ordinary R6G in methanol (S1), in 4:1 water/methanol (S2), and the spectra of the thiolated R6G in methanol (S3) and in water/methanol (4). The green scattering spectra represents the pure Ag discs, the magenta colored one, the Ag discs covered in dye, and the blue one the Ag discs covered in dye after photobleaching. Reprinted with permission from reference²¹⁰ (paper VIII) © 2016 American Chemical Society.

The thiolated R6G adsorbs in a higher density to the Ag nanostructures, due to the chemical affinity of thiols to the surface, this can be seen already in the photographs in **Figure 30** as well as with ligand exchange experiments.

As the density of molecules on the plasmonic particle increases, stronger spectral dips can be observed (sample 2 (S2) and sample 4 (S4), **Figure 31**). The density of molecules on the Ag nanoparticle was further increased by using water/methanol mixtures, probably due to a poor solubility of the dye R6G in water, which allows to form multiple overlayers of dye on the metal surface, possibly through π -stacking, these findings were confirmed by AFM measurements. Due to a higher density, stronger coupling between the NP and the dye molecules, resulted in stronger dips, upon comparing samples 1 to 2, or 3 to 4, can be observed.

Ligand exchange experiments indicate that in S1, which is the ordinary R6G in a water/methanol mixtures), a surface coverage of molecule/ 0.16 nm^2 can be estimated. The coverage is increased to around molecule/ 1.0 nm^2 due to a solvent change to pure methanol, shown in S2, which shows a more dominant spectral dip. A similar trend can be seen comparing S3 and S4, which shows the thiolated R6G in water/methanol and pure methanol. Here the coverage is determined to be increased from $\sim 1.0 \times 10^5$ molecules per nanodisc, which corresponds to a coverage of molecule/ 4.2 nm^2 to and $\sim 1.8 \times 10^6$ molecules per nanodisc, which is around molecule/ 5.45 nm^2 , see **Figure 31**. Indeed, we clearly observed an interaction between the molecule and the plasmon of the nanostructure, due to the modification in its scattering spectra. The mechanisms leading to spectral dips can be explained due to enhanced absorption or strong coupling. Calculation with the finite-difference time domain (FDTD) method, carried out by T. Antosiewicz, show that enhanced absorption is the main mechanism for spectral dipping in our experiments, but by achieving a high concentration of R6G on the surface a strong coupling regime can nearly be achieved.

The absorption spectra was obtained from transmission and reflection measurements at near normal incident ($A = 1-T-R$, neglecting diffuse scattering), and no spectral dips, were observed. This finding was also corroborated by FDTD calculations except for S4 (thiolated R6G in methanol) (Figure 32).

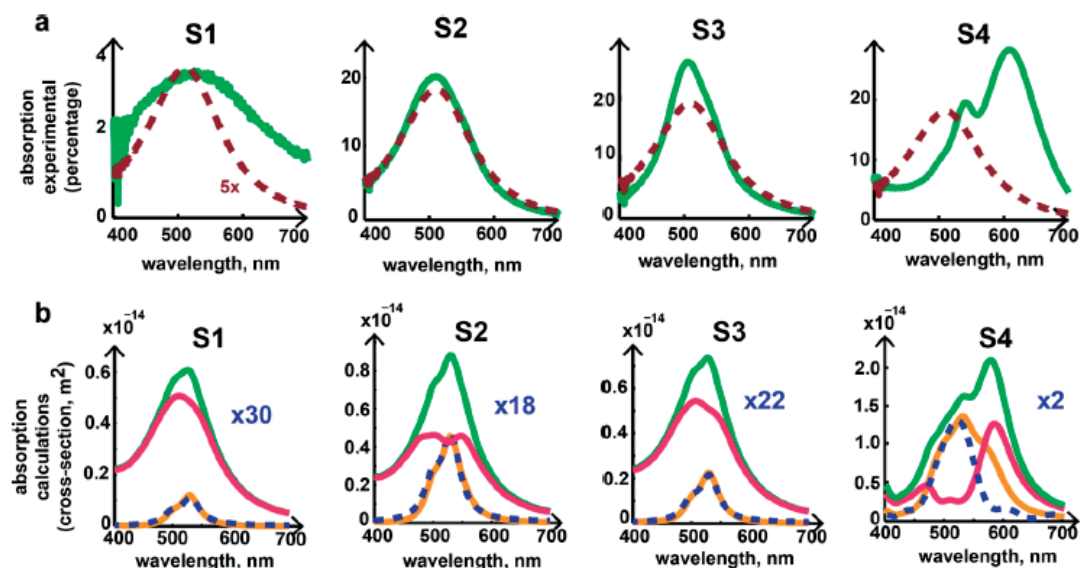


Figure 32: Absorption spectra of thiolated and ordinary R6G. Sample 1: ordinary R6G in methanol, sample 2 ordinary R6G in a 4:1 water/methanol mixtures, sample 3 thiolated R6G in methanol, sample 4 thiolated R6G in 4:1 water/methanol. A) Experimental absorption spectra of the R6G-Ag discs hybrids are plotted green, Ag discs without dye are plotted dashed brown; B) Simulated absorption cross sections: green shows the total absorption cross section of the R6G-Ag system, magenta and orange the separate contributions of metal and dye, the dashed curves the absorption of the same amount of R6G with no plasmonic particle present multiplied by the enhancement factor. Reprinted with permission from reference²¹⁰ (paper VIII) © 2016 American Chemical Society.

By plotting the total absorption of the metal-dye hybrid (green), the absorption contribution of the metal (magenta) and the dye (orange) as well as the same amount of dye without the plasmonic disc (dashed blue) multiplied by the effective enhancement factor, we observed a decrease of the enhancement factor for denser R6G coverage, see Figure 32. This can be explained by a fast decay of the electromagnetic field outside the Ag disc, meaning that just the sub-monolayers are enhanced as much as 30 times, as seen in Figure 32 (S1), but the molecules in a thick layer further away from the Ag disc are enhanced to a lesser extent. The spatial extent of the R6G goes beyond the decay length of the electric field, resulting in lower enhancement values and most R6G dye molecules do not interact with the plasmonic near-field. FDTD calculations for the scattering and the absorption behavior for sample 4 show further, that the thiolated R6G in water is just reaching the strong coupling regime.

All experiments were conducted with the protonated form, which shows the strong pink color. Comparing S1 to S2 and S3 and S4 show that the addition of water changes the absorbance properties of the dye.

These findings are very important, since this clarifies that the study of strong coupling between NP and chromophores cannot be determined merely done just by analyzing the scattering behavior.

In conclusion, we managed to clarify the nature of plasmon-exciton interaction for R6G and localized surface plasmons in Ag nanodiscs. The newly synthesized thiolated R6G binds specifically to the nanodiscs and allows the control of the molecular coverage compared to the unspecific binding of the original R6G used in many previous studies. Depending on the solvent, very dense layers can be achieved and FDTD calculations indicate that the surface enhanced absorption is the dominant effect for the spectral dips, but a strong coupling regime can only be achieved with the densest dye layers we prepared. A dye with a dipole moment of around 1 D like R6G requires an extreme density of molecules located in the near-field to reach the strong coupling regime, which has recently been confirmed in other experiment, in which high densities of dye placed in close proximity to the nanostructure could be achieved.^{163,164}

To achieve strong coupling a molecule with a high transition dipole moment such as in J-aggregates or quantum dots could be used for future experiments. But also smaller nanoparticle structures or dimers could lead it the wanted strong coupling event.

2.2 Photolabile Protection Groups

A useful class for molecular linkers are photolabile compounds, also called caged compounds, in which light with a specific wavelength¹⁶⁵ and appropriate intensity will cleave the molecule and release an active group of interest.¹⁶⁶ Alcohols,^{167,168} amines,¹⁶⁹ thiols,¹⁷⁰ phosphoric acids,^{171–173} carboxylic acids^{174–176} or internal alkynes are commonly released groups.

Adsorbing these photolabile compounds to nanostructures, the photo release can be strongly enhanced due to the LSPR of the plasmonic structures. This made it possible to specifically functionalize local surface areas with light and use them for microarrays¹⁷⁷ or obtain defined chemical patterns with nanometric resolution.¹⁷⁸ Moreover it gives rise to the idea, that one can only activate molecules in a nanogap of a dimeric structure and this newly generated functional groups can detect, bind or react with whatever one is interested in. By finding out the reaction conditions, we envisioned that this could lead *e.g.* to a single molecule functionality in a nanogap.

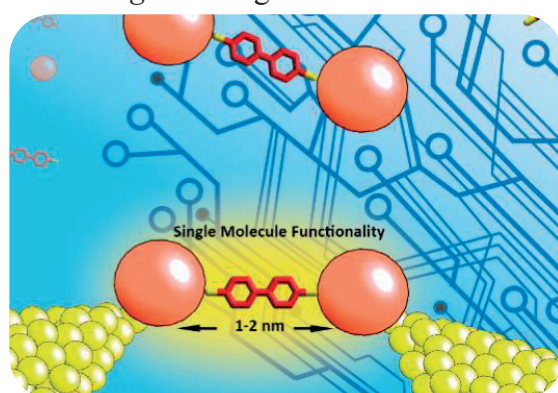
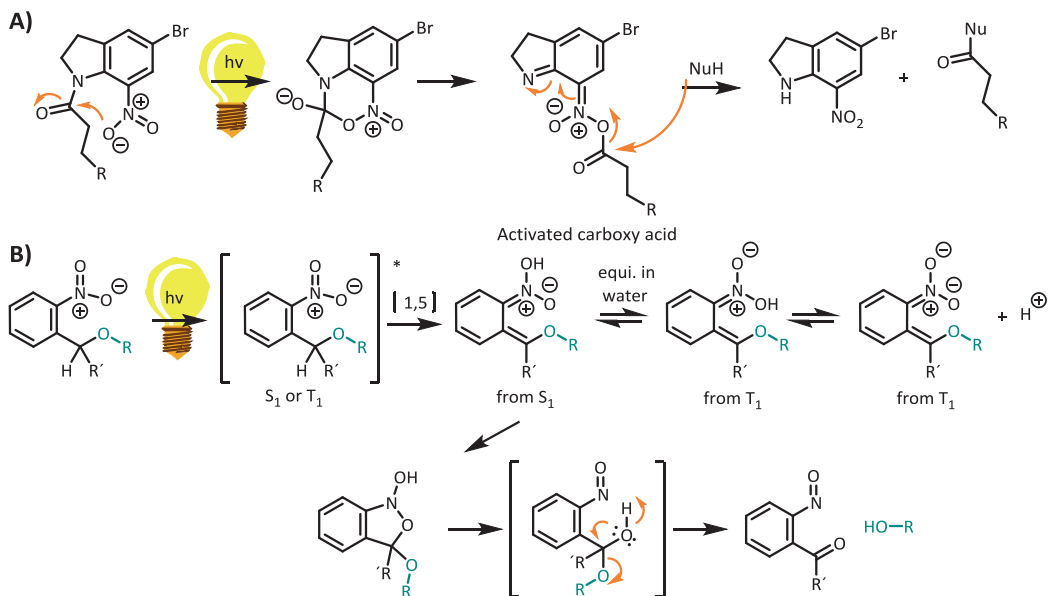


Figure 33: Self-Assembled molecules in a gap of two plasmonic structures.

Since the work of Kaplan¹⁷⁹ and Engels¹⁸⁰ in the 1970s, photolabile groups are of interest in many fields, such as biochemistry,¹⁷⁹ organic synthesis,^{181–183} surface science,^{165,184} natural product synthesis¹⁸⁵ and many more. Many type of molecules are known and very well studied, such as *o*-nitrobenzyl, (coumarin-4-yl)methyl, nitroindoline, and *p*-hydroxyphenacyl derivatives.

The mechanism of the photo release is different for each photolabile compound, but in any case an activated state is involved due to the absorption of a photon, so that an unoccupied state is populated as a singlet (spin up/spin down) or after intersystem crossing a triplet state (spin up/spin up). The excited state makes a molecule inherently a better electronic donor and acceptor. In case of nitroindoline, **Scheme 6A**, an activated carboxy ester results upon absorption of a photon, the ester then readily reacts with nucleophiles, see **Scheme 6**. In case of the *o*-nitrobenzyl derivatives **Scheme 6B** the nitro benzyl group forms nitronic acid, through a 1,5 sigmatropic shift from the photo excited state, which cyclizes and facilitates further reaction to cleaving the ether

and releasing it as an alcohol, see **Scheme 6**. More details about the mechanisms can be found in literature.^{183,186,187}



*Scheme 6: Reaction mechanism of the light induced photo cleavage of A) nitroindolines; B) *o*-nitrobenzyls.*

This Chapter presents the use of a photolabile compounds based on nitroindoline and *o*-nitrobenzyl. A nitroindoline derivative with possessing a thiol moiety was assembled on Au nanostructures in order to build a biosensor, activated by light and giving a sensitive plasmonic read out (**Chapter 2.2.1.**). Furthermore, we designed a new photolabile molecular linker for metal nanostructures, which releases terminal alkynes under irradiation (**Chapter 2.2.2.**). Terminal alkynes haven't been reported to undergo release via photolabile moieties before and due to fact that they undergo very specific reactions, see **Chapter 2.2.2**, these would be an ideal platform for biosensing in a very specific way.

2.2.1 Assembly of a Photolabile Nitroindoline on Gold Nanostructures as a LSPR based Biosensor (paper I)

Light induced surface functionalization can be very local and site-specific by using spatially structured illumination. The functionalization of surfaces with biomolecules has potential use for drug-screening, DNA chips, antiseptic surfaces and biosensors. As described in **Chapter 1**, sensors can be designed by exploiting the plasmonic properties of metal structures. Due to the refractive index dependency of the LSPR peak, they are very sensitive to the immediate surrounding. The idea for this project was to use light sensitive molecules, developed in the group of J.B. Christensen University of Copenhagen,¹⁸⁸ to demonstrate as proof-of principle, that light induced reactions on self-assembled monolayers on nanostructures can be used for biosensing applications. For the purpose of this study we used the photoactive motif indoline (5-bromo-7-nitroindolinyl) functionalized with a thiol unit, which self-assembles onto gold surfaces. In **Figure 34** it is envisioned that the indoline reacts with nucleophiles upon activation with UV irradiation.

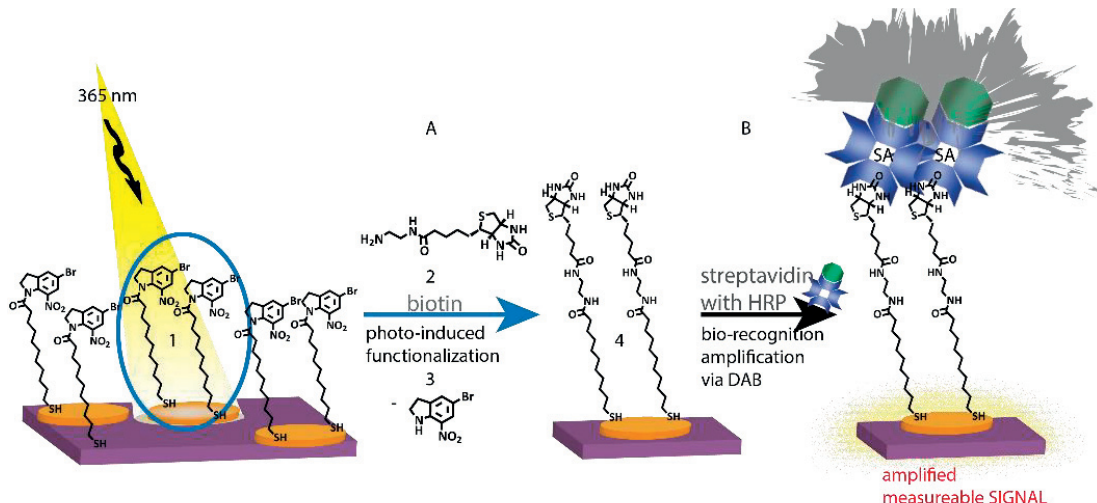


Figure 34: Schematic of the photoinduced reaction on a nanostructured gold sensor. The assembled monolayer of nitroindoline (1) reacts light induced with biotin (2) (step A), which is then recognized by streptavidin (SA) (step B) and the horse radish peroxidase enzyme (green circle) conjugated streptavidin (blue structure) enzymatic 3,3-diaminobenzidine to enhance the LSPR signal. Adapted from reference⁵⁰ (paper I) © 2013 American Chemical Society.

Indeed, under irradiation, the modified surface reacts through the reactive nitroindoline unit, which is expelled as bromonitroindoline upon nucleophilic attack from biotin ethylenediamine. From here, this biotin functionalized surface can be used to probe the well-studied specific binding between biotin and the protein streptavidin (SA). Streptavidin is available as conjugates with many proteins, which makes this a good platform for other biosensing events. We used streptavidin functionalized horse radish peroxidase (HRP) enzyme to polymerize 3,3-diaminobenzidine (DAB), see **Figure 34** green circle on the blue streptavidin structure. The polymerization step with DAB on

top of the light activated nanostructure helps to increase the mass of the attacked object and therefore makes an optical response of the plasmon resonance more obvious.

The performance of the biosensor was tested and confirmed using a combination of quartz crystal microbalance (QCM) and LSPR. QCM is an acoustic resonator, which measures the variation in mass per area by measuring its frequency shift. It can be used to determine the affinity to a special functionalized surface or to investigate molecular interactions. The sensitivity is around $1 \mu\text{g}/\text{cm}^2$. Quartz shows the so called piezoelectric effect, which is the relationship between the mechanical and the electrical state in the crystal. An electrical charge is created due to mechanical force and *vice versa*. An applied voltage can therefore generate a mechanical deformation, and an acoustic resonance can be measured electrically. The crystal oscillates in a standing wave, due to an applied alternating current (AC) through electrodes evaporated on both sides of the crystal. The voltage induces a shear deformation. Adding or removing mass on/off the crystal changes its resonance frequency, which is the measureable variable, see **Figure 35D**. The procedure shown in **Figure 34** was used to obtain a large frequency shift as shown in **Figure 35D** with the purple curve, even without precipitating the DAB on top of the streptavidin. The blue curve presents the QCM chip, passivated for streptavidin by the assembly of PEG-thiols on the surface. Furthermore, a small reversible frequency shift (orange curve) was detected, when an indoline/PEG layer was brought into contact with streptavidin. Most likely a non-specific, hydrophobic interaction between streptavidin and indoline gave rise to it. For all assemblies we used mixed layers of indoline and PEG, since pure light activated indoline surfaces reacted with biotin showed less binding of streptavidin. This might be explained with the size of streptavidin, which needs adequate space to properly bind to biotin. Streptavidin did not bind well to biotin if the biotin layers were too densely packed.

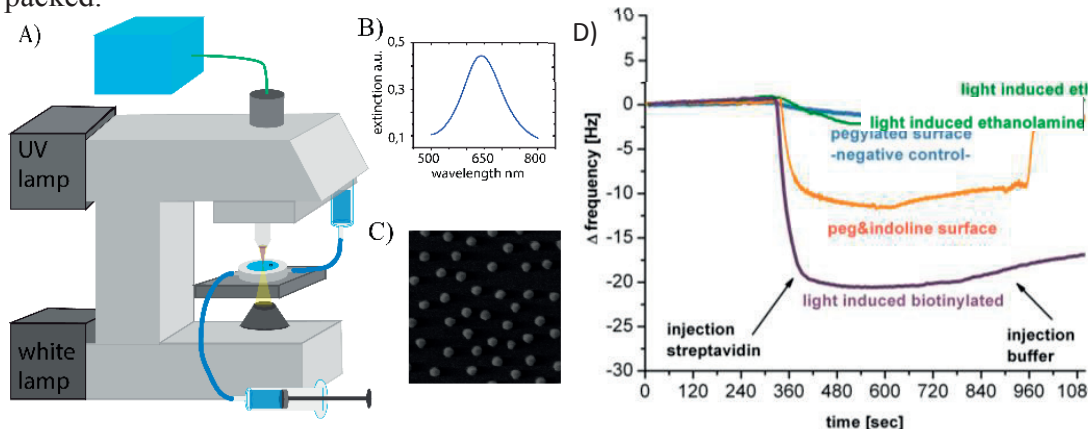


Figure 35:) A) Schematic diagram of the experimental setup to measure the LSPR shift in a mounted flow cell on an upright microscope; B-C) a typical UV/Vis of the plasmonic nanostructure and its SEM image; D) A typical QCM measurement showing a shift in the frequency after the injection of streptavidin, if the surface was light induced reacted with biotin (purple), but not without the light reaction (orange, blue). Adapted from reference⁵⁰ (paper I) © 2013 American Chemical Society.

The same experiment was performed on nanostructured Au surfaces measuring by LSPR, performed by Si Chen of Mikael Käll's group at Chalmers, as shown schematically in **Figure 35A**. The results of the LSPR shift are represented in **Figure 36D** and E and show similar behavior as seen with the QCM. The resonance frequency of the nanostructure (LSPR) shifts in case of a light induced reaction on the surface with biotin, due to a binding of streptavidin (blue curve). Pure indoline surfaces show some non-specific binding (red) and pure PEG surfaces show no binding of streptavidin. Very similar results are obtained with streptavidin, and the polymerization reaction of DAB afterwards. This proves, that just the binding event of streptavidin is enough to make this system usable as a biosensor.

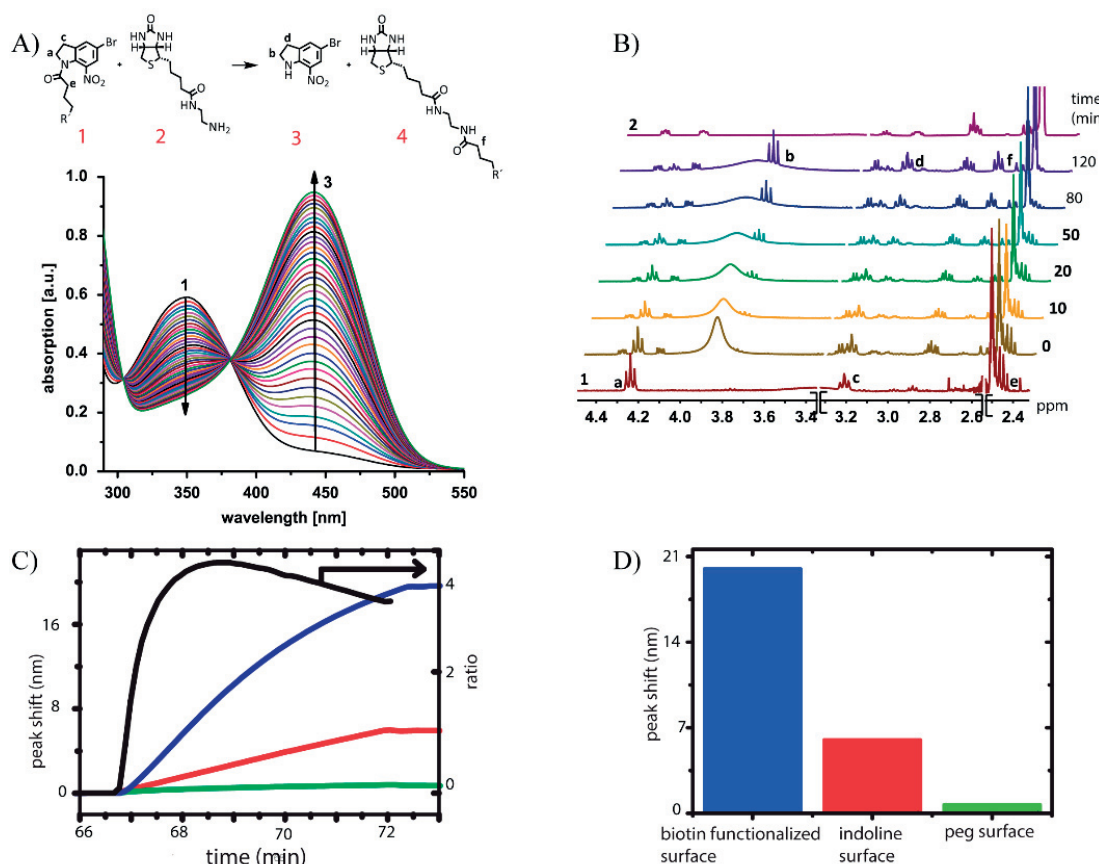


Figure 36: A) UV/Vis spectra of the light induced reaction in DMSO over 2 h. Due to the reaction of nitroindoline (1) with biotin-amine (2) the absorption shifts from 340 nm to 450 nm; B) this can be monitored with the NMR as well, recorded at a 20 min interval. Pure starting material (red and purple) are converted into the product; C/D) Plasmon Peak shift with time and as a column representation for the light reacted surface (blue), the pure nitroindoline (1) surface (red) and a passivated surface with PEG (green). The black curve represents the ratio between the light and not light reacted surface; Reprinted with permission from reference⁵⁰ (paper I) © 2013 American Chemical Society.

The light induced reaction was furthermore studied using UV/Vis and NMR as shown in **Figure 36A+B**, as well as with IRRA (grazing incidence reflection-absorption fourier transform infrared spectroscopy), contact angle and XPS/ESCA (x-ray photoelectron spectroscopy) measurements, see paper I. The UV/Vis spectra show the full conversion of the indoline (**1**) (absorption 340 nm) to **3** (450 nm absorption) without the appearance of byproducts. This is confirmed by two isosbestic points at 304 and 381 nm. NMR experiments during photolysis show the progressive decrease of sigthe signal intensity for the starting materials (signal a and c) **Figure 36B** as well as the appearance of a new set of signals b, d and f indicative of the coupling product and the nitroindoline. Contact angle measurements were done by reacting the indoline with a very hydrophobic amine terminated molecule (4-(trifluoromethyl)phenyl)methane amine) to drastically change the contact angle of the Au surface (**Figure 37**).



Figure 37: Contact angle measurements on gold surfaces, activated with 365 nm and reacted with the nucleophiles biotin (left), 4-(trifluoromethylphenyl)methanamine (CF₃). (right).

The IRRA on Au surfaces were performed by reacting the indoline with biotin as done in the sensor experiments, so that typical signals of biotin such as the carbonyl around 1697 cm⁻¹ can be detected, as well as the disappearance of the nitro group at around 1540 cm⁻¹. Furthermore, 4-(aminomethyl)benzonitrile was introduced to show the appearance of vibrations of the nitrile group (2237, 2268 cm⁻¹) and the aromatic C-H stretch around 2900 cm⁻¹.

For the ESCA measurements indoline on a Au surface was reacted with 4-(trifluoromethyl)phenyl)methanamine to detect the typical peaks for fluorines (F1s), with good correspondence to an expected chemical analysis.

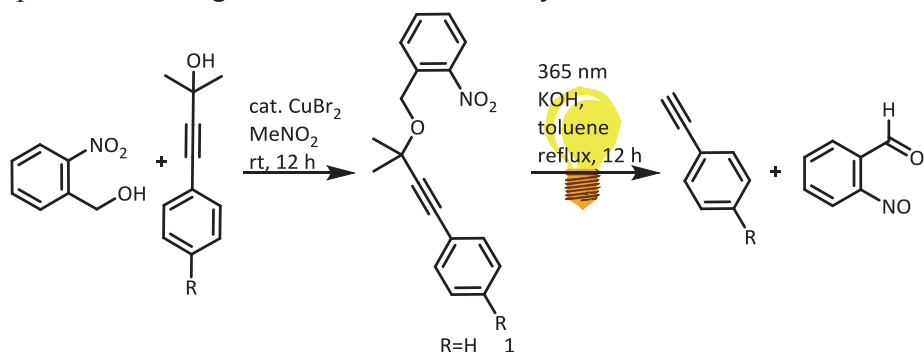
With the help of several techniques we presented here an efficient coupling of several amine nucleophiles of choice to a nanostructured Au surface *via* photoinduced surface chemistry. These self-assembled monolayers act as LSPR based biosensor with biological relevant recognition motifs. By using biotin-streptavidin, one can envision binding of any streptavidin fusion protein to specific position on gold surfaces and monitoring LSPR peak shifts. This might be a starting point for biomedical applications as drug-screening or microarrays. The LSPR based sensing has high sensitivity and is

a relatively simple method. Light induced reactions can be directly monitored in the same setup. Due to the use of light for the functionalization, spatially localized sensing regions with nanometric resolution are possible.

2.2.2 New Photolabile Protection Groups for Alkynes for self-assembly on plasmonic metal surfaces (paper III)

Due to our work with the photolabile nitroindolinyl group, see **Chapter 2.2.1.**, we realized that a more specific photolabile group is desirable, as indoline generates a activated carboxylic acid which can react with any nucleophile possible and under certain reaction conditions even with water. *O*-nitrobenzyls (NBs) are very robust photolabile compounds, well-studied since they were first reported in 1901¹⁸⁹ and used as a protection group in 1966 by Barltorp *et al.*¹⁹⁰ As described earlier, alcohols, amines, thiols, carboxylic acids and others can be protected by this type of photolabile moiety.

One idea was to extend this methodology to develop a protecting group for terminal alkynes, since these can only undergo very specific reactions such as 1,3-dipolar azide-alkyne click reactions, forming 1,2,3-triazoles, Sonogashira and Stephens-Castro reactions or Diels-Alder reactions. As mentioned earlier, a photolabile protection group for liberating terminal alkynes are not common. **Scheme 7** highlights the proposed idea for the photoactivated generation of terminal alkynes.



*Scheme 7: Basic concept of the synthesis of *o*-nitrobenzyl compounds, which can release terminal alkyne due to a photo cleavage under alkaline conditions. Procedure for compound 1, CuBr_2 , MeNO_2 , 12 h, rt. Photorelease is triggered by light of the wavelength around 365 nm ($200 \mu\text{W}/\text{cm}^2$) under alkaline (KOH , toluene, reflux) conditions. The byproduct of this reaction is *o*-nitrosobenzaldehyde. Reprinted with permission from reference²¹¹ (paper III) © 2013 Elsevier, Tetrahedron Letters.*

O-nitrobenzyl alcohol reacts with derivatives of a 2-methyl-3-butyn-2-ol (tertiary propargylic alcohol) in a copper-catalyzed nucleophilic substitution reaction to form the photocages of the family of the *o*-nitrobenzyls (NB), here a propargylic ether.

The formation of the necessary propargylic ethers is not common, even though they are interesting building blocks in organic chemistry.^{191,192} Lewis acids¹⁹³ or transition metals such as cobalt (Nicholas reaction)¹⁹⁴ or rhenium¹⁹⁵ and ruthenium¹⁹⁶ can be used to form primary and secondary propargyl ethers. Mild conditions to synthesize tertiary ethers are, however, not common. Here, the tertiary propargylic alcohol is activated by copper(II) bromide (CuBr_2) to form a propargylic ether through a nucleophilic substitution reaction ($\text{S}_{\text{N}}1$), see **Scheme 7**.¹⁹⁷ Huang *et al.*¹⁹⁷ assumed the formation of a propargylic cation, facilitate by copper coordinating and therefore a catalyzed $\text{S}_{\text{N}}1$ type substitution reaction. The lone pair of the hydroxyl interacts with the vacant coordination site on copper II, which lowers the energy of dissociation between the hydroxyl and the hydrocarbon, forming the carbocation. The empty d orbital of the copper can also overlap with π -cloud of the alkyne.

The two main reaction steps to synthesize a library of photolabile compounds were the above mentioned copper catalyzed $\text{S}_{\text{N}}1$ type substitution reaction to bind the *o*-nitrobenzyl motif to any kind of alkyne group. The other was the Sonogashira cross-coupling reaction, to introduce triple bonds, especially here to introduce the propargylic alcohol to the molecules.

The mechanism of a typical Sonogashira reaction is depicted in **Figure 38**. Firstly, the palladium catalyst ($\text{Pd}(\text{PPh}_3)_2\text{Cl}_2$) requires activation to a Pd^0 species. Pd^0 can be generated by addition of PPh_3 , but also from the amine base or from the terminal acetylene (this path requires copper, see catalyst activation **Figure 38**)

The main reaction is depicted in the palladium cycle, **Figure 38**. The active Pd^0L_2 reacts with aryl or vinyl halide in an oxidative addition, forming a palladium (II) complex. This complex undergoes a transmetalation with the copper acetylide (formed in the copper cycle). A *trans-cis* isomerization of the Pd complex follows, to bring the organic ligands close to each other, to finally eliminate the product under a reductive elimination step, regenerating the active Pd^0 .

To help the transmetalation, copper forms a π -alkyne complex, which helps to abstract the terminal proton of the alkyne and let it react with the Pd, see copper cycle in **Figure 38**.

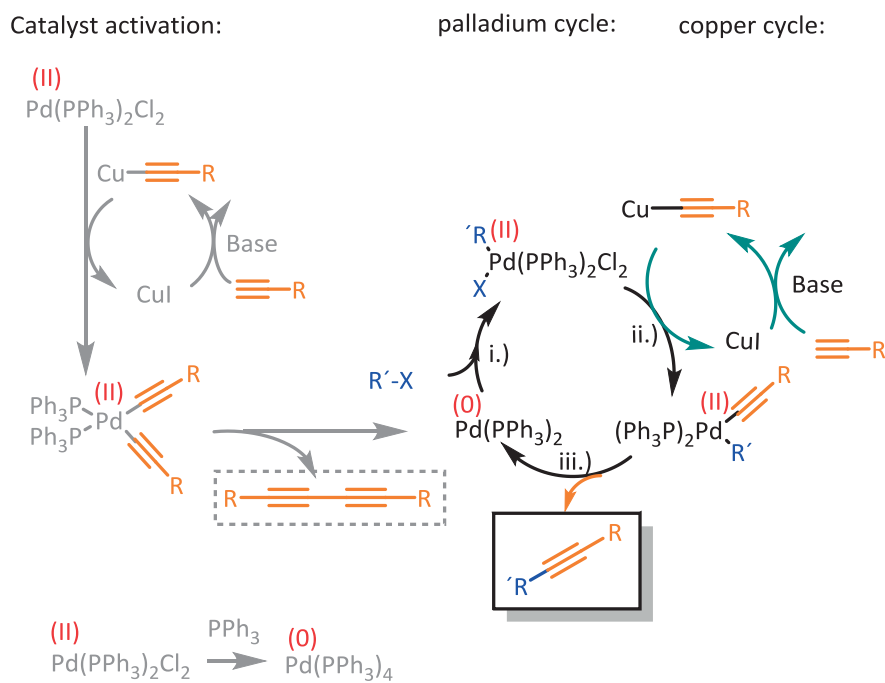
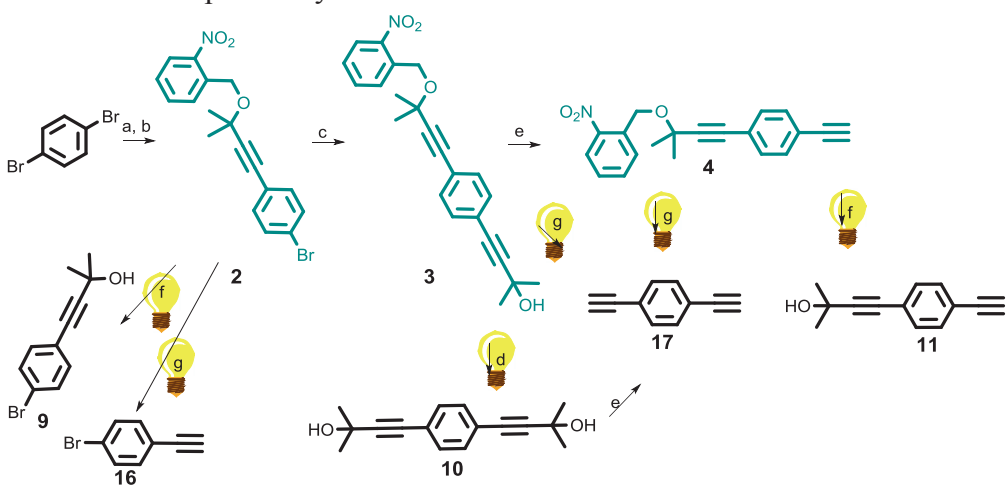


Figure 38: Reaction mechanism of a typical Sonogashira reaction; i) oxidative addition, ii) transmetallation and trans-cis isomerization, iii) reductive elimination. R is a hydrocarbon compound, X a halogen.

A library consisting of 7 photolabile compounds were synthesized using the same synthetic methodology to prove its versatility. All compounds could be used as photocleavable groups for terminal alkynes (**Scheme 8** and **Scheme 9**, all green structures). Furthermore, the orthogonality of the photolabile group to e.g. the traditional propargylic alcohol protected alkynes was demonstrated (**Scheme 8**) and the ability to be used as molecular linkers (**Scheme 9**) for self-assembly on plasmonic structures is realized by synthesizing a thiolated version.

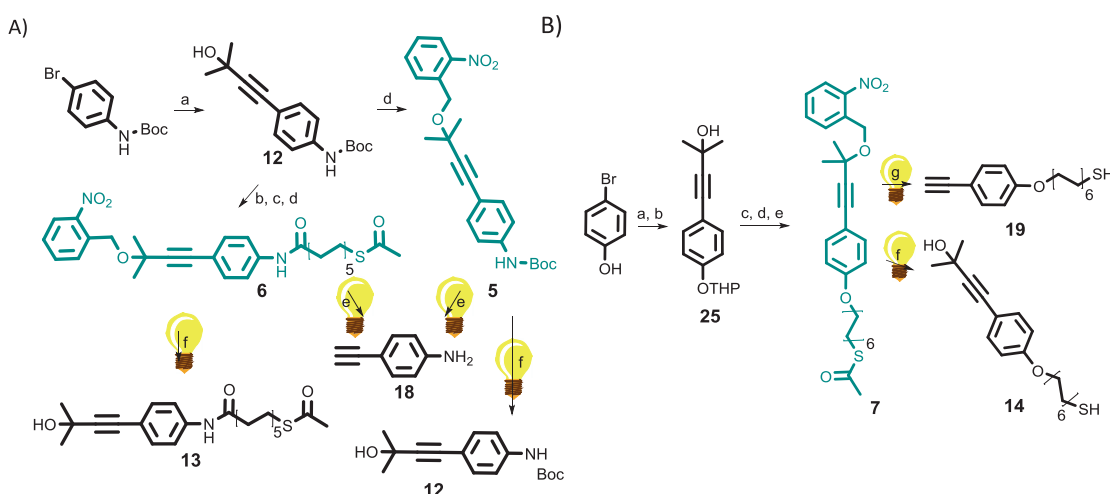
To prove the “orthogonality” of the photolabile group, compound **3** (**Scheme 8**) was synthesized, and deprotected to compound **4** under basic conditions with the exclusion of any light, while still carrying the photo-protection group. This demonstrated the robustness of this photolabile protection group for terminal alkynes. During illumination under alkaline conditions both the traditional and the photoprotection group in **3** are removed, forming compound **17**, see **Scheme 8**. By using illumination but neutral reaction conditions, compound **3** deprotects to compound **10**, in which the traditional protection group is still stable. In this way we demonstrated that they are in one direction independently addressable from each other.



*Scheme 8: Synthetic procedure for photolabile compound 2 and 3. a) $PdCl_2(PPh_3)_2$, NEt_3 , 2-methyl-3-butyn-2-ol, CuI , PPh_3 , THF; b) $CuBr_2$, $MeNO_2$, *o*-nitrobenzyl alcohol; c) $PdCl_2(PPh_3)_2$, NEt_3 , 2-methyl-3-butyn-2-ol, CuI , PPh_3 , THF; d) 365 nm, ethyl acetate; e) KOH , toluene; f) 365 nm ethyl acetate, g) 365 nm, KOH , toluene.*

Reprinted with permission from reference²¹¹ (paper III) © 2013 Elsevier, Tetrahedron Letters.

Furthermore, we wanted to demonstrate the concept of biosensing *via* LSPR and designed two compounds, carrying a thiol anchoring groups for metal, plasmonic nanostructures, see **Scheme 9**, compound **6** and **7**. These could be used as a very sensitive LSPR sensors as demonstrated in paper **I** (**Chapter 2.2.1.**), capable of undergoing very specific reactions, such as azide-alkyne click reactions. This would improve the selectivity compared to the nitroindoline photolabile group in paper **I**, which is susceptible to attack from all kinds of nucleophiles. Another possibility is to place these photolabile compounds in a gap, see **Figure 33**, and activate them just in the hot-spot. These compounds would allow to generate reactive alkynes just in the gap, which can then react specifically with reporter molecules, dyes or others for applications as described earlier, SERS, enhanced absorption, strong coupling, biosensing and many more.



Scheme 9: Synthesis procedure for photolabile compound 5, 6 and 7. *A)* a) $PdCl_2(PPh_3)_2$, NEt_3 , 2-methyl-3-butyn-2-ol, CuI , PPh_3 , THF; b) $TBAF$; THF; c) EDC ; $DMAP$, DMF, 11-acetylthio)undecanoic acid; d) $CuBr_2$, $MeNO_2$, *o*-nitrobenzyl alcohol; e) 365 nm, KOH , toluene; f) 365 nm ethyl acetate; *B*) a) $p\text{-}TsOH$, DCM, 3,4-dihydro-2H-pyran; b) $PdCl_2(PPh_3)_2$, NEt_3 , 2-methyl-3-butyn-2-ol, CuI , PPh_3 , THF; b) $p\text{-}TsOH$, THF/ $MeOH$; d) K_2CO_3 , DMF, 2-(12-bromododecyl)thioacetate; e) $CuBr_2$, $MeNO_2$, *o*-nitrobenzyl alcohol; f) 365 nm, ethyl acetate, g) 365 nm, KOH , toluene. Reprinted with permission from reference²¹¹ (paper III) © 2013 Elsevier, *Tetrahedron Letters*.

Scheme 7 visualizes already, that strong basic conditions during the photoreaction were needed to generate a primary alkyne. Therefore, some possible compounds containing the photolabile moiety were unstable, such as compound 6, which contains a amide bond, which is labile in basic conditions and breaks during the attempt to form a terminal alkyne, and forms instead compound 18 (**Scheme 9**).

The thioacetate moiety in compound 7 is a relatively robust moiety and reactions such as Sonogashira or others can be endured. Whereas a free thiol group can react as a nucleophile, which can poison catalysts or react in nucleophilic reactions. Strong basic conditions as needed in the photocleaving step with KOH, result in deprotecting the thioacetate and forming the free thiol, forming compound 19, with a free alkyne and the thiol anchor for the metal surface. Compound 7 lead us therefore to a compound, with a thiol anchored photolabile compound, which is a candidate for further studies for surface sensor applications.

The photo release of compound 1 can be monitored *via* 1H -NMR spectroscopy. The byproduct, *o*-nitrosobenzaldehyde (see **Scheme 7**) gives rise to two very distinctive signals, an aldehyde around 12 ppm and an upfield shifted aromatic resonance at 6.4 ppm (*para* position). Furthermore, the disappearance of the signals of the starting material can be observed, for instance the signal for the benzylic protons at 5.1 ppm diminish and eventually disappear after irradiation, see details in **Figure 39**.

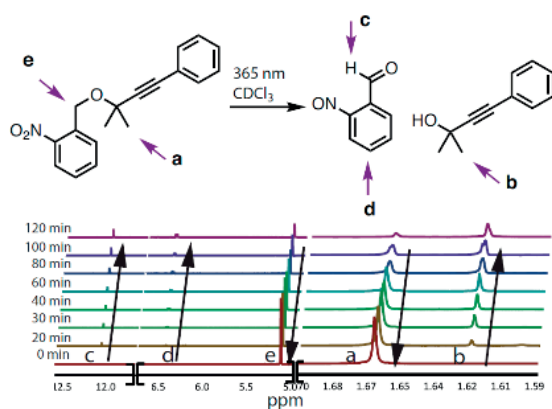


Figure 39: ^1H -NMR spectra of photolabile compound 1 in CDCl_3 upon irradiation with UV-light (365 nm, $200 \mu\text{W}/\text{cm}^2$) for 120 min. Product 8 and the byproduct o-nitrosobenzaldehyde is formed. Reprinted with permission from reference²¹¹ (paper III) © 2013 Elsevier, Tetrahedron Letters.

With this strategy we developed a novel methodology for the photolabile protection of terminal alkynes. The nitrobenzyl based compounds can be used orthogonal to the traditional alkyne protection for synthetic purposes as well as for plasmonic surfaces, which gives rise to many applications as plasmonic sensing.

The photocages need to be further tested for plasmonic applications and we are considering ways to further develop the system, and to eliminate the harsh alkaline conditions needed to form the terminal alkyne. Recently, our protection strategy has inspired the group of Kakiuchi et al.,¹⁹⁸ who employed a milder hydrolysis step for the release of the terminal alkyne, which definitely would allow testing these conditions on self-assembled monolayers in the future.

3

Assembly of Colloidal Nanoparticles

Chapter 2 discussed in detail the synthesis and the assembly of various molecular linkers which have been used in conjunction with plasmonic metal nanostructures to addressing questions such as plasmon-exciton interactions, the use of photolabile molecular linkers for biosensing, or the measuring of the binding force of complexes. To go one step further, nanoparticles were synthesized and assembled giving dimeric structures, in order to study some of the previously mentioned effects as indirect plasmonic sensing in assembled nanoparticles. This chapter will describe three ways to assemble dimeric nanostructures: A) Assembly using newly synthesized molecular linkers, B) Assembly using electrostatic interaction, and C) Assembly of nanostructures on surfaces, see **Figure 40**.

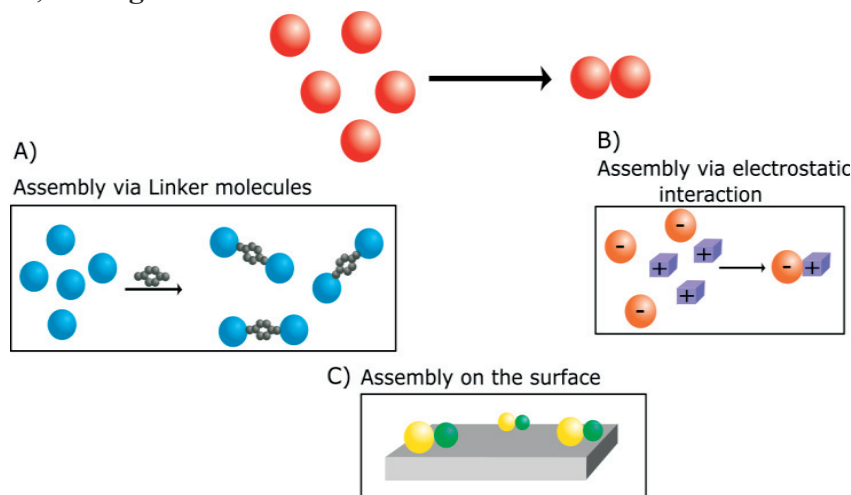


Figure 40: Schematic representation of the assembly of nanoparticles in three different ways A) Assembly via linker molecules; B) Assembly via electrostatic interaction; C) Assembly on the surface.

3.1.1 Terpyridine Linker to Assemble Dimeric Metal Nanoparticles (paper VI)

One such possibility to assemble nanoparticles is to use molecular linkers, as described in **Chapter 1 Figure 12**. Traditionally, molecules bearing two thiol units have been used to combine two nanoparticles (homodimers) of the same or different composition (heterodimers) or to form discrete nanoclusters.⁵¹ One desirable is a strategy to dimerize two nanoparticles in a dynamic equilibrium assisted process, achieving a monofunctionalization, where a single molecular linker resides between these particles.

For this purpose we designed an amine terminated terpyridine linker, since it is known that two terpyridine molecules form a stable but reversible complex with transition metal cations (see **Chapter 2.1**). However, by adding *e.g.* a strong complexing agent such as EDTA (ethylenediaminetetraacetic acid), HEEDTA (hydroxyethyl ethylenediamine triacetic acid)^{199,200} or by protonation of the amine groups by the addition of HCl,²⁰¹ this 2:1 complex can be disassociated (**Figure 41**).

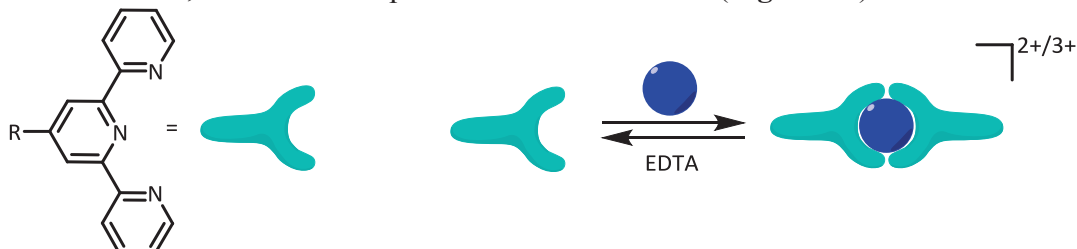
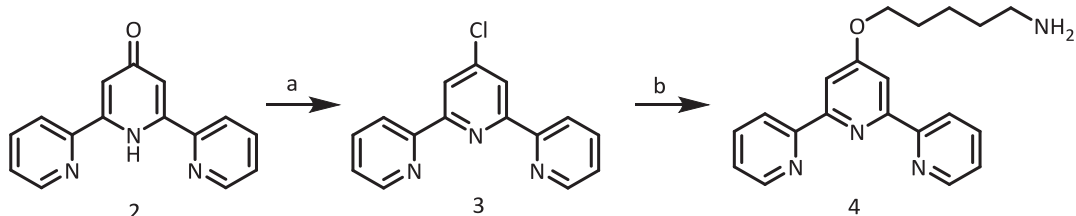


Figure 41: Schematic of the complexation of terpyridine with transition metals and the decomplexation with a competitive ligand such as EDTA.

This, in essence, gives one the opportunity to reversibly assemble NPs if all these components are present in conjunction with terpyridyl units attached nanoparticles.

In order to connect the terpyridine molecular linkers, we followed the analogous procedure shown in **Scheme 1** (step a and b) in **Chapter 2** to obtaining the terpyridine ketone compound 2. Ketone 2 was further reacted with a mixture of phosphoryl chloride (POCl_3) and phosphorus pentachloride (PCl_5) (step a **Scheme 10**), forming compound 3, followed by subsequent treatment with 5-aminopentan-1-ol, affording amine functionalized terpyridine, compound 4, see **Scheme 10** step b.



Scheme 10: Reaction scheme for an amine functionalized terpyridine. A) $\text{POCl}_3, \text{PCl}_5$, 0°C , 10 min; 110°C , 12 h; b) 5-aminopentan-1-ol, DMSO, KOH , 60°C , 12 h.

For this purpose we synthesized the aforementioned terpy molecular linker bearing a primary amine moiety, which can react with carboxylic acid functionalized SiO_2 NPs solid support (**Figure 43** step **A**) and indeed with metal NPs (**Figure 43** step **B**), here Fe_3O_4 and Au, which also have carboxylic acid coverage. SiO_2 NPs were prepared *via* a typical sol-gel synthesis and further functionalized with an amino silane (APTES, 3-aminopropyltriethoxysilane) and further coupled with tartaric acid using peptide chemistry (EDC/NHS) introducing a terminal carboxylic acid to the surface of the SiO_2 NPs. Iron oxide and gold NPs (Fe_3O_4 and Au) were surface functionalized with oxalic acid ($\text{C}_2\text{H}_2\text{O}_4$) and 3-mercaptopropionic acid, respectively, adding carboxylic acid groups to the surface of these NPs (**Figure 42**).

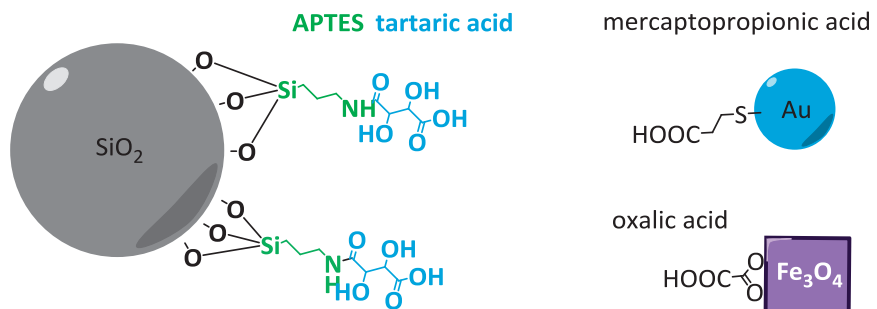


Figure 42: Preparation of the solid support SiO_2 and the Au or Fe_3O_4 NP to react with terpy amine.

To establish a route towards monofunctionalized NPs, we employed a solid support approach; binding a small NP *e.g.* Au on a larger SiO_2 NP, and functionalize the metal NP with the terpy molecule while sitting on the solid support. By releasing it from the solid support with EDTA, the monofunctionalized NPs can encouraged to dimerize with different or the same type of NP by adding a transition metal salt, in this case FeCl_3 , and form a supramolecular complex consisting of a single iron(terpy) bridging between two metal containing nanoparticles (**Figure 43**).

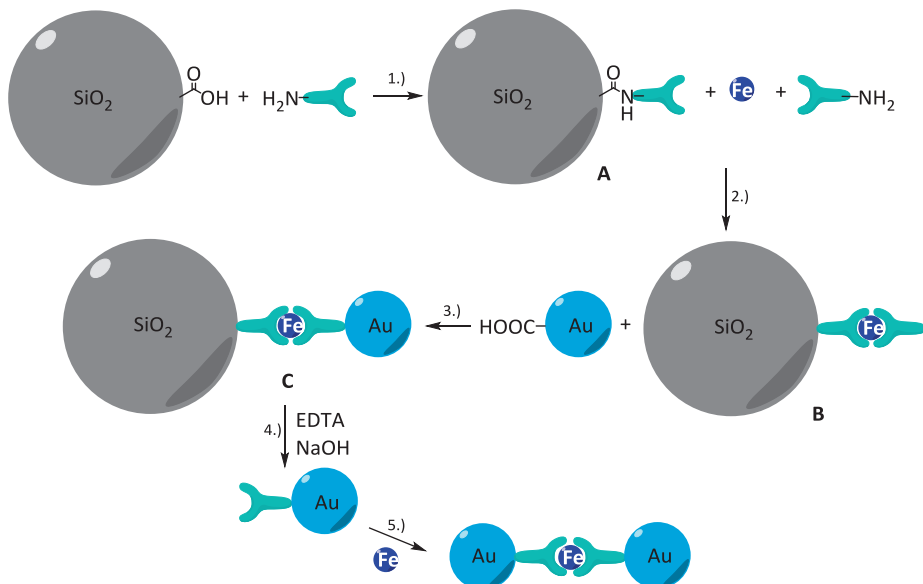


Figure 43: Strategy to assemble monofunctionalized dimeric NPs. The source of Fe^{III} comes from $\text{FeCl}_3 \cdot 6\text{H}_2\text{O}$. 1) Carboxylic acid decorated SiO_2 NPs react in a coupling reaction with the amine terpy to complex A. 2) A reacts binds via Fe^{III} a second terpy, forming complex B. 3.) B reacts with the carboxylic acids groups on the surface of Au NP, forming complex C. 4) EDTA extracts the iron from the system and the silicon support can be dissolved by adding 1M NaOH , releasing monofunctionalized Au- or Fe_3O_4 -terpy NPs, 5) which can react with another monofunctionalized Au-terpy NP with the help of Fe^{III} to a dimeric nanostructure, Au-Au.

Due to the presence of the carboxylic acid functionality of the surface of all nanostructures, the main synthetic protocol in this assembly process (**Figure 43**) was therefore done using peptide coupling reactions: This procedure was used to attach the terpy compound 4 via the terminal amine to the terminal carboxylic acid groups coated silicon dioxide (SiO_2) forming an amide bond (complex A, **Figure 43** step 1). A second terpyridine linker is then introduced to the SiO_2 solid support by forming a complex with iron, (step 2, **Figure 43** complex B). At this point, either carboxylic acid terminated Au or Fe_3O_4 NPs could then be bound to complex B via a second peptide coupling, see step 3, **Figure 43** complex C. Since this synthesis step happened on the solid support, all unreacted starting materials could be removed by both repeated centrifugation and washing. From here, monofunctionalized NPs could be conveniently obtained by decomplexation of complex C firstly with EDTA liberating the Au NP, step 4. Subsequent treatment of the reaction mixture with NaOH aids purification by dissolving the silicon based solid support. The reintroduction of FeCl_3 then allows for the highly selective formation of homo metallic NP dimers (step 5, **Figure 43**).

FTIR as well as TEM allowed us to follow the assembly of either Au or Fe_3O_4 NPs to the solid support (**Figure 44A** and **B**) as well as in the dimer formation steps (**Figure 44C** and **D**). In addition, ^1H NMR revealed a successful bonding between the terpy and

the silicon support. The aromatic signals broaden due to the immobilization on the support, and the signals of the terpy unit at 7.85 and 7.38 ppm are high-field shifted, indicating a strong electron-pushing effect from the particles into the terpy unit. Furthermore, UV-Vis spectra of the singles Au NPs to the dimeric Au NPs shifts from 523 to 533 nm.

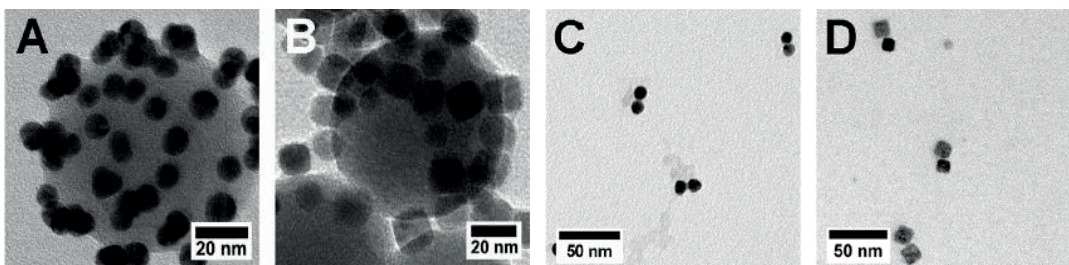


Figure 44: TEM images of A) SiO_2 -Au nanoparticles; B) SiO_2 - Fe_3O_4 NPs, C) Au dimers; D) Fe_3O_4 dimers. Reprinted with permission from reference²¹² (paper VI) © 2015 American Chemical Society.

Dimers of two monofunctionalized NPs could be reversibly formed *via* metal complexation in a yield around 50%. This versatile bottom-up approach can give rise to the formation of complex nanoclusters. Using the same approach to form heterodimers could be a logical progression of this methodology. Future goals would therefore be to employ this method to assemble all different kind of dimeric structures and use the monofunctionalization to test plasmonic properties, such as SERS, indirect nanosensing or in other applications.

The assembly of the nanoparticles was undertaken in the group of Thomas Nann in Australia, where the design and the synthesis of the reversible terpy linker as well as parts of the spectroscopic characterization of the samples were carried out by the author of this thesis.

3.1.2 Assembly of Dimers in Solution using Electrostatic Interactions and the Use of Heterodimers for Sensing Applications (paper IV and VII)

Aside from using molecular linkers to bridge nanoparticles, electrostatic interactions between oppositely charged NPs can also be used to assemble dimeric NPs, which was highlighted in **Chapter 1 Figure 12**. To develop a versatile synthetic strategy to assemble two metal NPs of different shapes, sizes and, metal composition, thus forming hetero- and homodimers, a method based on electrostatic interactions was developed. The aggregation process has to be carried out in a controlled way to achieve the highest possible yield of dimeric nanostructures, whilst avoiding over aggregation and thus sintering of NPs. For this purpose, the stability of each NP in the presence of its counter ions and the oppositely charged NP had to be studied and fine-tuned.

In this study, we used one NP functionalized with sodium 2-mercaptopethanesulfonate (MESNa), forming a negatively charged NP, in this case either Au or Ag. Positively charged nanostructures, could be made in different shapes using either Au or Pd, with coverage of surfactants CTAB or CTAC.

To develop this versatile method to assemble dimeric NPs we used well known and easily available NPs in order to access a wide range of homo- and heterodimeric structures. One particle family is the citrate stabilized particles, which are commercially available for many metals, and due to the high lability of citrate are easy to further functionalize. These were functionalized with stronger binding MESNa (sodium 2-mercaptopethanesulfonate), to form stable negatively charged particles. Another large and well described class of NPs are NPs stabilized with CTAB and to a lesser extent CTAC. Either CTAB or CTAC stabilized particles on the account of the quaternary ammonium cation, were used as the positively charged particle component.

The surface charge and the hydrodynamic radii on both the negatively and positively charged NPs were measured using zeta-potential and dynamic light scattering (DLS), moreover all these particles were further analyzed using TEM and SEM to confirm the size and the shape of these NPs. **Figure 45** visualize the idea of combining positively and negatively charged NPs, as well as the results we obtained by using several different citrate and CTAB particles forming heterodimeric NPs. We combined Au and Ag NP spheres with a range of shaped Au and Pd NPs, cubic, rhombic-octahedron, truncated cube, rhomic dodecahedron, showing different surface crystallographic facets.

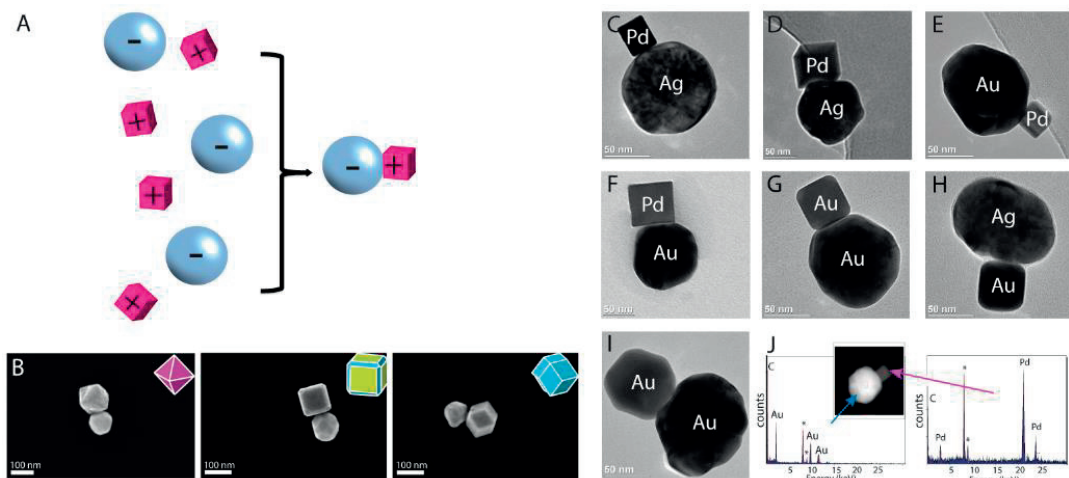


Figure 45: A) Schematic of the electrostatic interaction to assemble a wide variety of homo- and heterodimers. C-I) TEM images; B) SEM images of Au(spherical_{90 nm})-Pd of different shapes; C) Ag (spherical_{90 nm})-Pd (cube_{25 nm}); D) Ag (spherical_{90 nm})-Pd (cube_{70 nm}); E) Au (spherical_{90 nm})-Pd (cube_{25 nm}); F) Au (spherical_{90 nm})-Pd (cube_{70 nm}); G) Au (spherical_{90 nm})-Au (cube_{35 nm}); H) Ag (spherical_{90 nm})-Au (cube_{35 nm}), I) Au (spherical_{90 nm})-Au (rhombic octahedron_{50 nm}); J) EDX-STEM elemental analysis of dimer Au (spherical_{90 nm})-Pd (cube_{25 nm}). Adapted from reference²¹³ (paper IV) © 2014 American Chemical Society.

Crucial for a successful electrostatic assembly of dimeric structures is the mutual stability of two contributing NPs. In addition to coverage of the positively charged NP with CTAB, unbound CTAB is also present in the solution and cannot be completely removed without irreversible aggregation. On the other hand generation of negative MESNa NPs is accompanied by citrate in solution. It was found that the success of dimer formation had a strong dependency on relative concentration of these salts in solution when positively and negatively charged NPs were mixed. **Figure 46**, shows the results of addition of CTAB to negatively charged MESNa coated Au NPs which had varying citrate levels, showing the relative stability ranges for negatively charged Au NPs in the presence of CTAB. For the NPs hosted in 300 μM citrate, tolerance of CTAB up to as high as 20 μM was obtained, however, higher levels of CTAB lead to aggregation.

In order to find a window, in which both particles are stable, the same experiment was performed, instead adding sodium citrate to CTAB stabilized Pd NPs of different CTAB concentrations. The plotting of both lines (**Figure 46**) for these relative concentration stabilities, showed a window, highlighted in blue, where it seemed that both negative and positively charged NPs exhibited stability.

It was within this window that the controlled assembly of NP dimers was centered. To achieve the highest yield of dimeric nanoclusters a fine-tuning of the ratio of NPs was required as well. By changing the concentration of NP A: NP B the yield can be tuned to around 30-40% of aggregates being AB dimers. The remaining 60-70% composed

of both single A particles or bigger clusters of AB_n in which $n \geq 2$, as determined by microscopy.

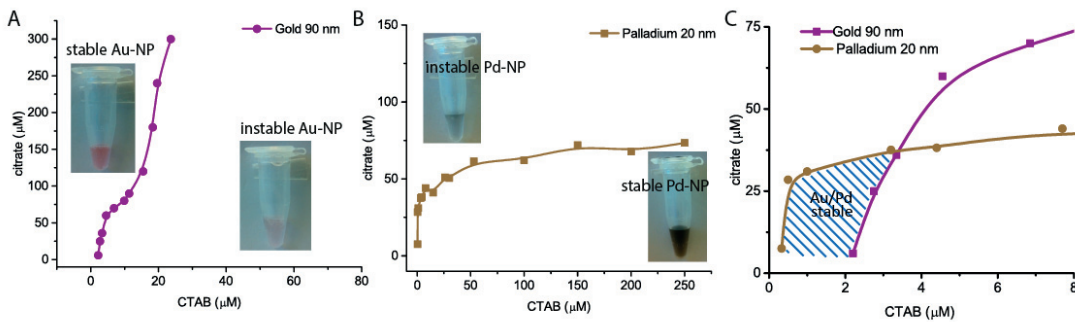


Figure 46: Stability diagram as a function of concentration of capping agents for A) Au sphere_{90 nm}, and B) Pd cube_{25 nm}. C) The blue zone visualize the citrate and CTAB concentration in which both particles are stable.

The mutual stability of oppositely charged NPs can be theoretically described by the nature of the interactions involved in the aggregation process using variations of DLVO theory (named after Derjaguin, Landau, Verwey, and Overbeek), which is in detail explained in paper IV, and will not be further described here.

In brief, this versatile approach following the model stability diagram allowed us to combine metallic NPs of different sizes, shapes and chemical composition. Following this model, could also lead to further work possibly extended to non-metallic particles. Furthermore, it would be desirable for plasmonic sensing applications to have shaped plasmonic nanoparticles as triangles or rods. This would enhance the hot-spot between the NPs and allow the testing of many plasmonic applications.

One of the heterodimeric structures (Au-Pd), prepared this way, was used for single-particle plasmonic nanospectroscopy, see Figure 47A, to test the utilization of these assembled structures (paper VII).

Our novel approach of forming heterodimers (see paper IV, described above) allowed the generation of combinations of NP dimers, consisting of many kinds of metals, in a range of sizes in addition to a great selection of surface facets. This potentially broadens the field of sensors already described in literature, such as hydrogen sensing with palladium NPs.^{9,29}

Hydrogen is known to be able to occupy interstitial sites in metal lattices such as Pd or Pt, forming hydrides. Hydrogen molecules (H_2) can adsorb on metal surfaces, dissociate into hydrogen atoms (H) and subsequently diffuse into the interstitial sites in the metal lattice leading to lattice expansion (Figure 48C). Hydrogen uptake in palladium nanostructures can be measured directly or indirectly using the LSPR of a metal nanoparticle, described earlier by e.g. the group of Langhammer et al.^{202,203} For direct sensing, the Pd NP changes its permittivity and the metal lattice expands due to the uptake of hydrogen, which causes the change of the resonance conditions for the LSPR.

Some metals, such as Pd show a very small LSPR, resulting in poor scattering, seen as broad flat features in the scattering spectrum. Therefore indirect sensing could be a means to overcome the issue, by using another metal NP as the sensor, to probe the hydride-formation in their local vicinity.

In order to study physicochemical properties, which might depend on the size, shape and facet of the Pd, particles needed to be synthesized in a bottom up approach, as our implemented heterodimer formation. Lithography or other top-down methods typically don't allow us to create special crystal facets of different sizes and shape. The aim was therefore to study single structures to learn about the hydride formation, thermodynamics and hysteresis in colloidal Pd nanocrystals of different sizes and shapes. This is the first attempt of sensing hydride formation in individual Pd NPs of different sizes and shapes.

As mentioned in **Chapter 1**, the LSPR of the Au NP placed next to the Pd nanocrystal is sensitive to permittivity changes of its surroundings. By adsorbing hydrogen in Pd NPs, forming palladium hydrides, the volume of Pd expands and the permittivity changes, which was detectable by a LSPR shift for the Au NP adjacent to it. Au shows a strong absorption and can therefore act as an antenna, i.e. a nanoprobe for the hydrogen adsorption in the adjacent Pd NP and as a signal transducer in dark field scattering spectroscopy (DFSS) (**Figure 22 Chapter 1**). The hydrogen uptake and release experiments were performed by Svetlana Syrenova in Christoph Langhammers group at Applied Physics in Chalmers and the results are discussed below.

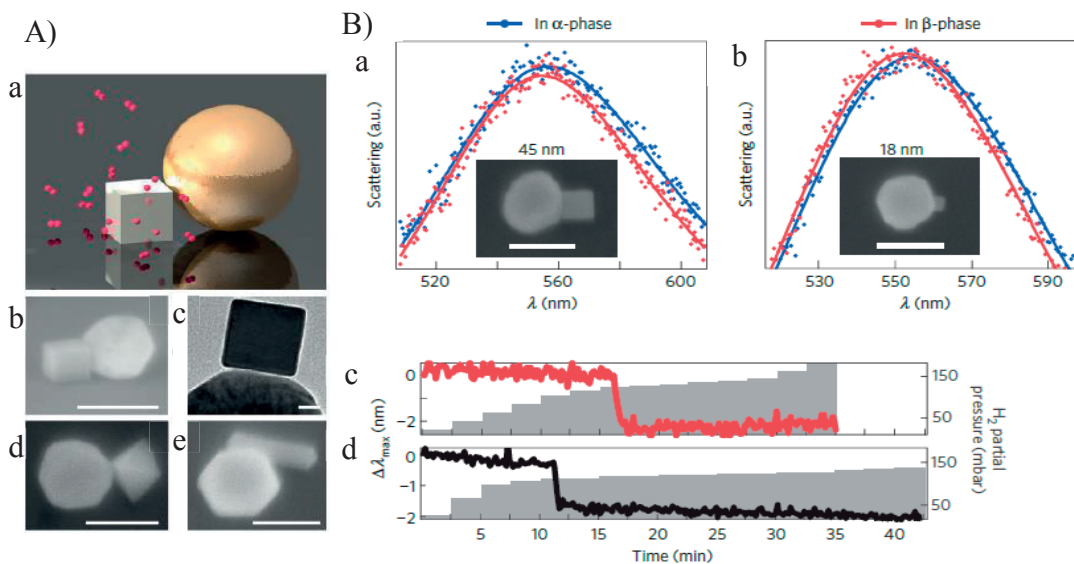


Figure 47: A) a) Artistic view of H_2 (red) dissociated and absorbs on Pd cubes; b, d, e) SEM images of an Au-Pd arrangement; c) TEM image of the gap between the Au sphere and a Pd cube; B) Representative scattering spectra of individual Au-Pd dimers. Blue (red) correspond to the raw scattering data before (after) hydride formation; a) 45 nm Pd cube; b) 18 nm Pd cube. The solid lines are the Lorentzian curve. The scale bar in the inset SEM is 100 nm. c, d) corresponding time evolution of $\Delta\lambda_{\text{max}}$ during hydrogen sorption and phase transition from metal to hydride for the particles shown in a,b. Reprinted with permission from reference²¹⁴ (paper VII) © 2015 Nature Publishing Group.

By exposing the heterometallic dimer to hydrogen gas, hydrogen molecules adsorb onto the surface and dissociate into atoms, as depicted in **Figure 47A**. With time a shift of the LSPR of the Au NP was observed, due to the hydrogen sorption and a phase transition of the Pd (**Figure 47B**). **Figure 47B** visualizes the $\Delta\lambda$ with an changing partial hydrogen pressure over time, before and after the hydride formation. (The following will go into detail about the different phases of the transition of Pd to PdH, and after **Figure 47** will be discussed further.)

After the dissociation into atoms, hydrogen diffuses into the metal lattice. Exposing Pd NPs to a low partial pressure of hydrogen, results in the so called α -phase being formed, which is a solid solution of hydrogen within the metal lattice. The amount of hydrogen is low and the distances between the hydrogen atoms are large. By absorbing more hydrogen, will result in the lattice being subjected to a local strain. At a certain hydrogen pressure/concentration hydrogen-hydrogen interactions in the lattice will lead to the formation of the so called β -phase, where a metal hydride is formed. At intermediate hydrogen pressure, α - and β -phase will coexist, but an increasing pressure of hydrogen will favor the β -phase. Being completely in the β -phase means that the metal in entirely has been transformed into a metal hydride, see **Figure 48C**.

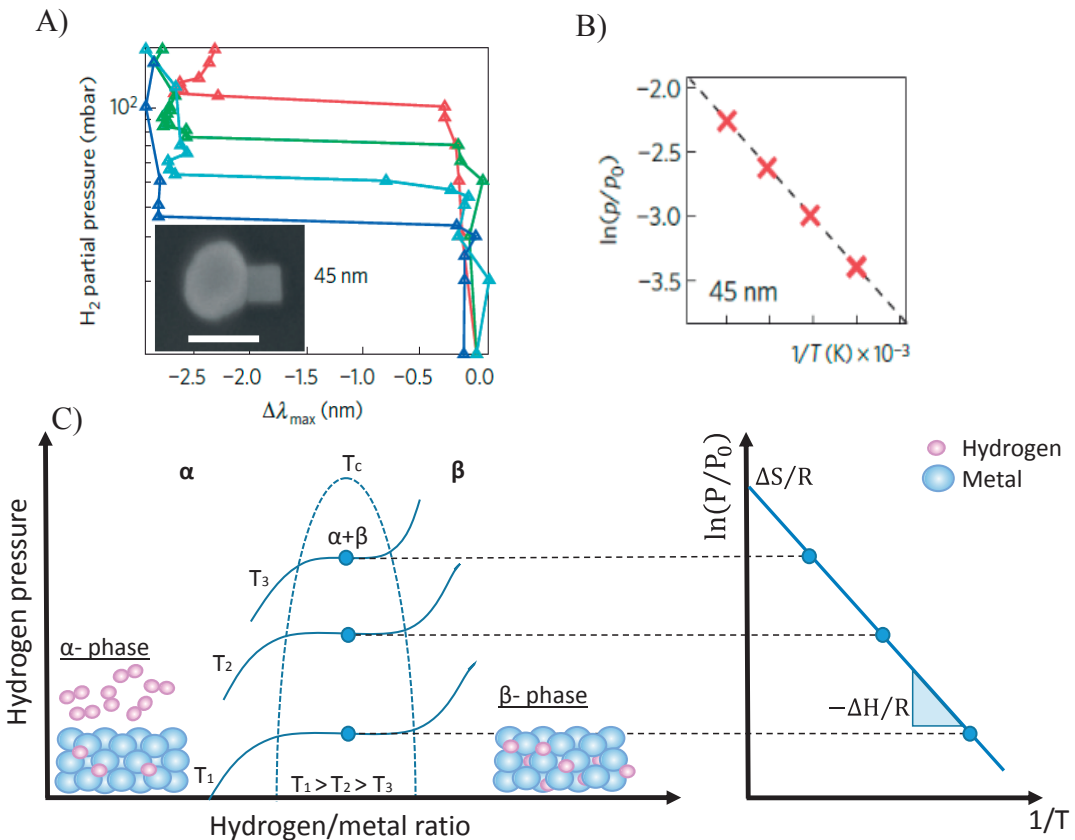


Figure 48: $p\text{-}\Delta\lambda_{\max}$ isotherm of a 45 nm Pd cube measured at four temperatures: red: 333 K, green 323 K, cyan 313, blue 303 K; B) Van't Hoff plots of corresponding absorption isotherm, giving the thermodynamic informations, ΔH and ΔS . Here $-\Delta H = 32 \text{ kJ/mol}_{(H_2)}$ and $-\Delta S = 77 \text{ J/K mol}_{(H_2)}$; Reprinted with permission from reference²¹⁴ (paper VII) © 2015 Nature Publishing Group. C) Schematic of a $p\text{-}C$ isotherm at different temperatures, allowing to map the phase diagram of the hydride formation/decomposition. Plotting the equilibrium plateau pressure allows for the calculation of ΔH and ΔS according to the Vant't Hoff plots to the right.

As discussed, hydrogen exposure to a palladium NP, placed next to a Au nanostructure, shifts the LSPR of the Au. **Figure 47B** (a and b) shows two characteristic scattering spectra, before (blue) and after (red) hydride formation for two different Pd – Au NP dimers. In all cases, the LSPR of the Au NP shifted clearly to shorter wavelengths, $\Delta\lambda_{\max}$. By increasing the hydrogen partial pressure stepwise (**Figure 47B** (c and d)), a continuous blue shift in the $\Delta\lambda_{\max}$ was observed. Sufficient time must be allowed for the new equilibrium state to be reached, as indicated by a stable peak position. This means that hydrogen was still being gradually absorbed into the so called α -phase (gas phase of hydrogen). Later a jump in the signal could be observed, which corresponded to the first order transition of the α -phase into the palladium hydride.

The thermodynamics of the hydride formation can be tracked by recording the $\Delta\lambda_{\max}$ with increasing hydrogen pressure. Plotting $p\text{-}\Delta\lambda_{\max}$, which is interpreted as a $p\text{-}C$ (pressure-composition) isotherm, showed the α –phase at low hydrogen pressures, β -

phase at high pressures and a phase transition as a sharp plateau (**Figure 48**). In the α -phase, the attraction between the hydrogen atoms in the lattice is very weak, due to the low loading of hydrogen, where hydrogen atoms are far away from each other. The Pd lattice feels, nonetheless, an induced strain due to the hydrogen atoms residing in the interstitial lattice. With an increasing hydrogen pressure, the hydrogen-hydrogen attraction becomes stronger, hence more lattice strain is felt within the Pd NP. In the β -phase all sites are occupied by hydrogen. **Figure 48A** shows the measured data for a Au-Pd dimer, and **Figure 48C**, a schematic of the transition between the two phases (α and β). The plateau describes the coexistence of both phases. In addition, an increase in temperature resulted in an increase the pressure required for hydride formation.

Above the so-called critical temperature (T_c), the transition between the phases takes place continuously, no plateau will be observed. The enthalpy (ΔH) and entropy (ΔS) can be determined with the help of such isotherm measurements. The enthalpy and entropy changes per hydrogen molecule during the hydride formation can be calculated with the Van't Hoff equation: $\ln\left(\frac{p}{p_0}\right) = \frac{\Delta H}{RT} - \frac{\Delta S}{R}$, see **Figure 48B** of a real measurement and **Figure 48C** of a schematic representation.

Measuring several sizes of Pd cubes, in conjunction with an adjacent Au NP, showed a small increase of ΔH with increasing cube size. Furthermore, the hysteresis can give more information on the equilibrium pressure for the hydride formation (p_{abs}) and hydride decomposition (p_{des}), which was determined from the absorption and desorption at the single particle level for the first time. The pressure for the hydride formation decreases with the cube size, whilst the pressure for the hydride desorption seemed independent of size and shape of the palladium nanostructure. This behavior implied that the transition from metal to metal hydride was asymmetric and size and shape impact the absorption of hydrogen, not its release. As with the absorption of hydrogen, It seems that the hydride decomposition also occurs *via* a coexistence between α - and β -phases until all the hydrogen has been released.

The hydrogen absorption properties of Pd NPs in size ranges from 20 to 110 nm did not show large variation, however, it was thought that exploring the behavior of Pd NPs, smaller than 10 nm, may show more significant changes. Smaller particles might show further a decrease in ΔH .

These measurements showed that more information can be gained by measuring colloidal heterodimeric structures for plasmonic nanospectroscopy compared to ensemble measurements made on a surface. Reference this. Compared to ensemble measurements, a very sharp hydride phase transition with very flat plateau can be seen. The hysteresis was much wider than for polycrystalline bulk Pd or thin films. The hydride formation enthalpy and entropy are nearly independent of size and shape. Future work should therefore consider particles below 10 nm, which should in principle

show a reduced enthalpy.²⁰⁴ Furthermore, Pd possessing different facets should be investigated to see whether there is a difference in the hydrogen uptake,

Other room for improvement could be to use different shaped probes, such as Au nanotriangles, thus giving bow tie structures in conjunction with Pd NPs (as opposed to this study which used spheres) should enhance the signal by creating a more localized hot-spot.

3.1.3 Assembly of Nanostructures on Surfaces (paper V)

A big topic aside from the assembly of nanostructures in solution is the controlled assembly of NPs on surfaces. The fields of molecular electronics, microprocessors and portable devices could benefit from miniaturization, using nanoparticles and/or molecules.

Semiconductor based transistors invented in 1954 decreased in size from several μm to around 14 nm node transistors in 2014.^{3,4} It is still desirable to miniaturize computer components in order to improve the computing power, and the speed. But as mentioned earlier, top-down methods as photo lithography are reaching their limits.²⁰⁵ Furthermore, some features, which are desirable like sizes and facets of particles cannot be reached with top down methods and therefore the field of supramolecular chemistry (bottom-up) is more of an attractive option.

Top down and bottom up methods each offer distinctive different advantages, such as mass production via top down or molecular approaches via bottom up. In our field of interest, combining both these methodologies was a very interesting prospect, having the controlled colloidal synthesis of special faceted NPs and their assembly on top-down produced solid surface in a selective and controlled way. The latter aspect could be made possible by using e.g. patterned surfaces to self-assemble particle in specific locations.

This leads to the idea of studying the positioning of NPs by electrostatic soft-template directed self-assembly. The electrostatic interaction between a silicon surface and Pd NPs covered in CTAB was studied. By passivating certain areas on a surface with lipid in this case 1-palmitoyl-2-oleyl-sn-glycero-3-phosphocholine check name giving bilayers which act as a soft template, which in principle block the adhesion of Pd NPs to these regions.

This in turn allowed for the selective placement of Pd particles to other desired areas with nanometric space-resolution. **Figure 49** visualizes the idea of positioning particles at specific positions.

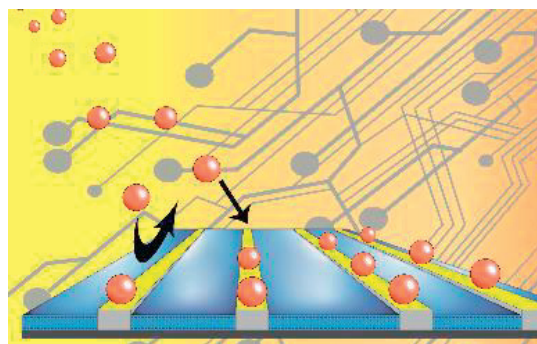


Figure 49: Schematic illustration of positioning nanoparticles on specific area of a surface by passivating other areas for example with lipid bilayers. Reprinted with permission from reference²¹⁵ (paper V) © 2014 Royal Society of Chemistry

The first approach was to study the interaction between an unmodified SiO_2 surface and the positively charged CTAB stabilized Pd NPs. Positively charged molecules and NPs adsorb non-covalently to a silicon surface. By removing as much CTAB as possible, but also maintaining Pd NP stability was necessary to achieve the greatest degree of NP coverage on the SiO_2 surface. (**Figure 50 a and b**). These results were reproduced using other NPs of different sizes and shapes as well. The cationic stabilizer CTAB promotes the adsorption of NPs on silicon surfaces, see SI paper V.

Treatment of the SiO_2 surface giving the bilayer, prior to the NP deposition prevented the adsorption of any NPs, see **Figure 50c**.

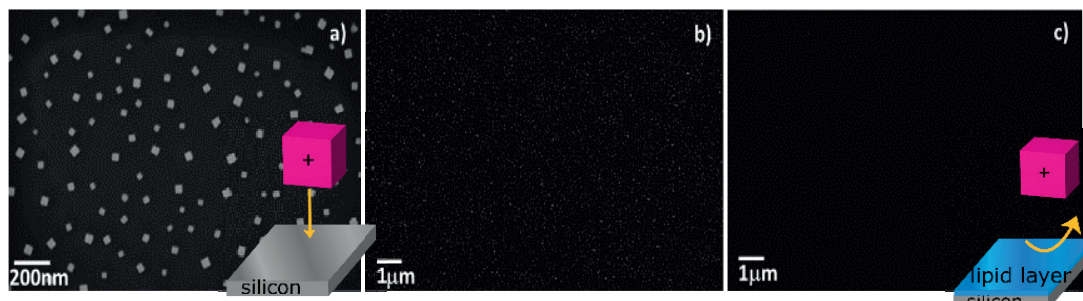


Figure 50: Self-assembled NP sub-monolayer on oxidized Si surface, a, b) SEM image of the Pd cubes 25 nm on silicon at different magnification; c) surface passivated by a lipid bilayer, preventing any Pd to bind to the SiO_2 surface. Reprinted with permission from reference²¹⁵ (paper V) © 2014 Royal Society of Chemistry. Insets show the schematic of the process on the surface.

Switching focus to assembly upon a gold surface, cationic Pd NPs, in addition to other positively charged NPs, could be achieved by firstly functionalizing the Au surface with sodium 2-mercaptoproethanesulfonate, MESNa. The anionic sulfonate group promoted the adhesion of positively charged NPs, whereas otherwise they did not stick to an untreated Au surface, (**Figure 51**). The thiol linker allows to bind to the Au surface, as discussed earlier.

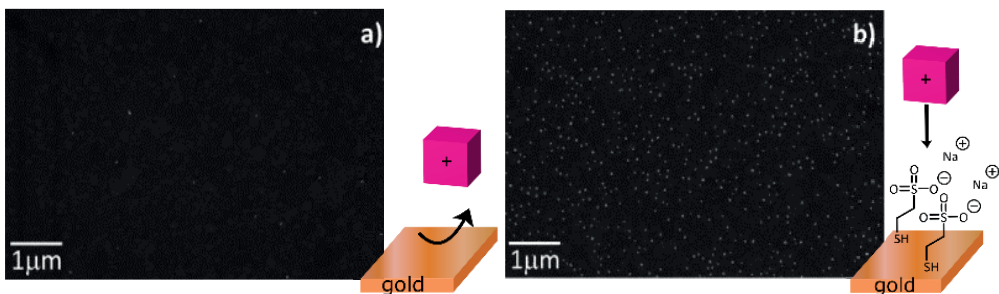


Figure 51: Self-assembled sub-monolayer of Pd cube 25 nm on a) plasma cleaned Au surface; b) MESNa functionalized Au surface. Reprinted with permission from reference²¹⁵ (paper V) © 2014 Royal Society of Chemistry. Insets show the schematic of the process on the surface.

These two experiments lead to the idea to attach Pd cubes on distinct Au areas, such as Au lines (**Figure 52**), patterned by e-beam lithography.

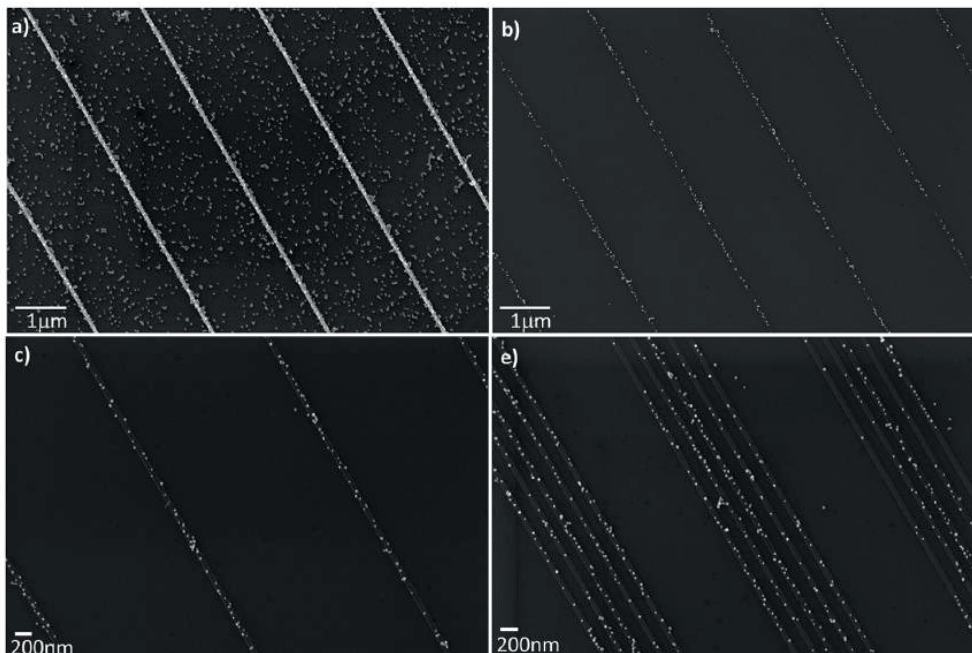
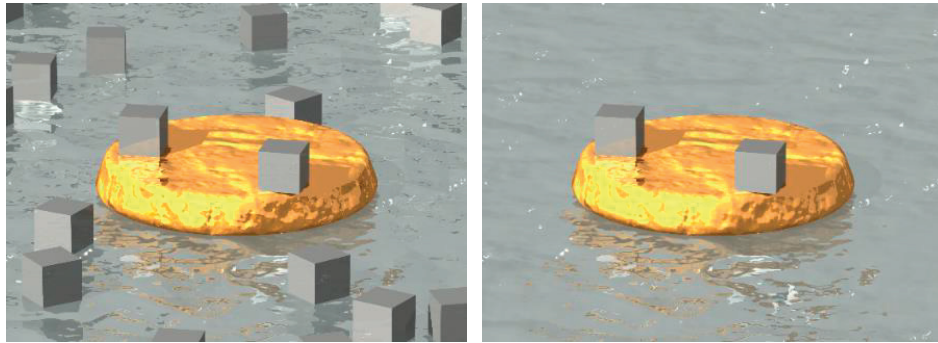


Figure 52: Pd NPs self-assembled on gold top-down fabricated structures: (a) clean Au lines patterns on clean oxidized Si wafer, (b–f) MESNa functionalized Au lines pattern on oxidized Si lipid bilayer passivated wafer (different magnification and different pattern).

By passivating the silicon surface with a lipid bilayer and activating the gold lines with MESNa, the Pd NPs stuck to the lines, but not to the silicon surface.

Furthermore, the principle was used to form a heterometallic dimer of Au with Pd, produced by a combination of top-down and bottom-up methods. Hole-mask colloidal lithography was used to produce small Au discs, whereas Pd cubes were synthesized in a bottom up approach. With this we combined two complementary features and designed a prototype of a self-assembled plasmonic sensor (**Scheme 11**).



Scheme 11: Schematic of the self-assembly of colloidal Pd cubes on Au discs, fabricated via hole-mask colloidal lithography. A) without passivating the silicon surface around the Au disc; B) with passivation of the silicon and functionalization of the Au disc with MESNa. Printed with the permission of Carl Wadell.

Figure 53 shows that a functionalization of the Au discs as well as a passivation of the silicon surface was necessary to achieve selective attachment of the Pd NPs to just the Au discs. As expected due to the previous experiments, the Pd cubes assemble everywhere but not on the Au discs when the neither the SiO₂ surface nor the Au discs had been treated (**Figure 53a**). Systematically, by only functionalizing the Au discs with a molecular linker with a thiol anchor group and a negative charge (MESNa), positively charged Pd NPs also now stick to the Au discs (**Figure 53b**). By passivating the silicon with the lipid bilayer and functionalizing the Au surface with the thiol linker Pd NPs attaching to just the Au discs, but not to the silicon anymore, as desired (**Figure 53d**).

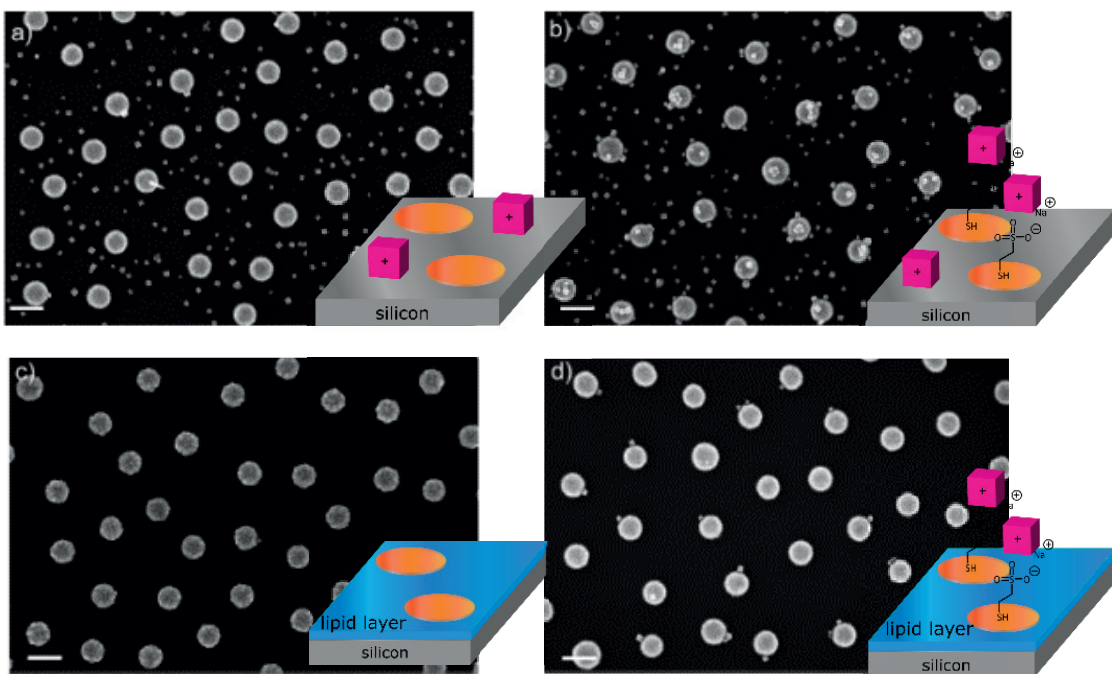


Figure 53:Self-assembled sub-monolayers of Pd cube 25 nm on plasma cleaned top-down nanofabricated Au discs on oxidized silicon surface, a) clean surface, b) Au functionalized with MESNa, c) SiO_2 passivated by self-assembled lipid bilayer, d) SiO_2 passivated by self-assembled lipid bilayer and Au functionalized with MESNa, scale bars are 200 nm; Reprinted with permission from reference²¹⁵ (paper V) © 2014 Royal Society of Chemistry. Insets show the schematic of the process on the surface.

To achieve this, we developed a method to form stable lipid bilayers. Bilayers diffuse laterally on open surfaces, therefore we fabricated a PMMA pool on the edges of the silicon surface. This pool was needed to act as a container for all additives, see **Figure 54**, since bilayers need to be in solution during the whole process in order to keep stable. We chose therefore to assemble everything by using source and drain pipettes simultaneously and just exchange one solution with the next. With this technique we functionalized the Au surface with MESNa first, washed away the remaining MESNa, followed by the formation of the lipid bilayer, again washing the surface and finally the deposition of the cationic Pd NPs. The gradual exchange of solvent was important for all steps, to form stable lipid bilayers and have a stable Pd NP solution to assemble on this surface, see **Figure 54**.

This method made it possible to exclusively position Pd NPs on 56% of the Au discs and prevented the adhesion to silicon. Without MESNa only 5% of the discs were functionalized with Pd. Furthermore, these structures were used to measure the hydride formation of palladium for indirect plasmonic sensing applications, by the group of Christoph Langhammer, Applied Physics, as described in **Chapter 3.1.2.**, see paper **VII** supporting information.

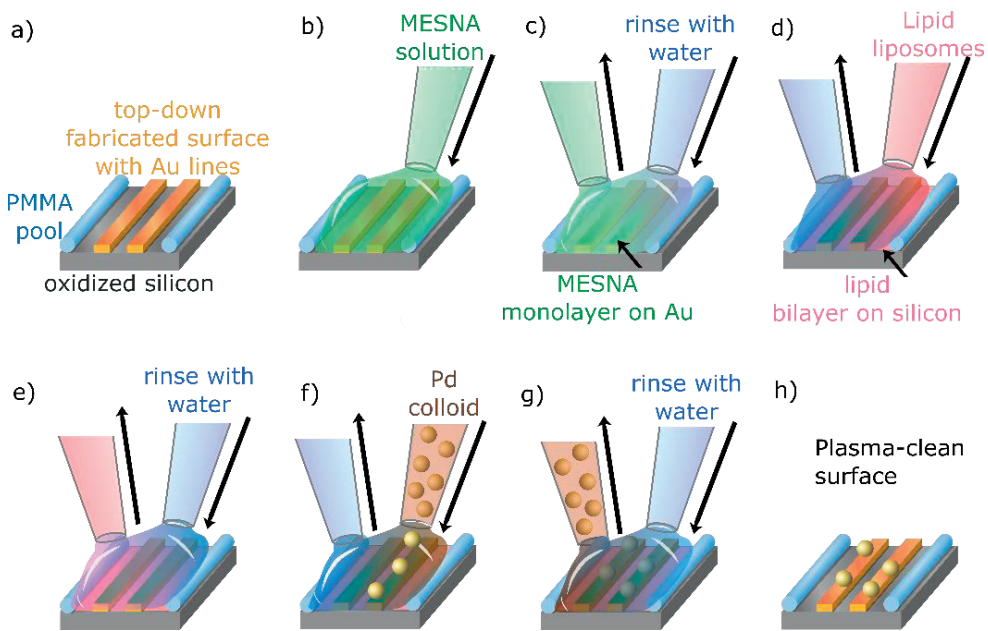


Figure 54: Schematic view of the procedure of the layer-by-layer strategy for the functionalization of top-down nanofabricated structures: a) starting surface, b-c) MESNa functionalization of Au surface, d-e) SiO_2 passivation with lipid bilayer, f-g) colloidal deposition, h) final surface.

This approach has the capacity to combine bottom-up and top-down methods to make it possible to, with high reproducibility and in a high yields, ordered assemblies of nanostructures on surface. The simultaneous fabrication makes it applicable to build independent devices on macroscopic surfaces, which is desirable when thinking about miniaturization of devices for all kinds of applications.

4

Concluding Remarks and Outlook

The overall aim of my thesis was to investigate different building blocks for the assembly of nanostructures. We were especially interested in improving and developing methods for the assembly of nanoparticle dimers, which may hold interest for a variety of applications. This was achieved in one way by synthesizing a specific molecular linker to assemble reversibly nanoparticle dimers in solution. Another route lead us to combine top-down and bottom-up synthesis of dimeric structures on a surface, which can be very interesting in order to build miniaturized nanodevices. We further developed a versatile methodology for the assembly of heterodimeric particles consisting of different sizes, shapes and composition by controlled electrostatic aggregation. Some of these heterodimeric aggregates were further studied for use in indirect plasmonic sensing, specifically for the hydride formation in palladium nanoparticles.

Another focus had been to synthesize molecular linkers for plasmonic surfaces for the purposes of studying a range of purposes; the plasmon-exciton interaction of a dye molecule and a plasmonic structure; The binding strength of molecular complexes, using a metal that access different oxidation states, self-assembled on a AFM tip and on flat Au surfaces was measured; and new photolabile compounds developed and used as molecular linker to build a LSPR based biosensor.

Weengaged in a broad spectrum of science, ranging from organic synthesis of molecular linkers, demonstrating their function as sensors, and eventually the assembly of dimeric particles and their applications.

All fields can be further improved and developed as already described in the different chapters. So should *e.g.* the new alkyne photolabile group be tested for sensing applications and a milder way for its cleavage be investigated, or the plasmon-exciton interaction be shifted into the regime of strong-coupling to achieve a real hybrid system. The assembly of heterodimers could be advanced to assemble all kind of non-metallic particles with metallic nanoparticles, or to assemble triangular plasmonic NPs to generate a stronger hot-spot to make them a better sensor or catalyst.

We are currently working already on different approaches to achieve some remaining goals. For example, the purity of dimeric structures, which can possibly be improved using gel electrophoresis. The assembly of heterodimeric structures is expanding, by using triangular Ag and Au structures to create a better hot spots, between a reactive entity and the LSPR of these noble metal NPs. These have already be combined with Pd, TiO₂ and Fe₂O₃ NPs, but may be extended to other catalytically active NPs. Our group is also seeking an improved photolabile alkyne protecting compound, which can generate a terminal alkyne under milder conditions and could soon in the short term future be tested on surfaces. There is plenty of room of improvement and further development, which is of interest for the future nanotechnology.

REFERENCES

- (1) Toumey, C. The Literature of Promises. *Nat. Nanotechnol.* **2008**, *3*, 180–181.
- (2) Wang, J. *Nanomachines- Fundamentals and Applications*; Wiley, 2013.
- (3) Brock, D. C. In Understanding Moore's Law Four Decades of Innovation. In *In Understanding Moore's Law Four Decades of Innovation*; Brock, D. C., Ed.; Chemical Heritage Press: Philadelphia, Pennsylvania, 2006; p. Chapter 3.
- (4) Advancing Moors Law in 2014: Road to 14 nm.
- (5) Jain, T.; Lara-Avila, S.; Kervennic, Y.-V.; Moth-Poulsen, K.; Nørgaard, K.; Kubatkin, S.; Bjørnholm, T. Aligned Growth of Gold Nanorods in PMMA Channels: Parallel Preparation of Nanogaps. *ACS Nano* **2012**, *6*, 3861–3867.
- (6) Williams, D. J.; White, A. J. P.; Stoddart, J. F.; Raymo, F. M.; Bravo, J. A. High Yielding Template-Directed Syntheses of [2] Rotaxanes. *European J. Org. Chem.* **1998**, 2565–2571.
- (7) Ball, P. Chemistry Meets Computing. *Nature* **2000**, *406*.
- (8) Moth-Poulsen, K.; Bjørnholm, T. Molecular Electronics with Single Molecules in Solid-State Devices. *Nat. Nanotechnol.* **2009**, *4*, 551–556.
- (9) Syrenova, S.; Wadell, C.; Langhammer, C. Shrinking-Hole Colloidal Lithography: Self-Aligned Nanofabrication of Complex Plasmonic Nanoantennas. *Nano Lett.* **2014**, *14*, 2655–2663.
- (10) Fredriksson, H.; Alaverdyan, Y.; Dmitriev, A.; Langhammer, C.; Sutherland, D. S.; Zäch, M.; Kaserno, B. Hole-Mask Colloidal Lithography. *Adv. Mater.* **2007**, *19*, 4297–4302.
- (11) Shegai, T.; Chen, S.; Miljković, V. D.; Zengin, G.; Johansson, P.; Käll, M. A Bimetallic Nanoantenna for Directional Colour Routing. *Nat. Commun.* **2011**, *2*, 481.
- (12) Lee, J.; Hasan, W.; Stender, C. L.; Odom, T. W. Pyramids: A Platform for Designing Multifunctional Plasmonic Particles. *Acc. Chem. Res.* **2008**, *41*, 1762–1771.
- (13) Niu, W.; Zhang, L.; Xu, G. Shape-Controlled Synthesis of Single-Crystalline Palladium Nanocrystals. *ACS Nano* **2010**, *4*, 1987–1996.
- (14) Busbee, B. D.; Obare, S. O.; Murphy, C. J. An Improved Synthesis of High-Aspect-Ratio Gold Nanorods. *Adv. Mater.* **2003**, *15*, 414–416.
- (15) Shiohara, A.; Novikov, S. M.; Sol, D. M.; Taboada, J. M.; Obelleiro, F.; Liz-Marzán, L. M. Plasmon Modes and Hot Spots in Gold Nanostar – Satellite Clusters. *J. Phys. Chem. C* **2015**, *119*, 10836–10843.
- (16) Pauly, M.; Pichon, B. P.; Albouy, P.-A.; Fleutot, S.; Leuvrey, C.; Trassin, M.; Gallani, J.-L.; Begin-Colin, S. Monolayer and Multilayer Assemblies of Spherically and Cubic-Shaped Iron Oxide Nanoparticles. *J. Mater. Chem.* **2011**, *21*, 16018.
- (17) Dinh, C.; Nguyen, T.; Kleitz, F.; Do, T. Shape-Controlled Synthesis of Highly Crystalline Titania Nanocrystals. *ACS Nano* **2009**, *3*, 3737–3743.
- (18) Wu, H.-L.; Kuo, C.-H.; Huang, M. H. Seed-Mediated Synthesis of Gold Nanocrystals with Systematic Shape Evolution from Cubic to Trisoctahedral and Rhombic Dodecahedral Structures. *Langmuir* **2010**, *26*, 12307–12313.
- (19) Jin, R.; Cao, Y. C.; Hao, E.; Métraux, G. S.; Schatz, G. C.; Mirkin, C. a. Controlling Anisotropic Nanoparticle Growth through Plasmon Excitation. *Nature* **2003**, *425*, 487–490.
- (20) Cheng, H.-M.; Hsu, H.-C.; Chen, S.-L.; Wu, W.-T.; Kao, C.-C.; Lin, L.-J.; Hsieh, W.-F. Efficient UV Photoluminescence from Monodispersed Secondary ZnO Colloidal Spheres Synthesized by Sol–gel Method. *J. Cryst. Growth* **2005**, *277*, 192–199.
- (21) Millstone, J. E.; Park, S.; Shuford, K. L.; Qin, L.; Schatz, G. C.; Mirkin, C. a. Observation of a Quadrupole Plasmon Mode for a Colloidal Solution of Gold Nanoprisms. *J. Am. Chem. Soc.* **2005**, *127*, 5312–5313.
- (22) Rossi, L. M.; Shi, L.; Quina, F. H.; Rosenzweig, Z. Stöber Synthesis of Monodispersed Luminescent Silica Nanoparticles for Bioanalytical Assays. *Langmuir* **2005**, *21*, 4277–4280.
- (23) Tedsree, K.; Li, T.; Jones, S.; Chan, C. W. A.; Yu, K. M. K.; Bagot, P. A. J.; Marquis, E. A.; Smith, G. D. W.; Tsang, S. C. E. Hydrogen Production from Formic Acid Decomposition at Room Temperature Using a Ag-Pd Core-Shell Nanocatalyst. *Nat. Nanotechnol.* **2011**, *6*, 302–307.
- (24) McFarland, A. D.; Van Duyne, R. P. Single Silver Nanoparticles as Real-Time Optical Sensors with Zeptomole Sensitivity. *Nano Lett.* **2003**, *3*, 1057–1062.

- (25) Zhao, J.; Zhang, X.; Yonzon, C. R.; Haes, A. J.; Van Duyne, R. P. Localized Surface Plasmon Resonance Biosensors. *Nanomedicine* **2006**, *1*, 219–228.
- (26) Novo, C.; Funston, A. M.; Mulvaney, P. Direct Observation of Chemical Reactions on Single Gold Nanocrystals Using Surface Plasmon Spectroscopy. *Nat. Nanotechnol.* **2008**, *3*, 598–602.
- (27) Seo, D.; Park, G.; Song, H. Plasmonic Monitoring of Catalytic Hydrogen Generation by a Single Nanoparticle Probe. *J. Am. Chem. Soc.* **2012**, *134*, 1221–1227.
- (28) Larsson, E. M.; Syrenova, S.; Langhammer, C. Nanoplasmonic Sensing for Nanomaterials Science. *Nanophotonics* **2012**, *1*, 249–266.
- (29) Liu, N.; Tang, M. L.; Hentschel, M.; Giessen, H.; Alivisatos, A. P. Nanoantenna-Enhanced Gas Sensing in a Single Tailored Nanofocus. *Nat. Mater.* **2011**, *10*, 631–636.
- (30) Faraday, M. Experimental Relations of Gold (and Other Metals) to Light. *Phil. Trans. R. Soc. Lond.* **1857**, *147*, 145–181.
- (31) Gothic Rayonnant Rose
<https://i0.wp.com/upload.wikimedia.org/wikipedia/commons/4/49/GothicRayonnantRose003.jpg> (accessed Jan 1, 2016).
- (32) Museum, B. Lycurgus cup
http://www.britishmuseum.org/collectionimages/AN00036/AN00036154_001_1.jpg (accessed Jan 1, 2016).
- (33) Kelly, K. L.; Coronado, E.; Zhao, L. L.; Schatz, G. C. The Optical Properties of Metal Nanoparticles: The Influence of Size, Shape, and Dielectric Environment. *J. Phys. Chem. B* **2003**, *107*, 668–677.
- (34) Romo-Herrera, J. M.; Alvarez-Puebla, R. A.; Liz-Marzán, L. M. Controlled Assembly of Plasmonic Colloidal Nanoparticle Clusters. *Nanoscale* **2011**, *3*, 1304–1315.
- (35) Halas, N. J.; Lal, S.; Chang, W.-S.; Link, S.; Nordlander, P. Plasmons in Strongly Coupled Metallic Nanostructures. *Chem. Rev.* **2011**, *111*, 3913–3961.
- (36) Wadell, C.; Syrenova, S.; Langhammer, C. Plasmonic Hydrogen Sensing with Nanostructured Metal Hydrides. **2014**, 11925–11940.
- (37) Kreibig, U.; Vollmer, M. *Optical Properties of Metal Clusters*; Springer: Berlin-NewYork, 1995.
- (38) Pallavicini, P.; Chirico, G.; Collini, M.; Dacarro, G.; Donà, A.; D’Alfonso, L.; Falqui, A.; Diaz-Fernandez, Y.; Freddi, S.; Garofalo, B.; et al. Synthesis of Branched Au Nanoparticles with Tunable near-Infrared LSPR Using a Zwitterionic Surfactant. *Chem. Commun.* **2011**, *47*, 1315–1317.
- (39) Shanthil, M.; Thomas, R.; Swathi, R. S.; Thomas, K. G. Ag@SiO₂ Core-Shell Nanostrucutres: Distance-Dependent Plasmon Coupling and SERS Investigation. *J. Phys. Chem. Lett.* **2012**, *3*, 1459–1464.
- (40) Lombardi, A.; Grzelcz(1) Lombardi, A.; Grzelczak, M. P.; Crut, A.; Maioli, P.; Pastoriza-Santos, I.; Liz-Marzán, L. M.; Fatti, N. Del; Vallée, F. Optical Response of Individual Au-Ag@SiO₂ Heterodimers. *ACS Nano* **2013**, *7*, 2522–2531.ak, M. P.; Crut, A.; Maioli, P.; Pastoriza-Santos, I.; Liz-Marzán, L. M.; Fatti, N. Del; Vallée, F. Optical Response of Individual Au-Ag@SiO₂ Heterodimers. *ACS Nano* **2013**, *7*, 2522–2531.
- (41) Shegai, T.; Johansson, P.; Langhammer, C.; Käll, M. Directional Scattering and Hydrogen Sensing by Bimetallic Pd-Au Nanoantennas. *Nano Lett.* **2012**, *12*, 2464–2469.
- (42) Nabika, H.; Takase, M.; Nagasawa, F.; Murakoshi, K. Toward Plasmon-Induced Photoexcitation of Molecules. *J. Phys. Chem. Lett.* **2010**, *1*, 2470–2487.
- (43) Baffou, G.; Quidant, R.; García De Abajo, F. J. Nanoscale Control of Optical Heating in Complex Plasmonic Systems. *ACS Nano* **2010**, *4*, 709–716.
- (44) Denisyuk, A. I.; Adamo, G.; MacDonald, K. F.; Edgar, J.; Arnold, M. D.; Myroshnychenko, V.; Ford, M. J.; García de Abajo, F. J.; Zheludev, N. I. Transmitting Hertzian Optical Nanoantenna with Free-Electron Feed. *Nano Lett.* **2010**, *10*, 3250–3252.
- (45) Moskovits, M. Spectroscopy: Expanding Versatility. *Nature* **2010**, *464*, 357.
- (46) Moskovits, M. Surface-Enhanced Spectroscopy. *Rev. Mod. Phys.* **1985**, *57*, 783–826.
- (47) Vesseur, E. J. R.; De Waele, R.; Kuttge, M.; Polman, A. Direct Observation of Plasmonic Modes in Au Nanowires Using High-Resolution Cathodoluminescence Spectroscopy. *Nano Lett.* **2007**, *7*, 2843–2846.
- (48) Novo, C.; Funston, A. M.; Pastoriza-Santos, I.; Liz-Marzán, L. M.; Mulvaney, P. Spectroscopy and High-Resolution Microscopy of Single Nanocrystals by a Focused Ion Beam Registration Method. *Angew. Chemie - Int. Ed.* **2007**, *46*, 3517–3520.

- (49) Chen, S.; Svedendahl, M.; Käll, M.; Gunnarson, L.; Dmitriev, A. Ultrahigh Sensitivity Made Simple: Nanoplasmonic Label-Free Biosensing with an Extremely Low Limit-of-Detection for Bacterial and Cancer Diagnostics. *Nanotechnology* **2009**, *20*.
- (50) Gschneidtner, T. a.; Chen, S.; Christensen, J. B.; Käll, M.; Moth-Poulsen, K. Toward Plasmonic Biosensors Functionalized by a Photoinduced Surface Reaction. *J. Phys. Chem. C* **2013**, *117*, 14751–14758.
- (51) Dadosh, T.; Gordin, Y.; Krahne, R.; Khivrich, I.; Mahalu, D.; Frydman, V.; Sperling, J.; Yacoby, A.; Bar-Joseph, I. Measurement of the Conductance of Single Conjugated Molecules. *Nature* **2005**, *436*, 677–680.
- (52) Gschneidtner, T. A.; Diaz Fernandez, Y. A.; Moth-Poulsen, K. Progress in Self-Assembled Single-Molecule Electronic Devices. *J. Mater. Chem. C* **2013**, *1*, 7127–7133.
- (53) Parveen, S.; Misra, R.; Sahoo, S. K. Nanoparticles: A Boon to Drug Delivery, Therapeutics, Diagnostics and Imaging. *Nanomedicine* **2012**, *8*, 147–166.
- (54) Liu, Z.; Gan, L. M.; Hong, L.; Chen, W.; Lee, J. Y. Carbon-Supported Pt Nanoparticles as Catalysts for Proton Exchange Membrane Fuel Cells. *J. Power Sources* **2005**, *139*, 73–78.
- (55) Hernandez-Fernandez, P.; Masini, F.; McCarthy, D. N.; Strelbel, C. E.; Friebel, D.; Deiana, D.; Malacrida, P.; Nierhoff, A.; Bodin, A.; Wise, A. M.; et al. Mass-Selected Nanoparticles of PtxY as Model Catalysts for Oxygen Electroreduction. *Nat. Chem.* **2014**, *6*, 732–738.
- (56) Barick, K. C.; Singh, S.; Bahadur, D.; Lawande, M. a.; Patkar, D. P.; Hassan, P. a. Carboxyl Decorated Fe₃O₄ Nanoparticles for MRI Diagnosis and Localized Hyperthermia. *J. Colloid Interface Sci.* **2014**, *418*, 120–125.
- (57) Gschneidtner, T. A.; Moth-Poulsen, K. *Handbook of Single Molecular Electronics, Chapter: Self-Assembly at Interfaces*; Moth Poulsen, K., Ed.; Pan Stanford Publishing, 2016.
- (58) Park, J.; Shumaker-parry, J. S. Structural Study of Citrate Layers on Gold Nanoparticles: Role of Intermolecular Interactions in Stabilizing Nanoparticles. *J. Am. Chem. Soc.* **2014**, *135*, 1907–1921.
- (59) Schulz, F.; Homolka, T.; Bastu, N. G.; Puntes, V.; Weller, H.; Vossmeyer, T. Little Adjustments Significantly Improve the Turkevich Synthesis of Gold Nanoparticles. *Langmuir* **2014**, *30*, 10779–10784.
- (60) Brust, M.; Walker, M.; Bethell, D.; Schiffrin, D. J.; Whyman, R. Synthesis of Thiol-Derivatised Gold Nanoparticles in Two-Phase Liquid-Liquid System. *J. Chem. Soc., Chem. Commun.* **1994**, 801–802.
- (61) Fink, J.; Kiely, C. J.; Bethell, D.; Schiffrin, D. J. Self-Organization of Nanosized Gold Particles. *Chem. Mater.* **1998**, *10*, 922–926.
- (62) Templeton, A. C.; Wuelfing, W. P.; Murray, R. W. Monolayer-Protected Cluster Molecules. *Acc. Chem. Res.* **2000**, *33*, 27–36.
- (63) Zheng, N.; Fan, J.; Stucky, G. D. One-Step One-Phase Synthesis of Monodisperse Noble-Metallic Nanoparticles and Their Colloidal Crystals. *J. Am. Chem. Soc.* **2006**, *128*, 6550–6551.
- (64) Stevenson, P. C.; Turkevich, J.; Hillier. A Study of the Nucleation and Growth Processe in the Synthesis of Colloidal Gold. *Discuss. Faraday. Soc.* **1951**, *11*, 55–75.
- (65) Enustun, B. V.; Turkevich, J. Coagulation of Colloidal Gold. *Jacs* **1963**, *85*, 3317–3328.
- (66) Frens, G. Particle Size and Sol Stability in Metal Colloids. *Kolloid-Zeitschrift und Zeitschrift für Polym.* **1972**, *250*, 736–741.
- (67) Frens, G. Controlled Nucleation for the Regulation of the Particle SIze in Monodisperse Gold Suspensions. *Nat. Phys. Sci.* **1973**, *241*, 20–23.
- (68) Hiramatsu, H.; Osterloh, F. E. A Simple Large-Scale Synthesis of Nearly with Exchangeable Surfactants. *Chem. Mater.* **2004**, *16*, 2509–2511.
- (69) Shenhar, R.; Rotello, V. M. Nanoparticles: Scaffolds and Building Blocks. *Acc. Chem. Res.* **2003**, *36*, 549–561.
- (70) Wan, Y.; Guo, Z.; Jiang, X.; Fang, K.; Lu, X.; Zhang, Y.; Gu, N. Quasi-Spherical Silver Nanoparticles: Aqueous Synthesis and Size Control by the Seed-Mediated Lee–Meisel Method. *J. Colloid Interface Sci.* **2013**, *394*, 263–268.
- (71) Polte, J.; Erler, R.; Thünemann, A. F.; Sokolov, S.; Ahner, T. T.; Rademann, K.; Emmerling, F.; Krahnert, R. Nucleation and Growth of Gold Nanoparticles Studied via in Situ Small Angle X-Ray Scattering at Millisecond Time Resolution. *ACS Nano* **2010**, *4*, 1076–1082.
- (72) Polte, J.; Ahner, T. T.; Delissen, F.; Sokolov, S.; Emmerling, F.; Thünemann, A. F.; Krahnert, R. Mechanism of Gold Nanoparticle Formation in the Classical Citrate Synthesis Method Derived from Coupled in Situ XANES and SAXS Evaluation. *J. Am. Chem. Soc.* **2010**, *132*,

- 1296–1301.
- (73) Polte, J. Fundamental Growth Principles of Colloidal Metal Nanoparticles – a New Perspective. *CrystEngComm* **2015**, *17*, 6809–6830.
- (74) Behera, M.; Ram, S. Inquiring the Mechanism of Formation, Encapsulation, and Stabilization of Gold Nanoparticles by Poly(vinyl Pyrrolidone) Molecules in 1-Butanol. *Appl. Nanosci.* **2014**, *4*, 247–254.
- (75) Pastoriza-Santos, I.; Liz-Marzán, L. M. Formation of PVP-Protected Metal Nanoparticles in DMF. *Langmuir* **2002**, *18*, 2888–2894.
- (76) Senthil Kumar, P.; Pastoriza-Santos, I.; Rodríguez-González, B.; Javier García de Abajo, F.; Liz-Marzán, L. M. High-Yield Synthesis and Optical Response of Gold Nanostars. *Nanotechnology* **2008**, *19*, 15606.
- (77) Jana, N. R.; Gearheart, L.; Murphy, C. J.; Carolina, S. Seeding Growth for Size Control of 5–40 nm Diameter Gold Nanoparticles. *Society* **2001**, 6782–6786.
- (78) Nikoobakht, B.; El-sayed, M. A. Preparation and Growth Mechanism of Gold Nanorods (NRs) Using Seed-Mediated Growth Method. *Growth (Lakeland)* **2003**, 1957–1962.
- (79) Attard, G. S.; Corker, J. M.; Göltner, C. G.; Henke, S.; Templer, R. H. Liquid-Crystal Templates for Nanostructured Metals. *Angew. Chemie Int. Ed. English* **1997**, *36*, 1315–1317.
- (80) Ye, X.; Jin, L.; Caglayan, H.; Chen, J.; Xing, G.; Zheng, C.; Doan-Nguyen, V.; Kang, Y.; Engheta, N.; Kagan, C. R.; et al. Improved Size-Tunable Synthesis of Monodisperse Gold Nanorods through the Use of Aromatic Additives. *ACS Nano* **2012**, *6*, 2804–2817.
- (81) Jana, N. R. Gram-Scale Synthesis of Soluble, Near-Monodisperse Gold Nanorods and Other Anisotropic Nanoparticles. *Small* **2005**, *1*, 875–882.
- (82) Jain, T.; Roodbeen, R.; Reeler, N. E. a.; Vosch, T.; Jensen, K. J.; Bjørnholm, T.; Nørgaard, K. End-to-End Assembly of Gold Nanorods via Oligopeptide Linking and Surfactant Control. *J. Colloid Interface Sci.* **2012**, *376*, 83–90.
- (83) Törnblom, M.; Henriksson, U. Effect of Solubilization of Aliphatic Hydrocarbons on Size and Shape of Rodlike C16TABr Micelles Studied by 2H NMR Relaxation. *J. Phys. Chem. B* **1997**, *101*, 6028–6035.
- (84) Thomas, N.; Mani, E. An Analytical Solution to the Kinetics of Growth of Gold Nanorods. *RSC Adv.* **2016**, *6*, 30028–30036.
- (85) Murphy, C. J.; Thompson, L. B.; Chernak, D. J.; Yang, J. A.; Sivapalan, S. T.; Boulos, S. P.; Huang, J.; Alkilany, A. M.; Sisco, P. N. Gold Nanorod Crystal Growth: From Seed-Mediated Synthesis to Nanoscale Sculpting. *Curr. Opin. Colloid Interface Sci.* **2011**, *16*, 128–134.
- (86) Pérez-Juste, J.; Liz-Marzán, L. M.; Carnie, S.; Chan, D. Y. C.; Mulvaney, P. Electric-Field-Directed Growth of Gold Nanorods in Aqueous Surfactant Solutions. *Adv. Funct. Mater.* **2004**, *14*, 571–579.
- (87) Liu, M.; Guyot-Sionnest, P. Mechanism of silver(I)-Assisted Growth of Gold Nanorods and Bipyramids. *J. Phys. Chem. B* **2005**, *109*, 22192–22200.
- (88) Park, K.; Drummy, L. F.; Wadams, R. C.; Koerner, H.; Fabris, L.; Vaia, R. A. Growth Mechanism of Gold Nanorods. **2013**.
- (89) Niu, W.; Li, Z.-Y.; Shi, L.; Liu, X.; Li, H.; Han, S.; Chen, J.; Xu, G. Seed-Mediated Growth of Nearly Monodisperse Palladium Nanocubes with Controllable Sizes. *Cryst. Growth Des.* **2008**, *8*, 4440–4444.
- (90) Gu, X.; Nie, C.; Lai, Y.; Lin, C. Synthesis of Silver Nanorods and Nanowires by Tartrate-Reduced Route in Aqueous Solutions. *Mater. Chem. Phys.* **2006**, *96*, 217–222.
- (91) Pastoriza-Santos, I.; Liz-Marzán, L. M. Formation and Stabilization of Silver Nanoparticles through Reduction by N,N-Dimethylformamide. *Langmuir* **1999**, *15*, 948–951.
- (92) Hostetler, M. J.; Templeton, A. C.; Murray, R. W.; Hill, C.; Carolina, N. Dynamics of Place-Exchange Reactions on Monolayer-Protected Gold Cluster Molecules Dynamics of Place-Exchange Reactions on Monolayer-Protected Gold Cluster Molecules. *Reactions* **1999**, 3782–3789.
- (93) Boal, A. K.; Rotello, V. M. Fabrication and Self-Optimization of Multivalent Receptors on Nanoparticle Scaffolds [12]. *J. Am. Chem. Soc.* **2000**, *122*, 734–735.
- (94) Lin, S. Y.; Tsai, Y. T.; Chen, C. C.; Lin, C. M.; Chen, C. H. Two-Step Functionalization of Neutral and Positively Charged Thiols onto Citrate-Stabilized Au Nanoparticles. *J. Phys. Chem. B* **2004**, *108*, 2134–2139.
- (95) Ivanov, M. R.; Bednar, H. R.; Haes, A. J. Investigations of the Mechanism of Gold Nanoparticle Stability and Surface Functionalization in Capillary Electrophoresis. *ACS Nano* **2009**, *3*, 386–

- 394.
- (96) Smith, A. M.; Marbella, L. E.; Johnston, K. A.; Hartmann, M. J.; Crawford, S. E.; Kozycz, L. M.; Seferos, D. S.; Millstone, J. E. Quantitative Analysis of Thiolated Ligand Exchange on Gold Nanoparticles Monitored by ^1H NMR Spectroscopy. *Anal. Chem.* **2015**, *87*, 2771–2778.
- (97) Lee, D.; Yoon, S. Gold Nanocube–Nanosphere Dimers: Preparation, Plasmon Coupling, and Surface-Enhanced Raman Scattering. *J. Phys. Chem. C* **2015**, *119*, 7873–7882.
- (98) Jones, M. R.; Macfarlane, R. J.; Lee, B.; Zhang, J.; Young, K. L.; Senesi, A. J.; Mirkin, C. a. DNA-Nanoparticle Superlattices Formed from Anisotropic Building Blocks. *Nat. Mater.* **2010**, *9*, 913–917.
- (99) Ma, X.; Xue, Y.; Dai, L.; Urbas, A.; Li, Q. Hydrophilic Cucurbit[7]uril-Pseudorotaxane-Anchored-Monolayer-Protected Gold Nanorods. *Eur. J. Inorg. Chem.* **2013**, *2013*, 2682–2686.
- (100) Indrasekara, a. S. D. S.; Wadams, R. C.; Fabris, L. Ligand Exchange on Gold Nanorods: Going Back to the Future. *Part. Part. Syst. Charact.* **2014**, *31*, 819–838.
- (101) Leonov, A. P.; Zheng, J.; Clogston, J. D.; Stern, S. T.; Patri, A. K.; Wei, A. Detoxification of Gold Nanorods by Treatment with Polystyrenesulfonate. *ACS Nano* **2008**, *2*, 2481–2488.
- (102) Lehn, J. Toward Complex Matter: Supramolecular Chemistry and Self-Organization. *PNAS* **2002**, *99*, 4763–4768.
- (103) Reder, A. S.; Spencer, N.; Stoddart, J. F. Olympiadane. *Angew. Chemie (Int. ed.)* **1994**, *33*, 1286–1290.
- (104) Harrowfield, J.; Lehn, J. Article Multifunctionality and Multivalency Generation by Self-Assembly of Grid-Type Metallosupramolecular Architectures. *Chem. New Zeal.* **2011**, 170–173.
- (105) Bumm, A. L. A.; Arnold, J. J.; Cygan, M. T.; Dunbar, T. D.; Burgin, T. P.; Ii, L. J.; Allara, L.; Tour, J. M.; Weiss, P. S. Are Single Molecular Wires Conducting? *Science (80-.).* **1996**, *271*, 1705–1707.
- (106) Alivisatos, A. P.; Johnsson, K. P.; Peng, X.; Wilson, T. E.; Loweth, C. J.; Bruchez Jr., M. P.; Schultz, P. G. Organization of Nanocrystal Molecules Using DNA. *Nature* **1996**, *382*, 609–611.
- (107) Mucic, R. C.; Storhoff, J. J.; Mirkin, C. A.; Letsinger, R. L. DNA-Directed Synthesis of Binary Nanoparticle Network Materials. *J. Am. Chem. Soc.* **1998**, *120*, 12674–12675.
- (108) Boal, A.; Ilhan, F.; DeRouchey, J.; Thurn-Albrecht, T.; Russell, T.; Rotello, V. Self-Assembly of Nanoparticles into Structured Spherical and Network Aggregates. *Nature* **2000**, *404*, 746–748.
- (109) Mastroianni, A. J.; Claridge, S. A.; Paul Alivisatos, A. Pyramidal and Chiral Groupings of Gold Nanocrystals Assembled Using DNA Scaffolds. *J. Am. Chem. Soc.* **2009**, *131*, 8455–8459.
- (110) Loweth, C. J.; Caldwell, W. B.; Peng, X.; Alivisatos, a. P.; Schultz, P. G. DNA-Based Assembly of Gold Nanocrystals. *Angew. Chemie Int. Ed.* **1999**, *38*, 1808–1812.
- (111) Zanchet, D.; Micheel, C. M.; Parak, W. J.; Gerion, D.; Williams, S. C.; Alivisatos, a. P. Electrophoretic and Structural Studies of DNA-Directed Au Nanoparticle Groupings. *J. Phys. Chem. B* **2002**, *106*, 11758–11763.
- (112) Brousseau III, L. C.; Novak, J. P.; Marinakos, S. M.; Feldheim, D. L. Assembly of Phenylacetylene-Bridged Gold Nanocluster Dimers and Trimers. *Adv. Mater.* **1999**, *11*, 447–449.
- (113) Jain, T.; Westerlund, F.; Johnson, E.; Moth-Poulsen, K.; Bjørnholm, T. Self-Assembled Nanogaps via Seed-Mediated Growth of End-to-End Linked Gold Nanorods. *ACS Nano* **2009**, *3*, 828–834.
- (114) Guttman, A.; Mahalu, D.; Sperling, J.; Cohen-Hoshen, E.; Bar-Joseph, I. Self-Assembly of Metallic Double-Dot Single-Electron Device. *Appl. Phys. Lett.* **2011**, *99*, 63113.
- (115) Peterle, T.; Ringler, P.; Mayor, M. Gold Nanoparticles Stabilized by Acetylene-Functionalized Multideterminate Thioether Ligands: Building Blocks for Nanoparticle Superstructures. *Adv. Funct. Mater.* **2009**, *19*, 3497–3506.
- (116) Hermes, J. P.; Sander, F.; Fluch, U.; Peterle, T.; Thompson, D.; Urbani, R.; Pfohl, T.; Mayor, M. Monofunctionalized Gold Nanoparticles Stabilized by a Single Dendrimer Form Dumbbell Structures upon Homocoupling. *J. Am. Chem. Soc.* **2012**, *134*, 14674–14677.
- (117) Busson, M. P.; Rolly, B.; Stout, B.; Bonod, N.; Larquet, E.; Polman, A.; Bidault, S. Optical and Topological Characterization of Gold Nanoparticle Dimers Linked by a Single DNA Double Strand. *Nano Lett.* **2011**, *11*, 5060–5065.
- (118) Lermusiaux, L.; Sereda, A.; Portier, B.; Larquet, E.; Bidault, S. Reversible Switching of the Interparticle Distance in DNA-Templated Gold Nanoparticle Dimers. *ACS Nano* **2012**, *6*, 10992–10998.

- (119) Bidault, S.; Abajo, F. J. G. de; Polman, A. Plasmon-Based Nanolenses Assembled on a Well-Defined DNA Template. *J. Am. Chem. Soc.* **2008**, *130*, 2750–2751.
- (120) Ma, W.; Sun, M.; Xu, L.; Wang, L.; Kuang, H.; Xu, C. A SERS Active Gold Nanostar Dimer for Mercury Ion Detection. *Chem. Commun.* **2013**, *49*, 4989–4991.
- (121) Sardar, R.; Heap, T. B.; Shumaker-Parry, J. S. Versatile Solid Phase Synthesis of Gold Nanoparticle Dimers Using an Asymmetric Functionalization Approach. *J. Am. Chem. Soc.* **2007**, *129*, 5356–5357.
- (122) Hofmann, A.; Schmiel, P.; Stein, B.; Graf, C. Controlled Formation of Gold Nanoparticle Dimers Using Multivalent Thiol Ligands. *Langmuir* **2011**, *27*, 15165–15175.
- (123) Cha, H.; Yoon, J. H.; Yoon, S. Probing Quantum Plasmon Coupling Using Gold Nanoparticle Dimers with Tunable Interparticle Distances Down to the Subnanometer Range. *ACS Nano* **2014**, *8*, 8554–8563.
- (124) Chen, G.; Wang, Y.; Tan, L. H.; Yang, M.; Tan, L. S.; Chen, Y.; Chen, H. High-Purity Separation of Gold Nanoparticle Dimers and Trimers. *J. Am. Chem. Soc.* **2009**, *131*, 4218–4219.
- (125) Akbulut, O.; MacE, C. R.; Martinez, R. V.; Kumar, A. a.; Nie, Z.; Patton, M. R.; Whitesides, G. M. Separation of Nanoparticles in Aqueous Multiphase Systems through Centrifugation. *Nano Lett.* **2012**, *12*, 4060–4064.
- (126) Pradhan, S.; Ghosh, D.; Chen, S. Janus Nanostructures Based on Au-TiO₂ Heterodimers and Their Photocatalytic Activity in the Oxidation of Methanol. *ACS Appl. Mater. Interfaces* **2009**, *1*, 2060–2065.
- (127) Feng, Y.; He, J.; Wang, H.; Tay, Y. Y.; Sun, H.; Zhu, L.; Chen, H. An Unconventional Role of Ligand in Continuously Tuning of Metal-Metal Interfacial Strain. *J. Am. Chem. Soc.* **2012**, *134*, 2004–2007.
- (128) Khanal, B. P.; Pandey, A.; Li, L.; Lin, Q.; Bae, W. K.; Luo, H.; Klimov, V. I.; Pietryga, J. M. Generalized Synthesis of Hybrid Metal-Semiconductor Nanostructures Tunable from the Visible to the Infrared. *ACS Nano* **2012**, *6*, 3832–3840.
- (129) Liang, S.; Liu, X.-L.; Yang, Y.-Z.; Wang, Y.-L.; Wang, J.-H.; Yang, Z.-J.; Wang, L.-B.; Jia, S.-F.; Yu, X.-F.; Zhou, L.; *et al.* Symmetric and Asymmetric Au-AgCdSe Hybrid Nanorods. *Nano Lett.* **2012**, *12*, 5281–5286.
- (130) Giljohann, D. A.; Seferos, D. S.; Daniel, W. L.; Massich, M. D.; Patel, P. C.; Mirkin, C. A. Gold Nanoparticles for Biology and Medicine. *Angew. Chemie Int. Ed.* **2010**, *49*, 3280–3294.
- (131) Alvarez-Puebla, R. a.; Liz-Marzán, L. M. SERS-Based Diagnosis and Biodetection. *Small* **2010**, *6*, 604–610.
- (132) Adleman, J. R.; Boyd, D. A.; Goodwin, D. G.; Psaltis, D. Heterogenous Catalysis Mediated by Plasmon Heating. *Nano Lett.* **2009**, *9*, 4417–4423.
- (133) Liu, N.; Tang, M. L.; Hentschel, M.; Giessen, H.; Alivisatos, A. P. Nanoantenna-Enhanced Gas Sensing in a Single Tailored Nanofocus. *Nat. Mater.* **2011**, *10*, 631–636.
- (134) Shegai, T.; Langhammer, C. Hydride Formation in Single Palladium and Magnesium Nanoparticles Studied by Nanoplasmonic Dark-Field Scattering Spectroscopy. *Adv. Mater.* **2011**, *7*, 4409–4414.
- (135) Sheikholeslami, S.; Jun, Y.-W.; Jain, P. K.; Alivisatos, A. P. Coupling of Optical Resonances in a Compositionally Asymmetric Plasmonic Nanoparticle Dimer. *Nano Lett.* **2010**, *10*, 2655–2660.
- (136) Lee, S. E.; Alivisatos, A. P.; Bissell, M. J. Toward Plasmonics-Enabled Spatiotemporal Activity Patterns in Three-Dimensional Culture Models. *Syst. Biomed.* **2013**, 1–9.
- (137) Lim, S. I.; Zhong, C.-J. Molecularly Mediated Processing and Assembly\rof Nanoparticles: Exploring the Interparticle\Interactions and Structures. *Acc Chem Res* **2009**, *42*, 798–808.
- (138) Sivapalan, S. T.; DeVetter, B. M.; Yang, T. K.; Schulmerich, M. V.; Bhargava, R.; Murphy, C. J. Surface-Enhanced Raman Spectroscopy of Polyelectrolyte-Wrapped Gold Nanoparticles in Colloidal Suspension. *J. Phys. Chem. C* **2013**, *117*, 10677–10682.
- (139) Chen, L.; Li, Z.; Meng, Y.; Lu, M.; Wang, Z.; Zhang, R.-Q. Chemical Mechanism and Tunability of Surface-Enhanced Raman Scattering of Pyridine on Heteronuclear Coinage Metal Diatomic Clusters: A Density Functional Study. *J. Phys. Chem. C* **2013**, *117*, 12544–12551.
- (140) Kinkhabwala, A.; Yu, Z.; Fan, S.; Avlasevich, Y.; Müllen, K.; Moerner, W. E. Large Single-Molecule Fluorescence Enhancements Produced by a Bowtie Nanoantenna. *Nat. Photonics* **2009**, *3*, 654–657.
- (141) Adato, R.; Yanik, A. A.; Amsden, J. J.; Kaplan, D. L.; Omenetto, F. G.; Hong, M. K.; Erramilli, S.; Altug, H. Ultra-Sensitive Vibrational Spectroscopy of Protein Monolayers with Plasmonic

- Nanoantenna Arrays. *PNAS* **2009**, *106*.
- (142) Oxide, M.; Shell, C. Å. Highly Efficient Plasmon-Enhanced Dye-Sensitized Solar Cells through. *ACS Nano* **2011**, *5*, 7108–7116.
- (143) Tang, Y.; Jiang, Z.; Tay, Q.; Deng, J.; Lai, Y.; Gong, D.; Dong, Z.; Chen, Z. Visible-Light Plasmonic Photocatalyst Anchored on Titanate Nanotubes: A Novel Nanohybrid with Synergistic Effects of Adsorption and Degradation. *RSC Adv.* **2012**, *2*, 9406–9414.
- (144) Chen, J.; Wu, J. C. S.; Wu, P. C.; Tsai, D. P. Plasmonic Photocatalyst for H₂ Evolution in Photocatalytic Water Splitting. *J. Phys. Chem. C* **2011**, *115*, 210–216.
- (145) Tanaka, A.; Nishino, Y.; Sakaguchi, S.; Yoshikawa, T.; Imamura, K.; Hashimoto, K.; Kominami, H. Functionalization of a Plasmonic Au/TiO₂ Photocatalyst with an Ag Co-Catalyst for Quantitative Reduction of Nitrobenzene to Aniline in 2-Propanol Suspensions under Irradiation of Visible Light. *Chem. Commun.* **2013**, *49*, 2551–2553.
- (146) Zhang, Z.; Sun, M.; Ruan, P.; Zheng, H.; Xu, H. Electric Field Gradient Quadrupole Raman Modes Observed in Plasmon-Driven Catalytic Reactions Revealed by HV-TERS. *Nanoscale* **2013**, *5*, 4151–4155.
- (147) Chen, Y.-S.; Hong, M.-Y.; Huang, G. S. A Protein Transistor Made of an Antibody Molecule and Two Gold Nanoparticles. *Nat. Nanotechnol.* **2012**, *7*, 197–203.
- (148) Bowman-James, K. Alfred Werner Revisited : The Coordination Chemistry of Anions. *Acc. Chem. Res.* **2005**, *38*, 671–678.
- (149) Claridge, S. A.; Schwartz, J. J.; Weiss, P. S. Electrons, Photons, and Force: Quantitative Single-Molecule Measurements from Physics to Biology. *ACS Nano* **2011**, *5*, 693–729.
- (150) Cottrell, F.; Merrill, E.; Smith, K.; Polym, J. P. S.; Ed, P.; Link, A.; Springer, J.; Grandbois, M.; Beyer, M.; Rief, M.; *et al.* How Strong Is a Covalent Bond ? *Science* (80-.). **1999**, *283*, 1727–1731.
- (151) Xue, Y.; Li, X.; Li, H.; Zhang, W. Quantifying Thiol-Gold Interactions towards the Efficient Strength Control. *Nat. Commun.* **2014**, *5*, 1–9.
- (152) Hantzsch, A. Concensationsprodukte Aus ALdehydammoniak Und Ketonartigen Verbindungen. *Chem. Ber.* **1881**, *14*, 1637–1638.
- (153) Hofmeier, H.; Schubert, U. S. Recent Developments in the Supramolecular Chemistry of Terpyridine – Metal Complexes. *Chem. Soc. Rev.* **2004**, *33*, 373–399.
- (154) Zhao, J.; Jensen, L.; Sung, J.; Zou, S.; Schatz, G. C.; Duyne, R. P. Van. Interaction of Plasmon and Molecular Resonances for Rhodamine 6G Adsorbed on Silver Nanoparticles. **2007**, *1272–1273*.
- (155) Koenderink, A. F. On the Use of Purcell Factors for Plasmon Antennas. **2010**, *35*, 4208–4210.
- (156) Sauvan, C.; Hugonin, J. P.; Maksymov, I. S.; Lalanne, P.; P, Q. Å. Theory of the Spontaneous Optical Emission of Nanosize Photonic and Plasmon Resonators. **2013**, *237401*, 1–5.
- (157) Juluri, B. K.; Lu, M.; Zheng, Y. B.; Huang, T. J.; Jensen, L.; Pennsyl, V. Coupling between Molecular and Plasmonic Resonances : Effect of Molecular Absorbance. **2009**, *18499–18503*.
- (158) Chen, H.; Shao, L.; Woo, K. C.; Wang, J.; Lin, H. Plasmonic – Molecular Resonance Coupling : Plasmonic Splitting versus Energy Transfer. *J. Phys. Chem. C* **2012**, *116*, 14088–14095.
- (159) Antosiewicz, T. J.; Apell, S. P.; Shegai, T. Plasmon – Exciton Interactions in a Core – Shell Geometry: From Enhanced Absorption to Strong Coupling. *acs photonics* **2014**, *1*, 454–463.
- (160) Dintinger, J.; Klein, S.; Bustos, F.; Barnes, W. L.; Ebbesen, T. W. Strong Coupling between Surface Plasmon-Polaritons and Organic Molecules in Subwavelength Hole Arrays. *Phys. Rev. B* **2005**, 1–5.
- (161) Ambjörnsson, T.; Apell, S. P.; Käll, M. Resonant Coupling between Localized Plasmons and Anisotropic Molecular Coatings in Ellipsoidal Metal Nanoparticles. *Phys. Rev. B* **2006**, 1–10.
- (162) Zengin, G.; Wersäll, M.; Nilsson, S.; Antosiewicz, T. J.; Käll, M.; Shegai, T. Realizing Strong Light-Matter Interactions between Single-Nanoparticle Plasmons and Molecular Excitons at Ambient Conditions. *Phys. Rev. Lett.* **2015**, *157401*, 1–6.
- (163) Väkeväinen, A. I.; Moerland, R. J.; Rekola, H. T.; Eskelinen, A.-P.; Martikainen, J.-P.; KIm, D.-H.; Törmö, P. Plasmonic Surface Lattice Resonances at the Strong Coupling Regime. *Nano Lett.* **2014**, *14*, 1721–1727.
- (164) Rodriguez, S. R. K.; Rivas, J. G. Surface Lattice Resonances Strongly Coupled to Rhodamine 6G Excitons : Tuning the Plasmon-Exciton-Polariton Mass and Composition Abstract : *Opt. Express* **2013**, *21*, 1065–1070.
- (165) San Miguel, V.; Bochet, C. G.; del Campo, A. Wavelength-Selective Caged Surfaces: How Many Functional Levels Are Possible? *J. Am. Chem. Soc.* **2011**, *133*, 5380–5388.

- (166) Givens, R. S.; Conrad, P. G.; Yousef, A. L.; Lee, J. Photoremoveable Protecting Groups. In *Handbook of Organic Photochemistry and Photobiology*; CRC Press LLC, 2004; pp. 1–43.
- (167) Tanabe, K. K.; Allen, C. a; Cohen, S. M. Photochemical Activation of a Metal-Organic Framework to Reveal Functionality. *Angew. Chemie (Int. ed.)* **2010**, *49*, 9730–9733.
- (168) Chamberlin, W. Use of the 3,5-Dimethoxybenzyloxycarbonyl Group as a Photosensitive N-Protecting Group. *J. Am. Chem. Soc.* **1966**, *31*, 1658–1660.
- (169) Cameron, J. F.; Frechet, J. M. J. Photogeneration of Organic Bases from O-Nitrobenzyl-Derived Carbamates. *J. Am. Chem. Soc.* **1991**, *113*, 4303–4313.
- (170) Smith, A. B.; Savinov, S. N.; Manjappara, U. V; Chaiken, I. M. Peptide-Small Molecule Hybrids via Orthogonal Deprotection-Chemoselective Conjugation to Cysteine-Anchored Scaffolds. A Model Study. *Org. Lett.* **2002**, *4*, 4041–4044.
- (171) Peng, L.; Goeldner, M. Synthesis and Characterization of Photolabile Choline Precursors as Reversible Inhibitors of Cholinesterases: Release of Choline in the Microsecond Time Range. *J. Org. Chem.* **1996**, *61*, 185–191.
- (172) Walker, J. W.; Reid, G. P.; Mccray, J. A.; Trentham, D. R. Photolabile 1 - (2-Nitrophenyl) Ethyl Phosphate Esters of Adenine Nucleotide Analogues . Synthesis and Mechanism of Photolysis. *J. Am. Chem. Soc.* **1988**, *110*, 7170–7177.
- (173) Pollock, J.; Crawford, J. H.; Wootton, J. F.; Corrie, J. E. T.; Scott, R. H. A Comparison between the Distinct Inward Currents Activated in Rat Cultured Dorsal Root Ganglion Neurones by Intracellular Flash Photolysis of Two Forms of Caged Cyclic Guanosine Monophosphate. *Neurosci. Lett.* **2003**, *338*, 143–146.
- (174) Gee, K. R.; Niu, L.; Schaper, K.; Jayaraman, V.; Hess, G. P. Synthesis and Photochemistry of a Photolabile Precursor of N-Methyl-D-Aspartate (NMDA) That Is Photolyzed in the Microsecond Time Region and Is Suitable for Chemical Kinetic Investigations of the NMDA Receptor. *Biochemistry* **1999**, *38*, 3140–3147.
- (175) Yoo, D. J.; Greenberg, M. M. Synthesis of Oligonucleotides Containing 3-Alkyl Carboxylic Acids Using Universal , Photolabile Solid Phase Synthesis. *J. Org. Chem.* **1996**, *60*, 3358–3364.
- (176) Amit, B.; Ben-Efraim, D. a.; Patchornik, a. Light-Sensitive Amides. The Photosolvolysis of Substituted 1-Acyl-7-Nitroindolines. *J. Am. Chem. Soc.* **1976**, *98*, 843–844.
- (177) Singh-Gasson, S.; Green, R. D.; Yue, Y.; Nelson, C.; Blattner, F.; Sussman, M. R.; Cerrina, F. Maskless Fabrication of Light-Directed Oligonucleotide Microarrays Using a Digital Micromirror Array. *Nat. Biotechnol.* **1999**, *17*, 974–978.
- (178) Álvarez, M.; Best, A.; Unger, A.; Alonso, J. M.; del Campo, A.; Schmelzeisen, M.; Koynov, K.; Kreiter, M. Near-Field Lithography by Two-Photon Induced Photocleavage of Organic Monolayers. *Adv. Funct. Mater.* **2010**, *20*, 4265–4272.
- (179) Kaplan, J. H.; Forbush, B.; Hoffman, J. F. Rapid Photolytic Release of Adenosine 5'-triphosphate from a Protected Analogue: Utilization by the Na:K Pump of Human Red Blood Cell Ghosts. *Biochemistry* **1978**, *17*, 1929–1935.
- (180) Engels, J.; Schlaeger, E.-J. Synthesis , Structure , and Reactivity of Adenosine Cyclic 3'-5'-Phosphate Benzyl Triester. *J. Med. Chem.* **1977**, *20*, 7–11.
- (181) Pillai, V. N. R. Photoremoveable Protecting Groups in Organic Synthesis. *Synthesis (Stuttg.)* **1980**, *1*.
- (182) Bochet, C. G. Photolabile Protecting Groups and Linkers. *J. Chem. Soc. Perkin Trans. I* **2002**, 125–142.
- (183) Pelliccioli, A. P.; Wirz, J. Photoremoveable Protecting Groups: Reaction Mechanisms and Applications. *Photochem. Photobiol. Sci.* **2002**, *1*, 441–458.
- (184) del Campo, A.; Boos, D.; Spiess, H. W.; Jonas, U. Surface Modification with Orthogonal Photosensitive Silanes for Sequential Chemical Lithography and Site-Selective Particle Deposition. *Angew. Chemie (Int. ed.)* **2005**, *44*, 4707–4712.
- (185) Saimoto, H.; Shibayama, K.; Smith, A. L.; Nakada, M.; Pitsinos, E. N.; Hummel, C. W.; Nicolaou, K. C. Total Synthesis of Calicheamicin gamma1. *J. Am. Chem. Soc.* **1992**, *114*, 10082–10084.
- (186) Klán, P.; Šolomek, T.; Bochet, C. G.; Blanc, A.; Givens, R.; Rubina, M.; Popik, V.; Kostikov, A.; Wirz, J. Photoremoveable Protecting Groups in Chemistry and Biology: Reaction Mechanisms and Efficacy. *Chem. Rev.* **2013**, *113*, 119–191.
- (187) Morrison, J.; Wan, P.; Corrie, J. E. T.; Papageorgiou, G. Mechanisms of Photorelease of Carboxylic Acids from 1-Acyl-7-Nitroindolines in Solutions of Varying Water Content. *Photochem. Photobiol. Sci.* **2002**, *1*, 960–969.

- (188) Moth-Poulsen, K.; Kofod-Hansen, V.; Kamounah, F. S.; Hatzakis, N. S.; Stamou, D.; Schaumburg, K.; Christensen, J. B. Optically Induced Linking of Protein and Nanoparticles to Gold Surfaces. *Bioconjug. Chem.* **2010**, *21*, 1056–1061.
- (189) Silber, P.; Ciamician, G. Berichte Der Deutschen Chemischen Gesellschaft Zu Berlin. *Chem. Ber.* **1901**, *34*, 2040–2046.
- (190) Barltrop, J. A.; Plant, P. J. Photosensitive Protective Groups. *Chem. Commun.* **1966**, 822–823.
- (191) Sherry, B. D.; Radosevich, A. T.; Toste, F. D. A Mild C–O Bond Formation Catalyzed by a Rhenium-Oxo Complex. *J. Am. Chem. Soc.* **2003**, *125*, 6076–6077.
- (192) Kudoh, T.; Mori, T.; Shirahama, M.; Yamada, M.; Ishikawa, T.; Saito, S.; Kobayashi, H. Intramolecular Anionic Diels-Alder Reactions of 1-Aryl-4-Oxahepta-1,6-Diyne Systems in DMSO. *J. Am. Chem. Soc.* **2007**, *129*, 4939–4947.
- (193) Sanz, R.; Martínez, A.; Álvarez-Gutiérrez, J. M.; Rodríguez, F. Metal-Free Catalytic Nucleophilic Substitution of Propargylic Alcohols. *European J. Org. Chem.* **2006**, 1383–1386.
- (194) Nicholas, K. M.; Mulvaey, M.; Bayer, M. Synthetic Application of Transition Metal Stabilized Carbenium-Ions. Selective Alkylation of Ketones and Ketone Derivates with Propargyldicobalt Hexacarbonyl Cations. *J. Am. Chem. Soc.* **1980**, *102*, 2508–2510.
- (195) Ohri, R. V.; Radosevich, A. T.; Hrovat, K. J.; Musich, C.; Huang, D.; Holman, T. R.; Toste, F. D. A Re (V)-Catalyzed C – N Bond-Forming Route to Human Lipoxygenase Inhibitors. *Org. Lett.* **2005**, *7*, 2501–2504.
- (196) Nishibayashi, Y.; Wakiji, I.; Hidai, M. Novel Propargylic Substitution Reactions Catalyzed by Thiolate-Bridged Diruthenium Complexes via Allenylidene Intermediates. *J. Am. Chem. Soc.* **2000**, *122*, 11019–11020.
- (197) Hui, H.; Zhao, Q.; Yang, M.; She, D.; Chen, M.; Huang, G. Copper(II) Bromide Catalyzed Novel Preparation of Propargylic Ethers and Sulfides by S N 1-Type Substitution between Propargylic Alcohols and Alcohols or Thiols. *Synthesis (Stuttg.)* **2008**, *2008*, 191–196.
- (198) Ma, C.; Zhang, Y.; Zhang, H.; Li, J.; Nishizama, Y.; Tanimoto, H.; Morimoto, T.; Kakiuchi, K. Synthesis and Photochemistry of a New Photolabile Protecting Group for Propargylic Alcohols. *Synlett* **2017**, *28*, 560–564.
- (199) Hofmeier, H.; Schubert, U. S. Supramolecular Branching and Crosslinking of Terpyridine-Modified Copolymers: Complexation and Decomplexation Studies in Diluted Solution. *Macromol. Chem. Phys.* **2003**, *204*, 1391–1397.
- (200) Schubert, U. S.; Schmatloch, S.; Ferna, M. Metallo-Supramolecular Diethylene Glycol: Water-Soluble Reversible Polymers. *Macromol. Rapid Commun.* **2002**, *23*, 957–961.
- (201) Haensch, C.; Chiper, M.; Ulbricht, C.; Winter, A.; Hoeppener, S.; Schubert, U. S. Reversible Supramolecular Functionalization of Surfaces: Terpyridine Ligands as Versatile Building Blocks for Noncovalent Architectures. *Langmuir* **2008**, *24*, 12981–12985.
- (202) Langhammer, C.; Zorić, I.; Kasemo, B.; Clemens, B. M. Hydrogen Storage in Pd Nanodisks Characterized with a Novel Nanoplasmmonic Sensing Scheme. *Nano Lett.* **2007**, *7*, 3122–3127.
- (203) Langhammer, C.; Larsson, E. M.; Kasemo, B.; Zoric, I. Indirect Nanoplasmmonic Sensing: Ultrasensitive Experimental Platform for Nanomaterials Science and Optical. *Nature* **2010**, *465*, 3529–3538.
- (204) Pundt, B. A. Hydrogen in Nano-Sized Metals. *Adv. Eng. Mater.* **2004**, *11*–21.
- (205) Ito, T.; Okazaki, S. Pushing the Limits of Lithography. *Nature* **2000**, *406*, 1027–1031.
- (206) Gole, A.; Murphy, C. J. Seed-Mediated Synthesis of Gold Nanorods: Role of the Size and Nature of the Seed. *Chem. Mater.* **2004**, *16*, 3633–3640.
- (207) Yuan, H.; Khouri, C. G.; Hwang, H.; Wilson, C. M.; Grant, G. A.; Vo-Dinh, T. Gold Nanostars: Surfactant-Free Synthesis, 3D Modelling, and Two-Photon Photoluminescence Imaging. *Nanotechnology* **2012**, *23*, 75102.
- (208) Albrecht, T.; Moth-poulsen, K.; Christensen, J. B.; Hjelm, J.; Bjørnholm, T.; Ulstrup, J. Scanning Tunneling Spectroscopy in an Ionic Liquid. *J. Am. Chem. Soc.* **2006**, *128*, 6574–6575.
- (209) Hao, X.; Zhu, N.; Gschneidtner, T.; Jonsson, E. Ö.; Zhang, J.; Moth-Poulsen, K.; Wang, H.; Thygesen, K. S.; Jacobsen, K. W.; Ulstrup, J.; et al. Direct Measurement and Modulation of Single-Molecule Coordinative Bonding Forces in a Transition Metal Complex. *Nat. Commun.* **2013**, *4*.
- (210) Zengin, G.; Gschneidtner, T.; Verre, R.; Shao, L.; Antosiewicz, T. J.; Moth-Poulsen, K.; Käll, M.; Shegai, T. Evaluating Conditions for Strong Coupling between Nanoparticle Plasmons and Organic Dyes Using Scattering and Absorption Spectroscopy. *J. Phys. Chem. C* **2016**, *120*, 20588–20596.
- (211) Gschneidtner, T. A.; Moth-Poulsen, K. A Photolabile Protection Strategy for Terminal Alkynes.

- (212) Dewi, M. R.; Gschneidtner, T. A.; Elmas, S.; Ranford, M.; Moth-Poulsen, K.; Nann, T. Monofunctionalization and Dimerization of Nanoparticles Using Coordination Chemistry. *ACS Nano* **2015**, *9*, 1434–1439.
- (213) Gschneidtner, T. a.; Fernandez, Y. a D.; Syrenova, S.; Westerlund, F.; Langhammer, C.; Moth-Poulsen, K. A Versatile Self-Assembly Strategy for the Synthesis of Shape-Selected Colloidal Noble Metal Nanoparticle Heterodimers. *Langmuir* **2014**, *30*, 3041–3050.
- (214) Syrenova, S.; Wadell, C.; Nugroho, F. a. a.; Gschneidtner, T. a.; Diaz Fernandez, Y. a.; Nalin, G.; Świtlik, D.; Westerlund, F.; Antosiewicz, T. J.; Zhdanov, V. P.; *et al.* Hydride Formation Thermodynamics and Hysteresis in Individual Pd Nanocrystals with Different Size and Shape. *Nat. Mater.* **2015**, *14*, 1236–1245.
- (215) Gschneidtner, T. A.; Diaz Fernandez, Y. A.; Wadell, C.; Fornander, L. H.; Lara Avila, S.; Langhammer, C.; Westerlund, F.; Moth-Poulsen, K. The Conquest of Middle-Earth: Combining Top-down and Bottom-up Nanofabrication for Constructing Nanoparticle Based Devices. *Nanoscale* **2014**, *6*, 14605–14616.

ACKNOWLEDGEMENTS

I want to thank the Chalmers Materials Area of Advance for funding my work here at Chalmers. Furthermore I acknowledge the financial support of the ERC Starting Grant SIMONE. The practical work was carried out at the division of Applied Chemistry, Department of Chemistry and Chemical Engineering, Chalmers University of Technology.

A very special thanks goes to Professor Kasper Moth-Poulsen, my main supervisor, who always knows how to motivate, guide and help. He has always been there for support and professional discussions, but also for issues not work-related in nature. During these years I am grateful to have had you as my supervisor and the honor of being your first PhD student. It was thrilling to watch the group grow (from the two of us to 15+) and develop so fast and I remain humbled that you trusted and helped me come a step further in becoming an independent researcher.

I also thank my Co-supervisor Professor Mats Andersson for taking me on as PhD student (formerly) in his group and for giving me the opportunity to do my PhD here at Chalmers.

I appreciate being able to work very interdisciplinarily due to the collaboration we established. Special thanks therefore to colleagues from other Universities: Professor Jens Ullstrup and Associate Professor Qijin Chi from DTU Denmark, Professor JØrn B. Christensen, his student Mario Ficker from the University of Copenhagen, Associate Professor Kasper NØrgaard and his PhD student Titoo Jain from the University of Copenhagen, who hosted me during a research visit. Thank you Titoo for a fun time in Copenhagen.

I further extend gratitude to some collaborators far away from Sweden, Professor Thomas Nann and his PhD student Melissa Dewi from the Ian Wark Research Institute at the University of South Australia, for the long distance scientific discussions and fruitful cooperation in the field of combining molecular linker with nanoparticles forming dimeric clusters. Sending samples back and forth took time but it was worth the effort when working with such wonderful people. We further collaborated with Prof. Thomas Nann and PhD student Shioban Bradley on the characterization of graphene. I am glad to have met all of you, you made my experience as a PhD student delightful.

Besides international collaborations, we also worked with local research groups inside of Chalmers. I am pleased to have been worked with the excellent group of Professor Mikael Käll, Bionanophotonics in the Applied Physics department, his PhD students Si Chen and Gülis Zengin, as well as the now Associate Professor Timur Shegai. It was challenging working together with a pure physics group and getting them to trust our chemical approach to doing things and *vice versa*. However, the results speak for themselves, so thank you for the thrilling challenge. Furthermore, I want to thank the highly motivated group of Professor Christoph Langhammer in

Applied Physics, especially Carl Wadell and Svetlana Syrenova. Our near constant exchange and meetings helped a lot in the understanding of each other's work and it was a great experience working with you.

All this work would not have been possible without the Chalmers Materials Analysis laboratory and the help of Stefan Gustafsson, Anders Kvist and the group of Professor Eva Olsson, who very patiently helped me with all small and bigger problems during the daily use of TEM and SEM. I thank you very much for that.

I am, of course, very happy for all the people I met during my PhD, who stood beside me, supported with the daily struggle as a PhD student, such as Tim, Agi, Wenliu, Renee, Anders, Ali, Guillermo and Harald. You made my professional and private stay here such a great experience. The Diamond division and all the people involved –former and present. It was a pleasure working together and all the *fika* we had together. Especially Frida and Lotta, for helping me daily and making my stay here a pleasurable one.

Particular and heartfelt gratitude goes to my very good friends at Chalmers and outside of Chalmers, Debby, Selda, Noushin, Johanna, Adele and especially Amaia, who was my biggest support and such a good friend to me and my kids, who was always there for me. Thank you so much *carino*. We will miss you here in Sweden a lot. I shared the last 5 years with you and we will never forget you. *Te quiero mucho*.

A special thanks goes to my family and my friends at home for always giving me the necessary support and love I needed. *Ich liebe euch und danke euch für Alles. Ohne eure Unterstützung und euer gutes Zureden, wäre ich nicht wo ich jetzt bin. Danke. Ich bin froh, dass es euch gibt, und dass wir uns trotz der Entfernung noch so nah sind.*

Finally, but most importantly, I would like to thank Luis for always being there for me, supporting me. We share the most important part of our lives, our adorable sons. You are what makes my day, I am so lucky and happy. I love you.